



LEHRSTUHL UND INSTITUT FÜR LEICHTBAU
Univ.-Prof. Dr.-Ing. H.-G. Reimerdes
– Fakultät für Maschinenwesen –



REpower Systems AG

DIPLOMARBEIT
DA-2010-02

**Fluttereffect analysis of horizontal windturbines in example of a
generic 61.5 m rotorblade via MBS-simulation with MBDyn**

Verfasser:
cand. Ing. Pay Thorben Sackniess

Betreuer:
Dr.-Ing. A. Dafnis
P. Rix - REpower Systems AG

Aachen, Juni 2010

Aufgabenstellung

„Flatterunteruchungen an Windturbinen Rotorblättern am Beispiel eines generischen 61.5m Rotorblattes mithilfe Mehrkörpersimulationen in MBDyn“
(Beginn: ab 01.Nov. 2009)

Es soll mittels aero-elastischer Simulationen von Mehrkörpersystemen (MKS) im Zeitbereich die Flatterneigung von Windturbinen-Rotorblättern untersucht werden.

Die Simulationen sollen mit der OpenSource MKS-Software "MBDyn" durchgeführt werden und diese auf ihre Eignung für Flattersimulationen an Windturbinen getestet werden. Dafür sollte zunächst eine generelle Einarbeitung in die Theorie der Strukturodynamik und der Aerodynamik während des Flattervorganges an Windturbinen erfolgen, sowie eine Einarbeitung in die Bedienung der Software und der Modellierungssprache anhand bestehender Rotorblatt-MKS-Modelle. Die anschließend durchzuführenden Simulationen sollen an Modellen von aktuellen, firmeneigenen Rotorblättern durchgeführt werden, um konkrete Aussagen über die Flatterneigung existierender Blätter zu erzielen. Dies beinhaltet die Beschreibung des Vorgehens u. der Methodik beim Modellaufbau (Topologie) und der Validierung (Plausibilisierung), welches als Grundlage für die Ausarbeitung einer allgemeinen Verfahrensanleitung / Prozessbeschreibung für zukünftige Untersuchungen dienen kann.

Der Aufbau eines generischen, "virtuellen" Modells eines fiktiven Rotorblattes könnte aufgrund wegfallender Geheimhaltungsvereinbarungen und somit unproblematischer Ergebnisdarstellung ebenfalls von Interesse sein.

Es soll durch eine noch näher zu bestimmende Anzahl an Simulationen eine Sensitivitätsanalyse durchgeführt werden, um die wichtigsten Parameter mit dem größten Einfluß hinsichtlich der Flatterdrehzahl (=Rotordrehzahl bei einsetzendem Flattern) zu identifizieren. Die erzeugten Ergebnisse (Zeitserien) sollten durch Vergleichssimulationen mit im Hause REpower verfügbaren proprietären (kommerziellen) Programmen wie z.B. SIMPACK, ADAMS und/oder ANSYS validiert werden.

Ansprechpartner:

Patrick Rix

Lasten und System Simulation
REpower Systems AG
TechCenter
Albert-Betz-Str. 1
D-24783 Osterrönfeld
e-mail: p.rix@repower.de
Internet: www.repower.de

Summary

By means of efficiency and cost savings the dimensions of rotorblades for windturbines constantly increased. Because of the dimension of nowadays used rotorblades new aeroelastic problems arise from structural compromises on rotorblade structures. The certification of rotorblades becomes more large scale by it. Therfore the Loads and System-Simulation department at REpower Systems develops a new tool on the base of MBDyn, a multi-body simulation software worked out for helicopter rotorblades, to make loads calculations for windturbines more realistic. MBDyn was deliberately taken because it allows an unlimited number of degrees of freedom in contrast to already existing multi-body simulation tools. MBDyn causes no licence-problems and -costs by its existing OpenSource code. The great share of own development leads to a funded knowledge which later on makes company internal solve of problems easier.

In a previous diploma thesis a modelgenerator for this tool was developed with which rotorblades as simulation models can be built. To check usability of the multi-body simulation tool as well as the modelgenerator, flutteranalysis are done to find out how the software deals with high dynamic oscillations. These flutter analysis precede a structural and aerodynamic validation of models of the modelgenerator.

The validation of the models done by the modelgenerator within the scope of this thesis showed mistakes in the structure dynamic modeling. By repair of this source of error and the next done validations there is a basis for following examinations. During the validations system parameters were determined to let them slip in the examination of dynamic instabilities.

The following done simulations on the rotor during this thesis in view of the appearence of aeroelastic instabilities at the rotorblades resulted in an arising of stall induced vibrations in the lower part of rotating speeds of the turbine. Aeroelastic flutter develops from a rotating speed of 14 rpm with the NREL-blade. The RE61.5 - blade attains higer rotation speeds when flutter occurs. During the examination of these instability areas problems as to the simulation stability of MBDyn arise. The thesis shows that it is possible to simulate high dynamic effects correctly, although at the moment with defined restrictions as to the aerodynamic model.

Zusammenfassung

Unter dem Gesichtspunkt der Effektivität und Kostensparnis ist die Größe von Rotorblättern für Windturbinen stetig angestiegen. Aufgrund der Größe von heutzutage verbauten Rotorblättern ergeben sich durch strukturelle Kompromisse für den Rotorblattbau neuartige aeroelastische Problemstellungen. Der Nachweis für die Zertifizierung von Rotorblättern wird hierdurch aufwendiger. Deshalb entwickelt die Abteilung Last und System-Simulation von REpower Systems auf Basis von MBDyn, ein Mehrkörpersimulationstool entwickelt für Hubschrauberrotoren, ein neues Tool um realistischer Lastenrechnungen für eine Windturbine anfertigen zu können. Hierbei wurde sich bewusst für MBDyn entschieden, da es im Gegensatz zu schon vorhandener Mehrkörpersimulationssoftware eine unbegrenzte Anzahl von Freiheitsgraden zulässt. Zudem verursacht MBDyn durch vorhandenen OpenSource Code keine Lizenz-Probleme und -Kosten. Auch verhilft der große Anteil an Eigenentwicklung zu einem fundierten Wissen, welches später betriebsinteres Losen von Problemen erleichtert.

In einer vorherigen Diplomarbeit wurde für dieses Tool ein Modelgenerator erstellt, mithilfe dessen sich Rotorblätter als Simulationsmodelle erstellen lassen. Um das Mehrkörpersimulations-tool sowie den Modelgenerator auf Verwendbarkeit in Zusammenhang mit hochdynamischen Schwingungen zu untersuchen, werden Flatteruntersuchungen durchgeführt. Diesen Flatteruntersuchungen geht eine strukturelle und aerodynamische Validierung von Modellen aus dem Modelgenerator voraus.

Die im Rahmen dieser Arbeit durchgeführte Validierung der vom Modelgenerator erstellten Modelle zeigte Fehler in der strukturdynamischen Modellierung auf. Durch die Behebung dieser Fehlerquellen und den anschliessend durchgeführten Validierungen besteht eine Grundlage für darauf folgende Untersuchungen. Während der Validierungen wurden Systemkennwerte ermittelt, um diese dann in die Untersuchung dynamischer Instabilitäten einfließen zu lassen.

Die des Weiteren im Rahmen dieser Arbeit durchgeführten Simulationen des Rotors mit Hinblick auf das Auftreten von aeroelastischen Instabilitäten an den Rotorblättern ergaben ein Auftreten von Stall induzierten Schwingungen im unteren Drehzahlbereich der Anlage. Aeroelastisches Flattern entwickelt sich bei einer Drehzahl von 14 rpm beim NREL-Blatt, beim RE61.5-Blatt ist dieser Wert strukturell bedingt höher. Im Laufe der Untersuchung dieser Instabilitätsbereiche traten Probleme hinsichtlich der Simulationsstabilität von MBDyn auf. Die Arbeit zeigt auf das es möglich ist, derzeit noch mit bestimmten Einschränkungen hinsichtlich des aerodynamischen Modells, hochdynamische Effekte richtig darzustellen, bzw. zu simulieren.

Declaration of Authorship

I hereby confirm that I have authored this thesis independently and without use of others than the indicated resources.

All passages, which are literally or in general manner taken out of publication or other sources, are marked as such.

location/date

signature

Contents

1	Introduction	1
2	Theoretical Foundations	4
2.1	Fundamentals of the functionality of a horizontal-axis-windturbine (HAWT)	4
2.2	The blade design	7
2.3	Actuator Disc Theory and Momentum Theory	9
2.4	Blade Element Theory	12
2.5	Blade Element Momentum Theory (BEMT)	14
2.6	A describtion of the aeroelastic instabilities	15
2.6.1	Determination between blades with a risk of flutter and those without	20
2.7	Theodorsen´s Theory	24
2.8	Simulations Tools	26
2.8.1	FLEX5®	27
2.8.2	Multibody-Dynamics-Simulation-Software MBDyn	27
2.8.3	Blender	29
2.8.4	ANSYS®	29
2.8.5	SIMPACK®	29
3	Accomplishment of model validations	30
3.1	The configuration of a rotor blade in MBDyn	30
3.1.1	Preprocessing	30
3.2	First Simulation	37
3.3	Structural validation	38

CONTENTS

3.3.1	The U-profile and L-profile validation with ANSYS	39
3.3.2	Structural analysis of the rotor blade	47
3.3.3	Research on the influence on the centrifugal force with the eigenfrequencies	54
3.4	Aerodynamic validations	55
3.4.1	Aerodynamic load on windturbine rotorblades	60
3.5	Researches on aeroelastic instabilities/flutter in running simulations	61
3.5.1	Looking on instabilities Region I	62
3.5.2	Looking on instabilities Region II	69
3.5.3	Influence of Theodorsen on the instabilities	74
4	Conclusion and outlook	80
Bibliography		82
5	Appendix	84
5.1	Simulation I	84
5.2	NREL - Blade - data	90
5.3	L-profile	94
5.4	CD	95

List of Figures

1.1	Accumulated Installed Capacity 1990-2009 (DEWI GmbH)	2
1.2	Power per Unit 1993-2009 (DEWI GmbH)	2
2.1	Design of an HAWT, schematic	5
2.2	Characteristics of c_p over $\frac{v_2}{v_1}$	6
2.3	Velocities, angles and forces on a rotor element	7
2.4	Basically blade construction	8
2.5	NREL-blade	8
2.6	Exposure of the NREL-blade 5.2	9
2.7	Top view of the NREL-blade to display the twist	9
2.8	Illustration of streamlines behind the rotor and the axial velocity and pressure upstream and downstream of the rotor	10
2.9	Axial Stream tube around a Wind Turbine	10
2.10	Rotating Annular Stream tube	11
2.11	Blade element	13
2.12	Forces on a turbine blade element	13
2.13	Fluttereffect	16
2.14	A typical blade section with two degrees of freedom	16
2.15	Positions of the different centers over the blade radius of the 61.5 NREL-blade .	21
2.16	A typical blade section with one degree of freedom	22
2.17	Dynamic stall loops in a $C_L-\alpha$ diagram	24
2.18	Mathematical model used by Theodorsen	24

LIST OF FIGURES

2.19	Damping coefficient of the flutter mode versus rotor speed for unsteady and quasi-steady aerodynamics [Lob04]	26
3.1	Approximation of a windturbine as a MBS	31
3.2	Assembly of nodes and beams for MBS	31
3.3	Structural assembling of a blade in MBDyn	32
3.4	Location of the Gausspoints	32
3.5	Aerodynamic assembling of a blade	33
3.6	Structure of the model created by the preprocessor	34
3.7	Global definition and coordinate system of a windturbine in MBDyn	35
3.8	The different coordinate systems of a windturbine	36
3.9	Section from the flapwise- and torsionmotion of a 61.5m blade	37
3.10	U-profile parameters	39
3.11	Loads on an U-profile (unmodified preprocessor)	40
3.12	Beam Section	42
3.13	Loads on an U-profile (modified preprocessor)	43
3.14	L-profile parameters	44
3.15	L-profile beam with a twist of 15 degree in ANSYS(2.8.4)	45
3.16	Loads on a L-profile (modified preprocessor)	46
3.17	Blade assembling, with nodes and elements	48
3.18	Blade with applied Forces on five nodes in ANSYS(2.8.4)	49
3.19	Cut-out with spider-node 44	49
3.20	Diagram of the deformation in MBDyn	50
3.21	Deviation from results(ANSYS/MBDyn) of applied loads in x-direction	51
3.22	Deviation from results (ANSYS/MBDyn) of applied loads in y-direction	52
3.23	Deviation from results(ANSYS/MBDyn) of applied moments around z-axis	53
3.24	Alteration of the eigenfrequencies over rpm corresponding to a standstill rotor	55
3.25	Bladelement for static aerodynamic validations	56
3.26	Exemplary $C_L(\alpha)$ -diagram	57
3.27	Arrangement of AC, SC, CG, EC and node position on a profile	58

LIST OF FIGURES

3.28 Influence of Theodorsens aerodynamic on an blade element	59
3.29 Examination of the effect of the distance between SC and AC	60
3.30 Different loadcases on a windturbine rotorblade	61
3.31 Time serie 95 - 140sec of simulation no.1	62
3.32 Detailed time serie	63
3.33 Aerodynamic forces over the blade	65
3.34 Interpolation areas on the blade	65
3.35 Aerodynamic forces of a constant profile in spanwise direction	66
3.36 Aerodynamic forces of a constant profile in spanwise direction in consideration of gauss points positions	66
3.37 Force-characteristic 112-119sec of node 7120	67
3.38 Angle of Attack	68
3.39 Time serie 195 - 230 sec	69
3.40 RegionII	70
3.41 Three time sections of Region No.II	71
3.42 Detailed characteristics, torsion scaled by 1/50 and the middle value of flap charged with minus four, torsion (red), flap (blue), edge (green)	72
3.43 flapwise and torsionwise displacement	73
3.44 Failure during Theodorsen Simulation	74
3.45 C81 Aerodynamic	75
3.46 Theodorsen Aerodynamic	76
3.47 Time section around 40sec	77
3.48 Comparison between NREL 5 beam and 10 beam model	79

List of Tables

3.2	Position of the nodes in MBDyn and ANSYS and the applied forces	47
3.3	NREL-eigenfrequencies on comparison	54
3.4	Detail information about the profile	56
3.5	Results of aerodynamic comparison	57
3.6	Dynamic structure properties of the blade element	58
3.7	Example list of test-simulations-paramaters	74

Nomenclature

Abbreviations

AC	Aerodynamic center
AoA	Angle of Attack
BEMT	Blade-element-momentum-theory
BET	Blade element theory
CG	Center of gravity
CP	Collocation point
DOF	Degree of freedom
EC	Elastic center
FEM	Finite-element-method
GPR	Glass fibre reinforced plastic
HAWT	Horizontal-axis-windturbines
MBS	Multi-body-system
MW	Megawatt
NREL	National Renewable Energy Laboratory
SC	Shear center

Chapter 1

Introduction

Due to the permanent rising of mankind all over the world the energy demand is growing fast. The fossil fuels like coal, gas, oil, etc. are dwindling resources and will be exhausted in the near future. They have provided the civilization with a high standard of living but they have taken a toll on the environment. The industry is starting to look for other sources of renewable, clean energy sources. Some of the most common alternative sources of energy are windpower and solar power. During the last decades these alternative energies became more important and will displace the conventional ones in the future. The oil shortages of the 1970's changed the energy picture for the world. It created an interest in alternative energy sources, paving the way for the re-entry of the windmill to generate electricity.

Among the renewable energy sources the wind energy sector got the most important in the last years. This bases on the currently best degree of efficiency by cost and power compared to other renewable energies like solar- or waterenergy.

Since 1990 the wind energy sector is booming and still expanding (Figure 1.1).

The windturbines become bigger, more efficient and new locations are discovered, onshore as well as offshore. Today the forecasts say this market will grow rapidly until 2030, then all regions are covered, where windturbines can be set up [Ins10]. The new challenge of windturbine manufacturers will then be to build more effective and noise reduced turbines. This process already starts nowadays, as Figure 1.2 shows, the energy yield per unit is steadily rising. The production of 5 Megawatt windturbines has began over a year ago, the 6 Megawatt turbines development will be finished in the next months and there are still plans for 10 MW constructions.

Because of that the windturbine blades get bigger, which means mainly bigger in span wise. With the longer span the bending-stiffness goes down by the length and the blade gets more bending and torsion "softer", considering the overall-weight should be as small as possible. The tip speed of a blade rises by the diameter of the rotor.

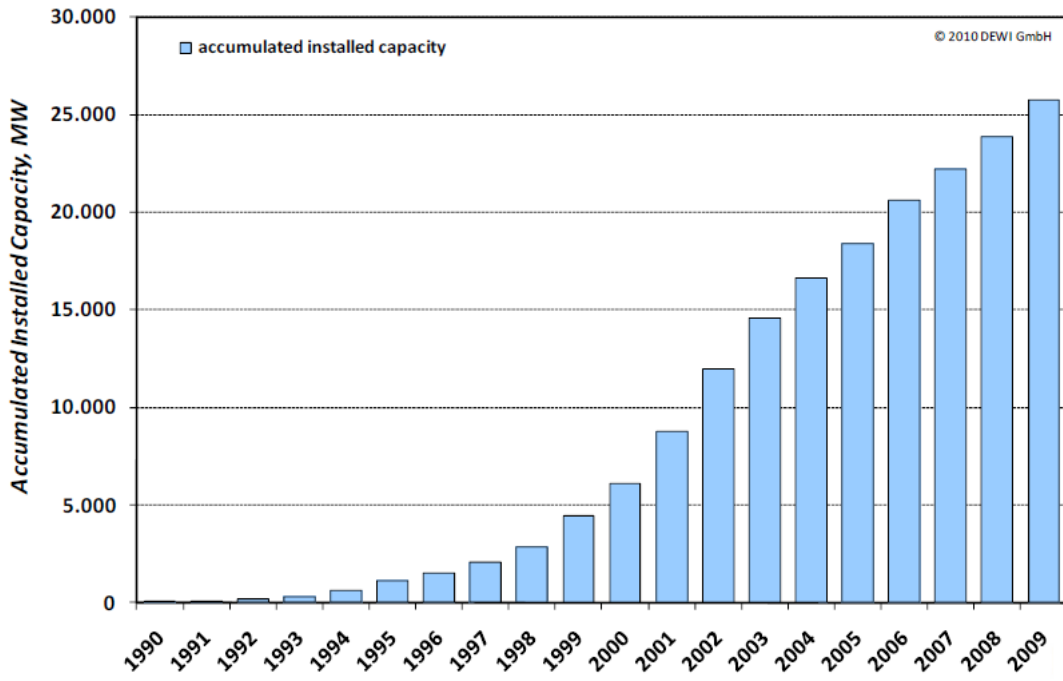


Figure 1.1: Accumulated Installed Capacity 1990-2009 (DEWI GmbH)

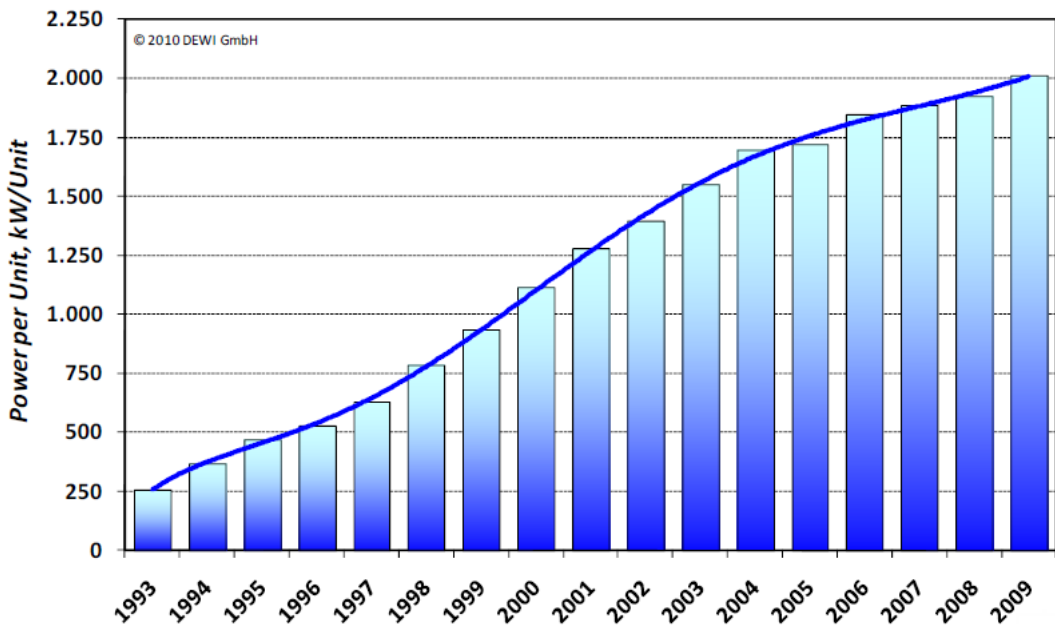


Figure 1.2: Power per Unit 1993-2009 (DEWI GmbH)

These things make it among others more susceptible to structural and aerodynamic blades oscillations. Therefore the proof of flutter stability becomes more important on windturbine

rotorblades, on one hand for the certification and security and on the other hand for the most effective building costs. Each layer of fiber glass costs more and makes the blade heavier so that all other components, like the nacelle, tower and the fundament, have to be layed up stronger.

To build the best cost effective wind turbines simulations proof their worth in industry. The simulation software steady continues development and today there is a hole bunch of commercial software for the wind industry. This commercial software is often quite expensive and the code cannot be modified for special purposes. As an example the range of costs of a single full-featured license is about 20.000 - 50.000 Euro (depending on the system). These have to be multiplied by the anticipated total amount of licences for all workplaces. OpenSource software on the other hand is for free and can be modified in many ways. REpower Systems AG will develop a new simulation tool for calculating load cases on wind turbines based on MBDyn.

But before a new software is integrated in the way of a certification of a new windturbine, this new software has to be validated, tested and the results must be compared with the results of the programms that were used in former times. It is meaningful to examine a high dynamic problem for the validation of the rotor, so you can be right about the model you build, if the results are all realistic and related compared to other multi-body simulations (MBS).

Grounded on the high dynamic coherence by the appearance of flutter it is important to use MBS with a high number of degrees of freedoms and changing time steps. For this purpose MBDyn is perfectly qualified because there are no limits concerning the degrees of freedoms and it is not limited like i.e. FLEX5[®], another multi-body software industry works with.

This diploma thesis shows the proceeding and results of the validation of a windturbine rotor with 61.5 m blades in consideration of the high-dynamic problem of flutter with the OpenSource software MBDyn. The proceeding can be arranged in following steps:

- Become acquainted with the literature of aerodynamic and structure-dynamic of windturbine-rotorblades
- Classification of windturbine-rotorblades in structure-dynamic and aerodynamic in problematical cases / riskanalysis
- Get into MBDyn and the established rotor-blade model
- Prove if the preprocessor is building up correct MBDyn models
- Validation and modification of the established rotor-blade model if necessary / comparison with other simulation-software
- Analytical aeroelastic validation, parameterstudies, sensitivity-analysis with MBDyn
- Examination of the results and interpretation

Chapter 2

Theoretical Foundations

2.1 Fundamentals of the functionality of a horizontal-axis-windturbine (HAWT)

Horizontal-axis-windturbines are nowadays those with the best yield of windpower. Therefore this is the most popular and assembled design in the world, besides i.e. vertical axis wind turbines. There are often many differences in details, but the basic design of an horizontal-axis-windturbine is always the same (Figure 2.1). It consists of a fundament, a tower, a rotor with the blades and a nacelle that contains the generator, gearbox, brakesystem, etc..

The primary component of a windturbine is an energy converter, who converts the kinetic energy of the moved air, the wind, into mechanical energy. The act of removal mechanical energy from a moved airstream with the help of a rotating windenergy-converter is described by Albert Betz (1885-1968).

The kinetic energy of an airmass m , moved with a velocity v , can be described as:

$$E = \frac{1}{2}mv^2 \text{ (Nm)}$$

Considering an appropriate sectional area A , crossing by air with a velocity v , the flow rate \dot{V} and the mass rate \dot{m} is:

$$\begin{aligned}\dot{V} &= vA \left(\frac{m^2}{s} \right) \\ \dot{m} &= \varrho \cdot v \cdot A \left(\frac{kg}{s} \right)\end{aligned}$$

With the approach of the kinetic energy of moved air and the mass rate a formula for the Power P_0 can be described:

$$P_0 = \frac{1}{2}\varrho v^3 A \text{ (W)}$$

2.1. FUNDAMENTALS OF THE FUNCTIONALITY OF A HORIZONTAL-AXIS-WINDTURBINE (HAWT)

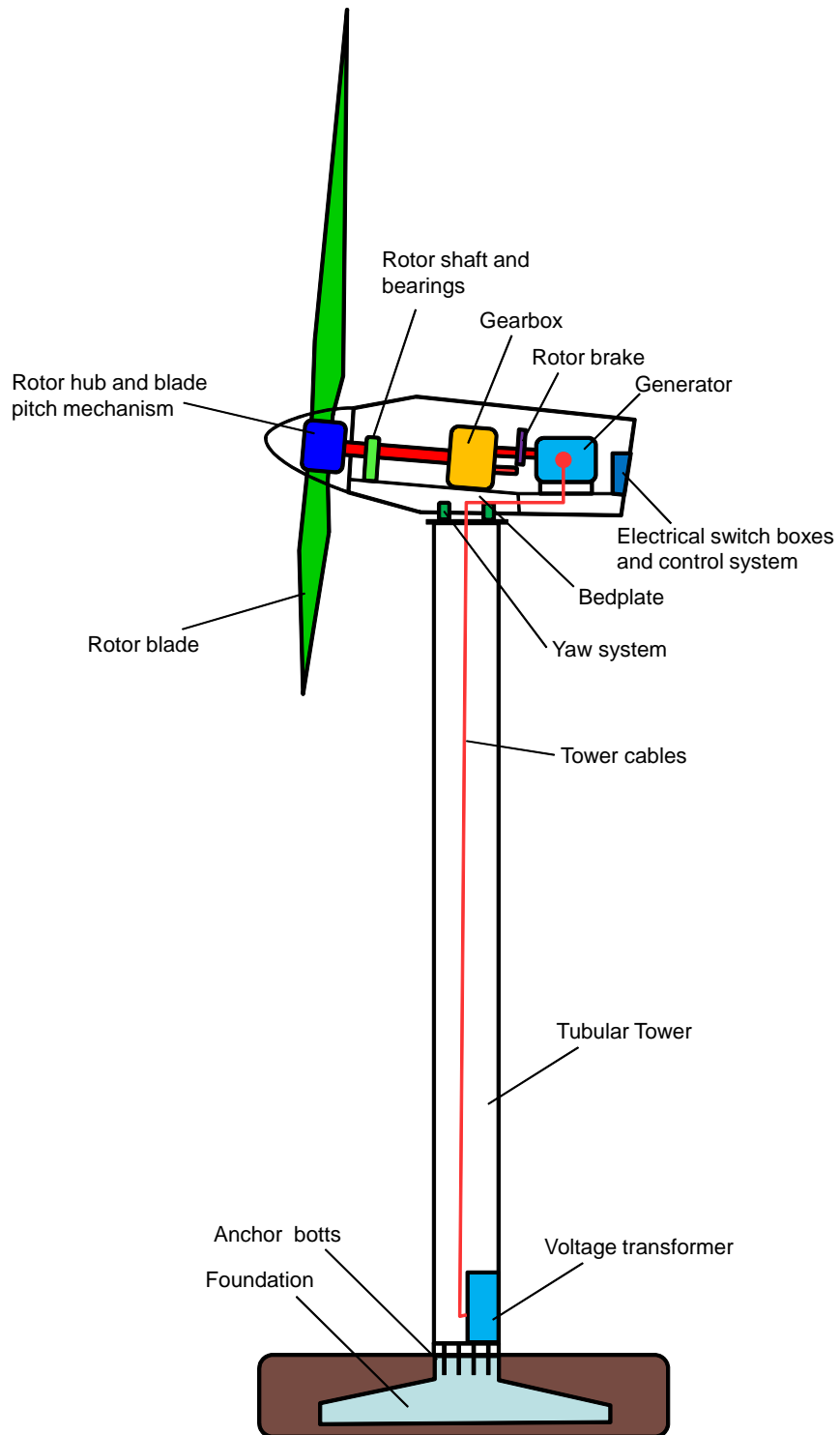


Figure 2.1: Design of an HAWT, schematic

The problem is to find out how much mechanical energy can be abstracted by the airstream with an energyconverter. The mechanical power equates the powerdifference of the airstream before

2.1. FUNDAMENTALS OF THE FUNCTIONALITY OF A HORIZONTAL-AXIS-WINDTURBINE (HAWT)

and after the converter. The mechanical power of the converter can be phrased like this:

$$P = \frac{1}{4} \rho A (v_1^2 - v_2^2) (v_1 + v_2) \text{ (W)}$$

The percentage between the converter mechanical power and the undisturbed airstream is called power coefficient c_p and can be described, considering some conversions, as a function from the velocity percentage $\frac{v_2}{v_1}$:

$$c_p = \frac{P}{P_0} = \frac{\frac{1}{4} \rho A (v_1^2 - v_2^2) (v_1 + v_2)}{\frac{1}{2} \rho v^3 A} = \frac{1}{2} \left| 1 - \left(\frac{v_2}{v_1}\right)^2 \right| \left| 1 + \frac{v_2}{v_1} \right|$$

Figure 2.2 displays the ratio between c_p and $\frac{v_2}{v_1}$ and it can be identified as the “ideal” power coefficient is $\frac{v_2}{v_1} = \frac{1}{3}$. Here c_p has a value of 0.593. This factor was first deduced by Betz and is therefore called the “Betz-Factor”.

This factor means that only 59.3% of the airstream power can convert under optimal requirements (ideal, no losses) into mechanical power [Bur01].

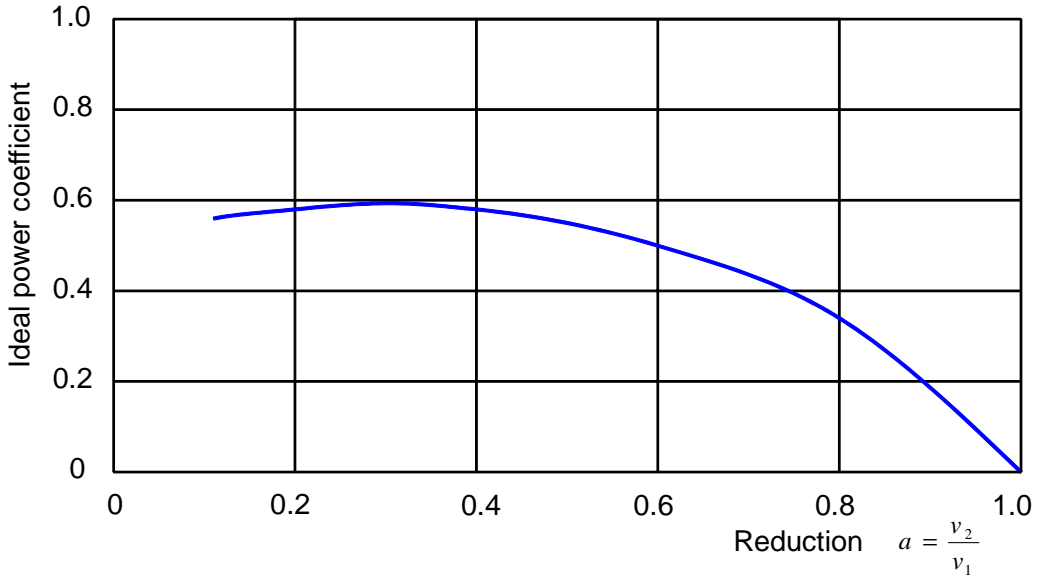


Figure 2.2: Characteristics of c_p over $\frac{v_2}{v_1}$

The Betz-theory gives the ideal limit for the removal of mechanical power from an airstream, impartial of the construction of the converter. In reality the recoverable power cannot be impartial of the characteristics of the converter itself. The HAWT has a lift gaining rotor. The wind velocity v_w overlays vectorial itself with the rotary speed u of the blade (Figure 2.3). The emerging velocity v_t composes with the chordline of the aerodynamic angle of attack (AoA).

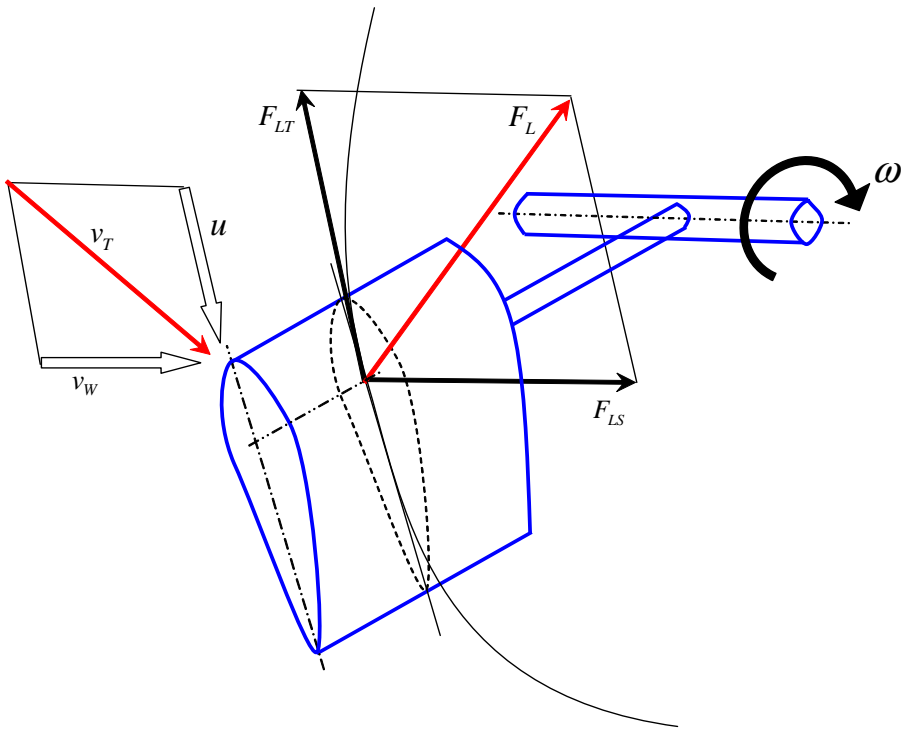


Figure 2.3: Velocities, angles and forces on a rotor element

The aerodynamic force can be differentiated into one component in direction of the approach velocity, the drag F_D , and one component normal to it, the lift F_L . F_L can be divided into F_{LT} , tangential force in the rotation plane and F_{LS} , normal force to the rotational plane. F_{LT} forms the drive moment while F_{LS} is responsible for the rotorthrust. Under normal operation the rotary speed u is much bigger than the wind velocity v_w , so the AoA is small. Note that the F_{LS} component is considerable bigger than F_{LT} . F_{DS} is added also to this resulting thrust force that acts on the structure of the rotor and bends it. Only the comparatively little F_{LT} produces the rotation and resulting from it the mechanical energy for the electric generator.

To sum it up it can be said that of the possible 60% useable windpower the largest part arrives in the deformation of the blade and only a small part in the rotation, the impulse that drives the rotor. It is necessary to optimise this small part as much as possible to emerge the most of the windturbine.

2.2 The blade design

The rotorblades are the only components of a windturbine, that had to be developed in the past completely new. All other components can be taken from other parts out of the engineering field. The building technique bases generally on knowledge out of the aircraft construction. REpower commonly uses blades based on fiber composite materials with two half-shells that are glued

2.2. THE BLADE DESIGN

together. The stabilization achieved by one to three light holmbars. These holmbars consist of GPR laminate with ninety degrees orientated fibers or sandwich-structures and they are the basic supporting components (Figure 2.4).

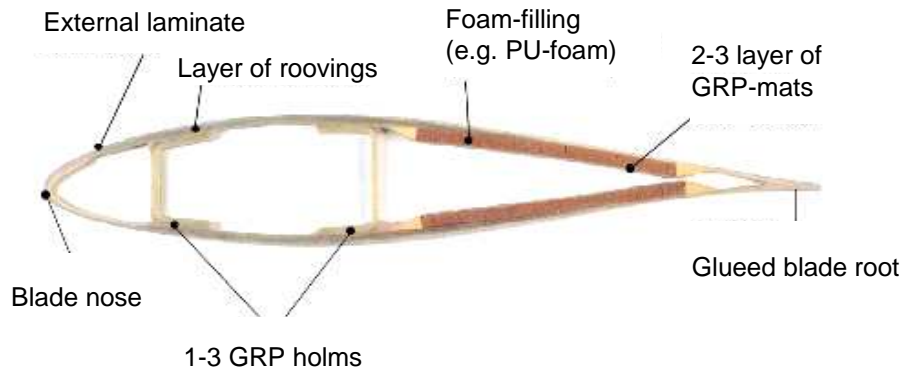


Figure 2.4: Basically blade construction

The 61.5 meter blade, this thesis is based on, has a total number of over 40 different profil types over the hole span. A blade with such a big span weights about 17 to 20 tons, according to the design status. Its maximum chordline length is 4.6 meter and it has an aerodynamic twist in position of the root of ca. 15 degrees. This twist is optimised for the operation condition by a wind of 13.2 m/s, a rotation of 12 rpm and a pitch angle of zero degrees. Than it guarantees optimal approaching flow of the particular profiles. Additional the blade has a prebending of 3 meters at the tip. This prebending allows bigger deflection before the tip enters the security zone near the tower and with this prebending you can build up the blade less more bending stiffer and this saves weight and costs among other things.

In following pictures (Figure 2.6, 2.7, 2.5) are shown screenshots of the Blender model from the NREL- blade.

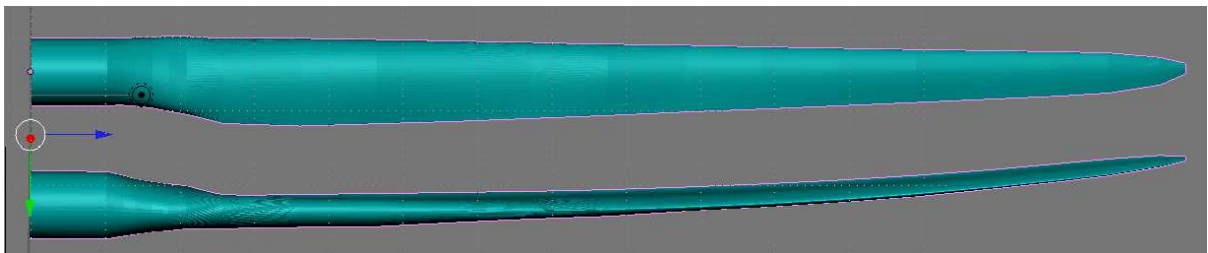


Figure 2.5: NREL-blade

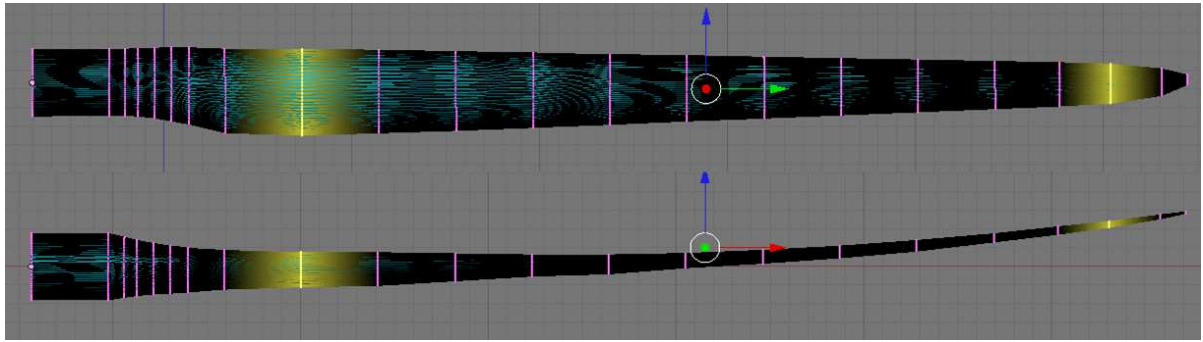


Figure 2.6: Exposure of the NREL-blade 5.2

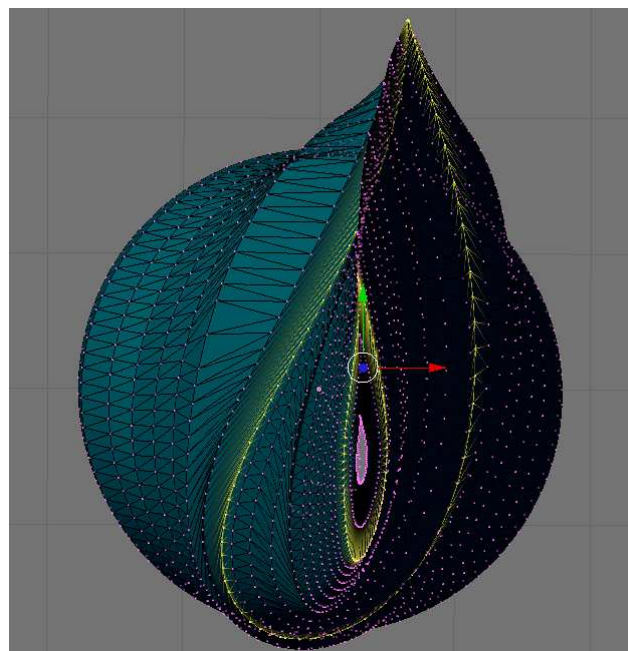


Figure 2.7: Top view of the NREL-blade to display the twist

2.3 Actuator Disc Theory and Momentum Theory

A windturbine extracts mechanical energy from the kinetic energy of the wind. The rotor is a permeable disc in a simple 1-D model.

This disc is considered ideal, i.e. it is frictionless, an infinitely thin disc and there is no rotational velocity component in the wake. The rotor disc acts as a drag device, slowing the wind speed down from U_∞ far upstream of the rotor to U_d at the rotor plane and to U_W in the wake. The disc supports a pressure difference and this decelerates the air through the disc. Therefore the streamlines must diverge as shown in Figure 2.8.

$$\rho A_\infty U_\infty = \rho A_d U_d = \rho A_W U_W$$

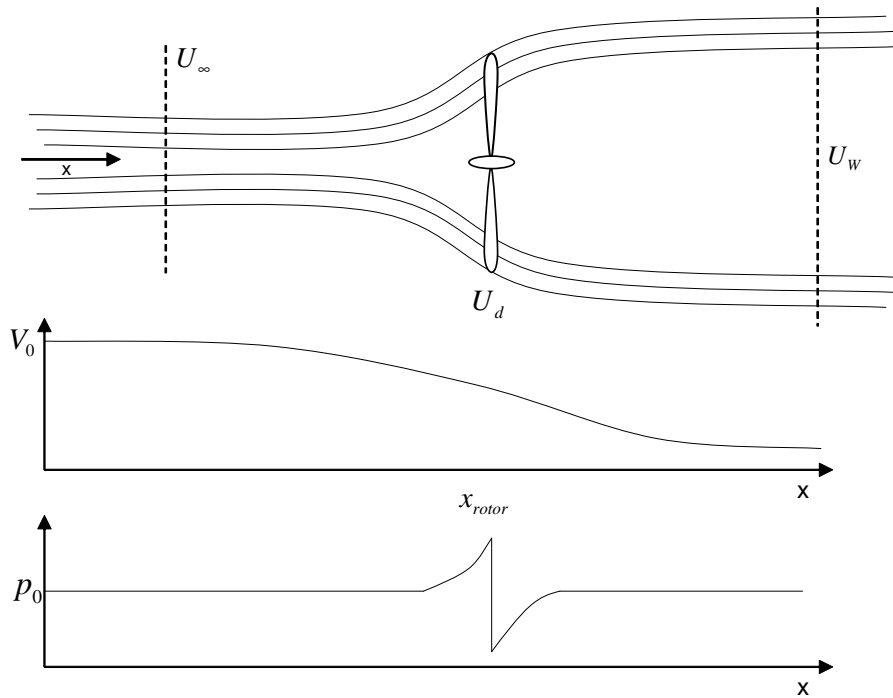


Figure 2.8: Illustration of streamlines behind the rotor and the axial velocity and pressure upstream and downstream of the rotor

The Momentum Theory method uses a momentum balance on a rotating annular stream tube which passes through a turbine. A stream tube around a wind turbine is shown in Figure 2.9. Four stations are shown, 1 way upstream of the turbine, 2 just before the blades, 3 just after the blades and 4 some way downstream of the blades. Between 2 and 3 energy is extracted from the wind and there is a change in pressure as a result.

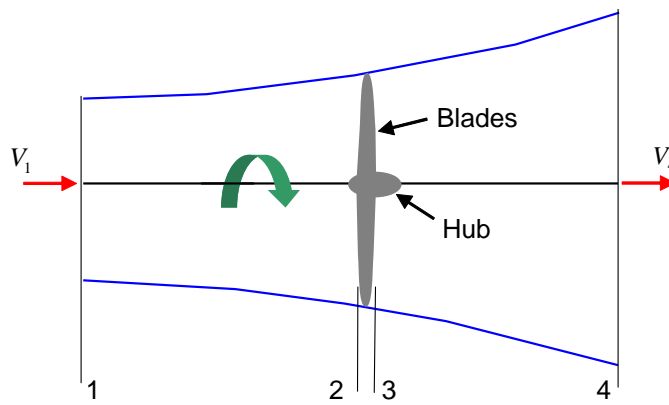


Figure 2.9: Axial Stream tube around a Wind Turbine

With Bernoulli's equation and some algebra the axial force can be measured:

$$p_2 - p_3 = \frac{1}{2}\rho(V_1^2 - V_4^2)$$

2.3. ACTUATOR DISC THEORY AND MOMENTUM THEORY

Note that force is pressure times area:

$$dF_x = (p_2 - p_3)dA$$

$$\Rightarrow dF_x = \frac{1}{2}\rho(V_1^2 - V_4^2)dA$$

Define the axial induction factor a as:

$$a = \frac{V_1 - V_2}{V_1}$$

It can also be shown that:

$$V_2 = V_1(1 - a)$$

$$V_4 = V_1(1 - 2a)$$

Substituting yields and the axial force can be written like this:

$$dF_x = \frac{1}{2}\rho V_1^2 [4a(1 - a)] 2\pi r dr \quad (2.1)$$

The tangential force can be calculated in consideration of conservation of angular momentum in the annular stream tube (Figure 2.10).

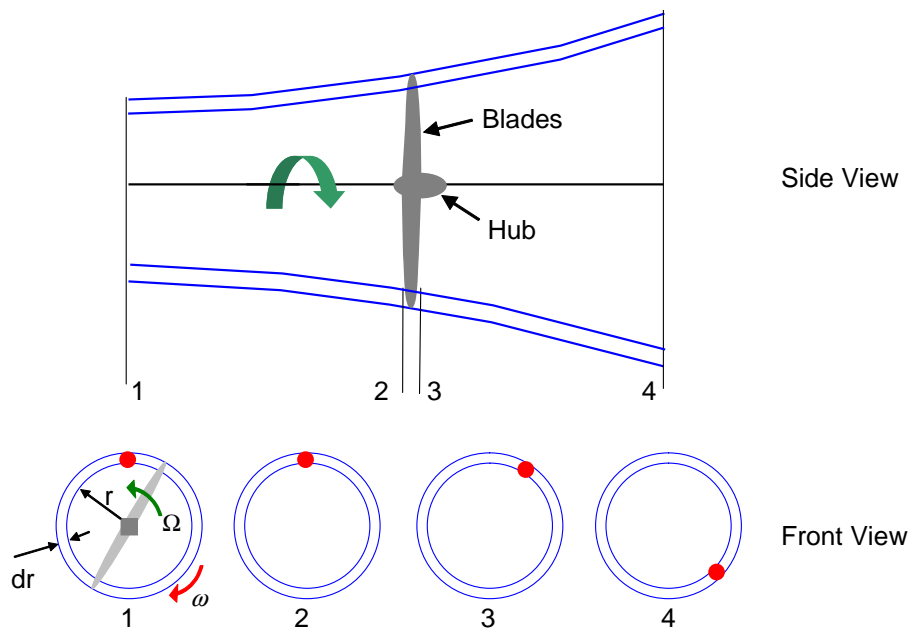


Figure 2.10: Rotating Annular Stream tube

The blade wake rotates with an angular velocity ω and the blades rotate with an angular velocity of Ω . Recall from basic physics that:

2.4. BLADE ELEMENT THEORY

Moment of Inertia of an annulus: $I = mr^2$

$$\text{Angular Moment:} \quad L = I\omega$$

$$\text{Torque:} \quad T = \frac{dL}{dt}$$

$$\Rightarrow T = \frac{dI\omega}{dt} = \frac{d(mr^2\omega)}{dt} = \frac{dm}{dt}r^2\omega$$

For a small element the corresponding torque will be:

$$dT = dm\omega r^2$$

For the rotating annular element

$$dm = \rho AV_2$$

$$dm = \rho 2\pi r dr V_2$$

$$\Rightarrow dT = \rho 2\pi r dr V_2 \omega r^2 = \rho V_2 \omega r^2 2\pi r dr$$

Define angular induction factor a' :

$$a' = \frac{\omega}{2\Omega}$$

Recall that $V_2 = V(1 - a)$ so:

$$dT = 4a'(1 - a)\rho V \Omega r^3 \pi dr \quad (2.2)$$

Formula 2.1 and 2.2 allow the determination of the momentum balance on a rotating annular stream tube passing through a turbine [Hau03, Bur01, Han01].

2.4 Blade Element Theory

The blade element theory (BET) describes the basis of the most modern analyses of rotor blade aerodynamics because it provides estimates of the radial and azimuthal distributions of blade aerodynamic loading over the rotor disk.

Blade element theory relies on two key assumptions:

- There are no aerodynamic interactions between different blade elements
- The forces on the blade elements are solely determined by the lift and drag coefficients

A rotating blade induces on every point across the whole length lift- and dragforces. It is necessary for the loads of a windturbine to know the total forces of a blade. The idea of the BET is to split the whole rotor area in infinite elements. Each blade section acts as a quasi-2-D airfoil to produce aerodynamic forces (and moments). The rotor performance can be obtained by integrating the sectional airloads at each blade element across the length of the blade and averaging the results across the whole rotor area. Considering a blade is divided up into N

2.4. BLADE ELEMENT THEORY

elements with a finite length of dy as shown in Figure 2.11.

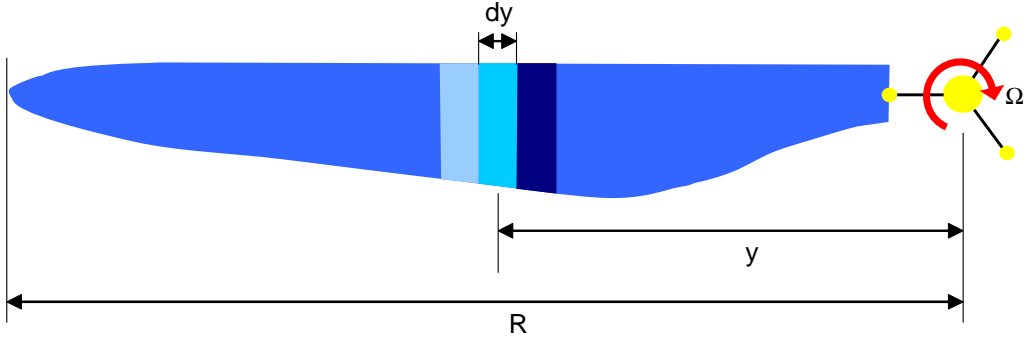


Figure 2.11: Blade element

Each of the blade elements will experience a slightly different flow as they have a different rotational speed (Ω_r), a different chord length (c) and a different twist angle (γ). The entire performance characteristics are determined by numerical integration along the blade span.

The forces on the blade element are shown in Figure 2.12, note the lift and drag forces are by definition perpendicular and parallel to the incoming flow.

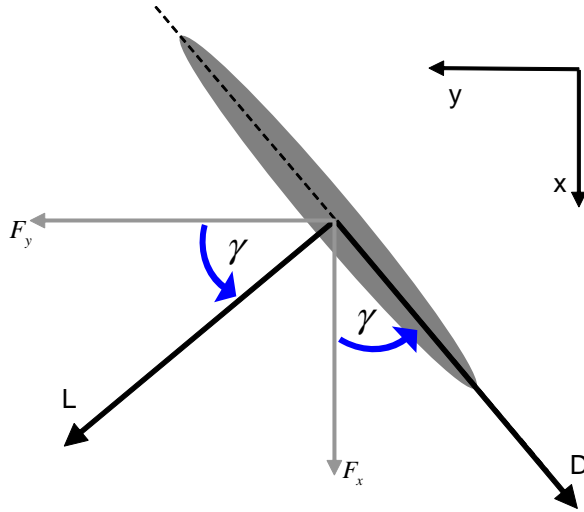


Figure 2.12: Forces on a turbine blade element

For each blade element the forces are:

$$dF_y = dL \cos \gamma - dD \sin \gamma$$

$$dF_x = dL \sin \gamma + dD \cos \gamma$$

where dL and dD are the lift and drag forces on the blade. dL and dD can be found by the definition of the lift and drag coefficients as follows:

$$dL = C_L \frac{1}{2} \rho V^2 c dr$$

$$dD = C_D \frac{1}{2} \rho V^2 c dr$$

If there are N blades the forces and the torque dT on an element shown are like this:

$$dF_x = N \frac{1}{2} \rho V^2 (C_L \sin \gamma + C_D \cos \gamma) c dr \quad (2.3)$$

$$dF_y = N \frac{1}{2} \rho V^2 (C_L \cos \gamma - C_D \sin \gamma) c dr$$

$$dT = N \frac{1}{2} \rho V^2 (C_L \cos \gamma - C_D \sin \gamma) c r dr = dF_y r \quad (2.4)$$

The principles of BET assume no mutual influence of adjacent blade element sections, based on the idealization as 2-D-airfoils.

However the effects of a nonuniform “induced inflow” across the blade (it causes from the rotor wake) is accounted through a modification to the angle of attack (AoA) at each blade element. If this induced velocity can be calculated, or even approximated, then forces and moments acting on the rotor can be readily obtained. This approximation is done with merging the BET together with the Momentum Theory [Bur01, Hau03, Han01].

2.5 Blade Element Momentum Theory (BEMT)

The BEMT combines the basic principles of both, the blade element and momentum theory approaches. The integration of the changed inflow as a result of the induced airmovement or other influences into the BEMT is lightly done.

The BET reveals that for a higher induced velocity the amount of the Lift is going down. Compared to this the MT declares for a lower Lift a lesser induced velocity.

To calculate rotor performance equations 2.3 and 2.4 from a momentum balance are equated with equations 2.1 and 2.2. Once this is done the following useful relationships arise:

$$\frac{a}{1-a} = \frac{\sigma' [C_L \sin \gamma + C_D \cos \gamma]}{4Q \cos^2 \gamma}$$

$$\frac{a'}{1-a} = \frac{\sigma' [C_L \cos \gamma - C_D \sin \gamma]}{4Q \lambda_r \cos^2 \gamma}$$

$$Q = \text{correction factor}, \sigma' = \frac{Nc}{2\pi r}, \lambda_r = \frac{\Omega r}{V}$$

This complex system of equations has to be solved by a numerical procedure.

The combined approach of the BEMT allows to calculate the allocation of the induced velocity, the aerodynamic forces, moments and the influences of wind can be considered.

The BEM theory needs several corrections for the approximation to conditions that are more realistic [Bur01, Han01, Hau03]:

1. Tip and roots effects:

The rotor consists of a finite number of blades and therefore the force applying to the stream cannot be seen as constant over the annulus. These effects can be modelled by Prandlt or more accurately by Goldstein approximation.

2. Turbulent wake State:

For heavily loaded turbines, the vortex structure disintegrates and the wake becomes turbulent and, in doing so, entrains energetic air from outside the wake by a mixing process. This is the turbulent wake state. Thus, the axial induction factor has to be replaced by an empirical relation. Anderson's, Garrad Hassan's, Glauert's, Johnson's and Wilson's can be used according to it.

3. Dynamic Inflow:

Load situation is changing continuously (wind velocities fluctuation and pitch control of the blades) the “wake” time between two stable states is approximate to a first order system.

4. Dynamic stall:

During the wind turbine runtime, the aerodynamic stall can change the coefficients C_L and C_D behaviour. The linear evolution of these coefficients (observable during static mode) is replaced by an hysteresis loop measured empirically.

5. 3D correction:

Important for stall regulated wind turbines.

2.6 A description of the aeroelastic instabilities

The worst aeroelastic instability is classical flutter. Here the first torsional blade mode couples to a flapwise bending mode in a flutter mode through the aerodynamic forces. The change of AoA due to torsion changes the lift in an unfavorable phase to the flapwise bending (Figure 2.13). The flutter mode has highly negative damping which cannot be compensated by structural damping.

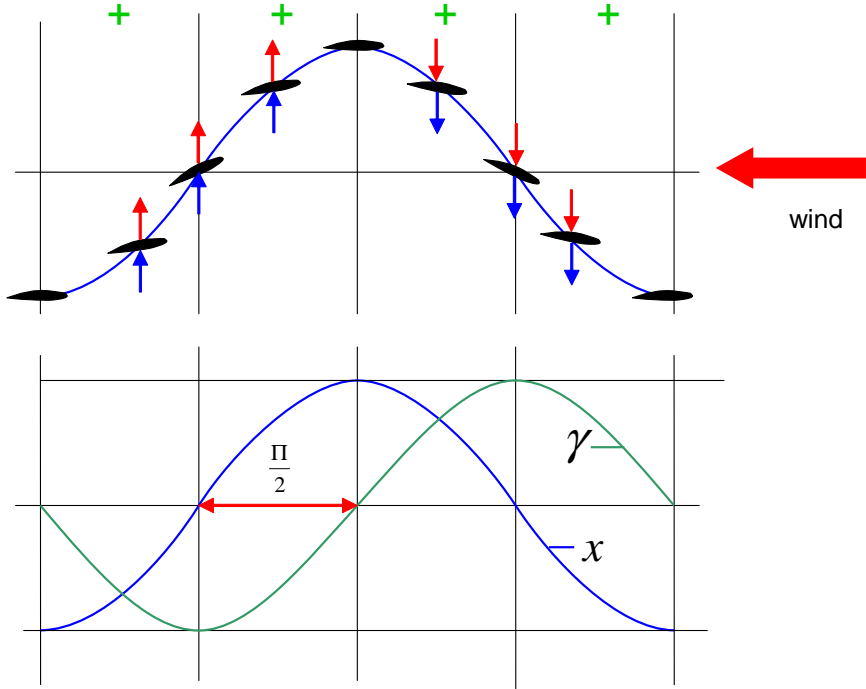


Figure 2.13: Fluttereffect

To understand the instability mechanism of classical flutter, it is sufficient to consider a typical blade section with two degrees of freedom (Figure: 2.14) subjected to quasi-steady aerodynamic lift without apparent mass terms. The inflow to the airfoil is presumed parallel to the chord. The flapwise translation of the airfoil $h(t)$ is presumed perpendicular to the inflow and the torsional rotation $\phi(t)$ about a chord point in the distance ca_{CG} in front of the center of gravity (CG) on the chord. The section is subjected to aerodynamic lift L at the aerodynamic center (AC) in the distance ca_{AC} in front of the torsional point.

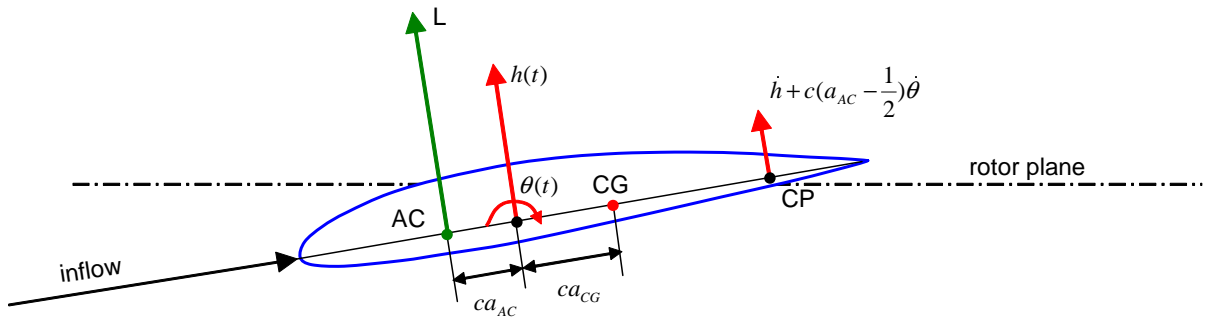


Figure 2.14: A typical blade section with two degrees of freedom

The linear equations of motions can be derived as:

$$m\ddot{h} - mca_{CG}\ddot{\theta} + k_f h = L \quad (2.5)$$

$$-mca_{CG}\ddot{h} + mc^2(r_{CG}^2 + a_{CG}^2)\ddot{\theta} + k_t \theta = ca_{AC}L \quad (2.6)$$

where m is the mass per unit-length of the section, r_{CG} is the radius of gyration about CG normalized with the chord length c , and k_f and k_t are the flapwise and torsional stiffnesses.

Neglecting apparent mass terms, the quasi-steady aerodynamic lift L per unit-length is:

$$L = \frac{1}{2}\rho c V^2 C_L(\alpha) \quad (2.7)$$

where ρ is the air density, V is the relative speed, α is the AoA, and C_L is the lift coefficient at α . To capture the effects of torsional velocity $\dot{\theta} \neq 0$ on the AoA, it is computed at the collocation point (CP) in the three-quarter chord. The relative speed and the AoA are therefore (noting that the inflow is presumed parallel to the chord):

$$\begin{aligned} V &= \sqrt{V_0^2 + \dot{h}^2} \text{ and} \\ \alpha &= \arctan\left(\frac{V_0 \sin\theta - \dot{h} - c(\frac{1}{2} - a_{AC})\dot{\theta}}{V_0 \cos\theta}\right) \end{aligned} \quad (2.8)$$

where V_0 is the steady state relative speed of the inflow. Substitution into aerodynamic lift L and linearization about $\phi = h = \dot{\phi} = 0$ leads to the linear approximation to the lift:

$$L \approx L_0 + \frac{1}{2}c\rho V_0^2 C'_L[\theta - \frac{\dot{h}}{V_0} - (\frac{1}{2} - a_{AC})\frac{c\dot{\theta}}{V_0}] \quad (2.9)$$

where the lift coefficient and its derivative $C'_L = \frac{dC_L}{d\alpha}$ are evaluated at $\alpha_0 = 0$, which for the thin airfoils is $C'_L = 2\pi$. The steady state lift L_0 may change the steady state equilibrium of the section, but it has no influence on the stability of this equilibrium.

Neglecting the camber of the airfoil the steady state lift is zero and the linear equations of motions with the linear lift can be written as:

$$M\ddot{x} \times C\dot{x} \times Kx = 0 \quad (2.10)$$

where the vector $x = \left\{ \frac{h}{c}, \phi \right\}^T$ contains non-dimensional degrees of freedom. The structural mass, aerodynamic damping, and aeroelastic stiffness matrices are

$$M = \begin{bmatrix} 1 & -a_{CG} \\ -a_{CG} & r_{CG}^2 + a_{CG}^2 \end{bmatrix}$$

$$C = \frac{c\kappa}{V_0} \begin{bmatrix} 1 & \frac{1}{2} - a_{AC} \\ a_{AC} & a_{AC}(\frac{1}{2} - a_{AC}) \end{bmatrix}$$

$$K = \begin{bmatrix} \omega_f^2 & -\kappa \\ 0 & r_{CG}^2\omega_t^2 - \kappa a_{AC} \end{bmatrix}$$

where $\omega_f = \sqrt{\frac{k_f}{m}}$ and $\omega_t = \sqrt{\frac{k_t}{(mc^2r_{CG}^2)}}$ are the natural frequencies of the flapwise and torsional modes without inertia coupling and $\kappa = \frac{\rho}{2m}V_0^2C'_L$ is aerodynamic stiffness depend on the air-section mass ratio $\frac{\rho}{m}$, the relative speed V_0 , and the lift gradient C'_L .

For high relative inflow speed V_0 and moderate frequencies of section vibrations ω as for the wind turbine blades, the reduced frequency is small $k = \frac{c\omega}{2V_0} \ll 1$. Hence the elements of the aerodynamic damping matrix C is an order smaller than the aerodynamic stiffness elements of the aerodynamic stiffness matrix K describing the lift change due to rotation of the section given by the torsion ϕ . Furthermore the aerodynamic damping matrix is positive semi-definite $C \geq 0$ if the aerodynamic center lies within the airfoil. These small, purely dissipative aerodynamic forces are similar to material damping forces and influence on the accurate predictions of flutter mechanism. Dissipative forces may have a destabilizing effect on systems other than non-gyroscopic, conservative systems, but such an effect is assumed to be quantitative for the present circulatory system.

Neglecting the aerodynamic damping matrix $C = 0$ and inserting the solution $x = ve^{\lambda t}$ into, leads to the eigenvalue problem

$$(\lambda^2 M + K)v = 0 \quad (2.11)$$

Non-trivial solutions of this problem require that it is singular, i.e., the determinant of $\lambda^2 M + K$ is zero leading to the characteristic equation:

$$r_{CG}^2\lambda^4 + ((r_{CG}^2 + a_{CG}^2)\omega_f^2 + r_{CG}^2\omega_t^2 - \kappa(a_{AC} + a_{CG}))\lambda^2 + \omega_f^2(r_{CG}^2\omega_t^2 - \kappa a_{AC}) = 0 \quad (2.12)$$

Its zeros are the eigenvalues of the eigenvalue problem, which generally are complex $\lambda = \beta + i\omega$. If the real part of the one eigenvalue is positive then the equilibrium of the section is unstable, because the solution $x = ve^{\lambda t} = ve^{\beta t}(cos\omega t - isin\omega t)$ in this case will grow exponentially in time. Stability limits for the section are therefore defined by the parameters where the real part of an eigenvalue becomes positive. The Routh-Hurwitz criteria states that the real part of all zeroes of the characteristic equation are negative if its coefficient are positive:

$$(r_{CG}^2 + a_{CG}^2)\omega_f^2 + r_{CG}^2\omega_t^2 - \kappa(a_{AC} + a_{CG}) > 0 \text{ and}$$

$$r_{CG}^2\omega_t^2 - \kappa a_{AC} > 0 \quad (2.13)$$

On the limit of the first criterion, there is one complex eigenvalue with a positive real part, because the characteristic equation corresponds $\lambda^4 = -\gamma^2$ (γ is a real constant) if the second criterion is satisfied. The non-zero imaginary part of this complex eigenvalue shows that the instability is oscillatory, hence this criterion defines the flutter limit of the section as

$$\frac{\rho}{2m} V_0^2 C'_L < \omega_f^2 \frac{r_{CG}^2 + a_{CG}^2}{a_{AC} + a_{CG}} + \omega_t^2 \frac{r_{CG}^2}{a_{AC} + a_{CG}} \text{ for}$$

$$a_{AC} + a_{CG} \geq 0 \quad (2.14)$$

where the aerodynamic stiffness κ has been inserted. This inequality must be turned for $a_{AC} + a_{CG} < 0$. The second criterion in RH defines the divergence limit of the section as

$$\frac{1}{2} c \rho V_o^2 C'_L c a_{AC} < k_t \quad (2.15)$$

where κ and ω_t has been inserted. On this limit, the structural and aerodynamic torsional stiffnesses (lower right element of K) cancel out. Beyond this limit, an increase in torsion will increase the lift which again increases the torsion, leading to divergence.

The simple analytical expression of the flutter limit in equation 2.14 derived from the simple typical section model confirms the main criteria for the risk of flutter. The flutter may occur under attached flow conditions $C'_L > 0$ if the air-mass ratio represented by $\frac{\rho}{m}$, and the tip speed represented by V_0 , are sufficiently high for the aerodynamic forces to overcome the dynamic elastic forces represented by the uncoupled flapwise and torsional factors $\frac{r_{CG}^2 + a_{CG}^2}{a_{AC} + a_{CG}}$ and $\frac{r_{CG}^2}{a_{AC} + a_{CG}}$ that may go to infinity if the center of gravity lies in the aerodynamic center ($a_{AC} + a_{CG} < 0$) then the turned inequality will always be satisfied for attached flow C'_L , which is why mass added to leading edges of aircraft wings is a practical solution to flutter problems.

All flutter speed limits have a vertical asymptote when the center of gravity lies at the aerodynamic center. The flutter speeds reduce as the center of gravity is moved aft on the section which is directly related to the coupling factor $\frac{r_{CG}^2}{a_{AC} + a_{CG}}$ on the uncoupled torsional frequency ω_t in equation 2.14. The coupling factor on the uncoupled frequency ω_f has a minor effect because the torsional frequency is three times higher. Hence the main reduction in flutter speed as the center of gravity is moved aft is due to the increased flapwise-torsional coupling. However a part of the flutter speed reduction is due to the decreased torsional frequency as the moment of inertia about the torsional point increases for increasing distance to the center of gravity.

Another characteristic of flutter is that the lowest damping of the modes suddenly becomes negative as the flutter modes arises. The critical speed range is small which has given pilots a fatal surprise in the early days of aviation . This narrow critical speed range also leads to the question

if a blade on a wind turbine running at nominal rotor speed but with large yaw misalignment in high winds can experience flutter on the part of the azimuth rotation where its blades meet the incoming wind leading to a higher relative speed [Han07, Bur01, Lob04, Lob05, Lei06].

2.6.1 Determination between blades with a risk of flutter and those without

The determination can be encountered by getting a closer view in the aerodynamic and structural details of a rotor blade. Also a differentiation of the operation mode makes sense. The two types of aeroelastic instabilities for modern commercial wind turbines are stall-induced vibrations mostly on stall-regulated wind turbines and the classical flutter on pitched-regulated wind turbines. This thesis only regards wind turbines that are pitched-regulated, based on the fact that pitch regulating is a standard today especially on multi-MW-windturbines. On this big constructions the pitch system is also used as an aerodynamic brake while the mechanical brake is only used to fix the rotor for maintenance.

From further studies it is assumed that a wind turbine may have the risk of flutter if the following main criteria come true [Han07]:

1. Attached flow: The flow over the blade must be attached to ensure that nose-up (towards stall) blade torsion leads to increased lift. This criteria shows that flutter may only become a problem for pitch-regulated turbines, for which the blades are operating below stall.
2. High tip speeds: The relative speed of the attached flow must be sufficiently high to ensure sufficient energy in the aerodynamic forces. This appears if the tip speed of pitched-regulated and variable speed windturbines are increased. Although the tip speed is limited by noise and load requirements.
3. Low stiffness: The natural frequencies of a torsional mode and a flapwise bending mode must be sufficiently low for them to couple in a flutter mode.
4. Aft center of gravity: The center of mass in the cross-sections on the outboard part of the blade must lie aft the aerodynamic center to ensure the right phasing of the flapwise and torsional components of the flutter.

Other parameters such as the air-blade mass ratio, blade aspect ratio, material damping and structural bending-torsion couplings (elastic and shear center positions) influence the flutter limit as well but the listed criteria are the fundamental ones.

In Figure 2.15 is given as an example for point four the positions of the different centers over the blade radius from an 61.5 meter NREL (National Renewable Energy Laboratory)-Blade (Section: 5.2).

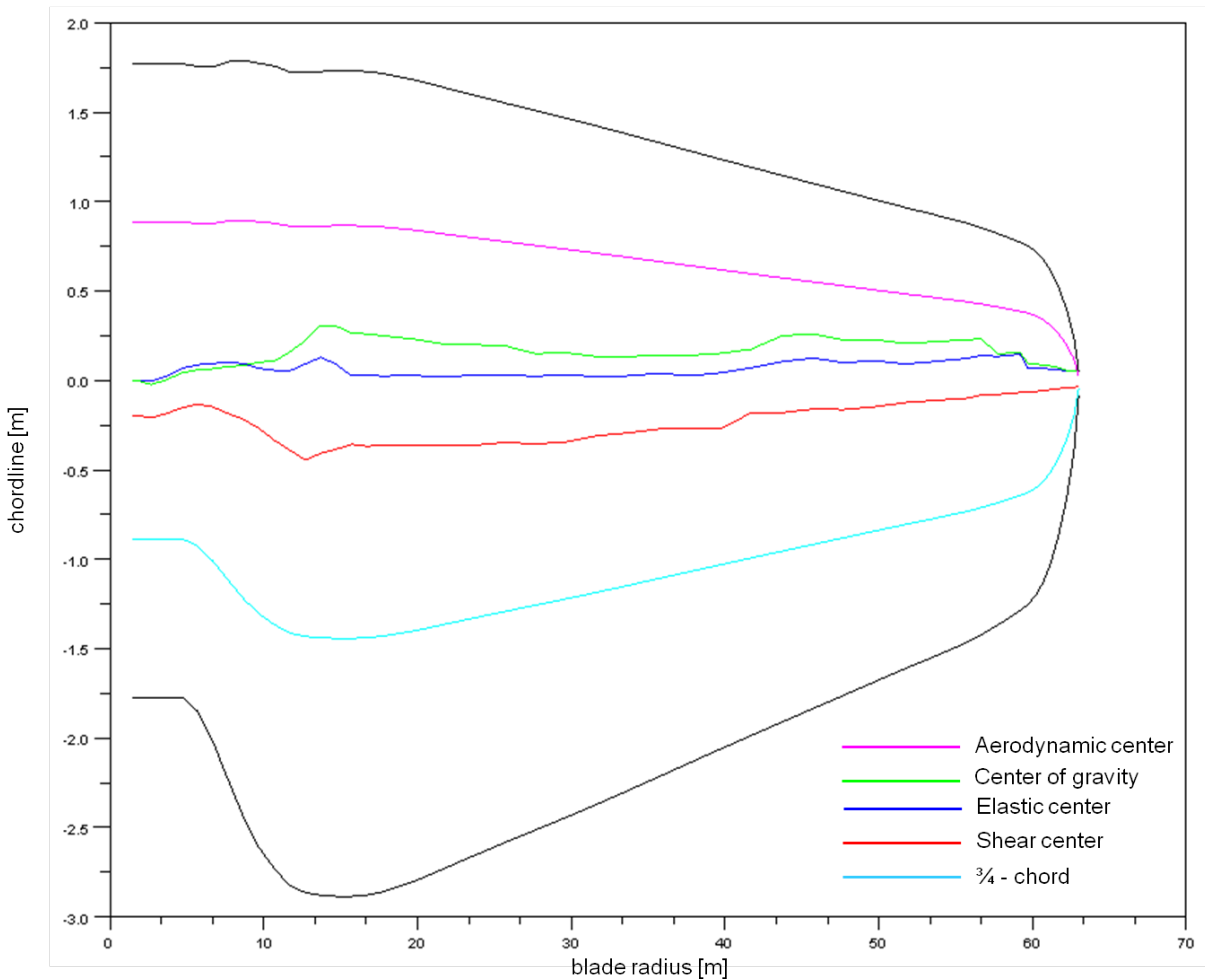


Figure 2.15: Positions of the different centers over the blade radius of the 61.5 NREL-blade

Next to classical flutter are stall-induced vibrations one of the main mechanisms that may lead to aeroelastic instabilities of three blades turbines with negative damping of an aeroelastic mode. But note that classical flutter is a much more violent instability than stall-induced vibrations. The three parameters that dominate the risk of stall-induced vibrations are:

- Airfoil characteristic: If the blades have airfoils with abrupt stall characteristics, the risk of stall-induced vibrations is larger for the rotor
- Direction of vibration: Dependent on the airfoil characteristic, there are directions of blade vibrations relative to the rotor plane where the risk of stall-induced vibrations is larger. Directions of blade vibrations depend on the entire turbine dynamics
- Structural damping: If a turbine mode has a slightly negative aerodynamic damping due to stall-induced vibrations it may be compensated by structural damping.

To understand the instability mechanism of stall-induced vibrations, it is sufficient to consider a typical blade section with one degree of freedom, subjected to quasi-steady aerodynamic forces as illustrated in Figure 2.16. The translation of the airfoil $x(t)$ is defined by the direction of vibrations ϕ relative to the rotor plane.

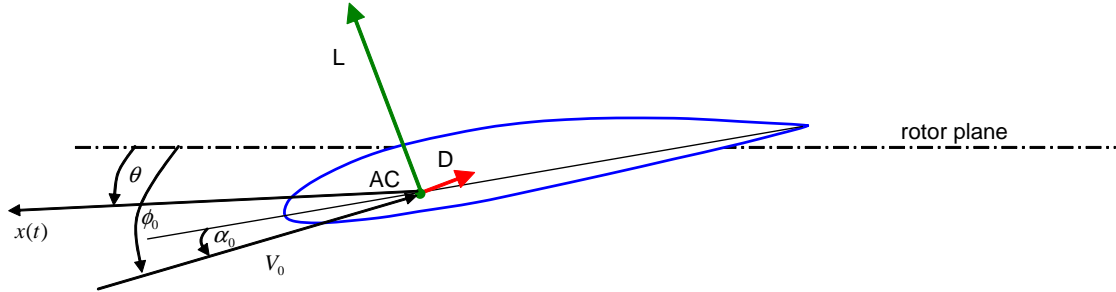


Figure 2.16: A typical blade section with one degree of freedom

The quasi-steady aerodynamic forces L and D per unit-length can be determined for the steady state inflow angle ϕ_0 and the relative speed V_0 , and the steady state angle of attack α_0 as follows:

$$L = \frac{1}{2}\rho cV^2 C_L(\alpha) \text{ and}$$

$$D = \frac{1}{2}\rho cV^2 C_D(\alpha) \quad (2.16)$$

where C_D is the drag coefficient evaluated at α . The relative speed and the AoA are functions of the velocity of the blade section:

$$V = \sqrt{(V_0\cos\phi_0 + \dot{x}\cos\theta)^2 + (V_0\sin\phi_0 + \dot{x}\sin\theta)^2} \quad (2.17)$$

$$\alpha = \phi - \phi_0 + \alpha_0$$

where ϕ is the inflow angle relative to the rotor plane:

$$\phi = \arctan \left(\frac{V_0\sin\phi_0 + \dot{x}\sin\theta}{V_0\cos\phi_0 + \dot{x}\cos\theta} \right) \quad (2.18)$$

Projection of the aerodynamic forces onto the direction of the vibration leads to the force:

$$F_x = \frac{1}{2}\rho cV^2 C_L(\alpha)\cos(\phi - \theta) - \frac{1}{2}\rho cV^2 C_D(\alpha)\sin(\phi - \theta) \quad (2.19)$$

Substitution of the flow variables (2.17) and (2.18) into this expression, it is seen that the aerodynamic force is a function of the velocity \dot{x} as the only independent variable.

Linearization of the aerodynamic force (2.19) using Taylor expansion about $\dot{x} = 0$ leads to the approximation $F_x \approx F_0 - \eta\dot{x}$, where the coefficient is given by:

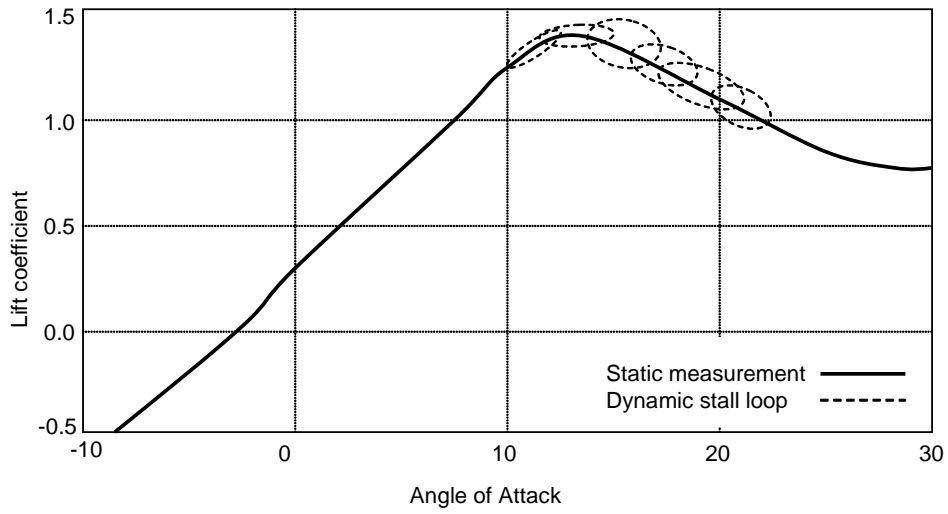
$$\eta = \frac{1}{2}\rho c V_0 \left[C_D(3 + \cos(2\theta - 2\phi_0)) + C'_L(1 - \cos(2\theta - 2\phi_0)) + (C_L + C'_D)\sin(2\theta - 2\phi_0) \right] \quad (2.20)$$

where the lift and drag coefficients and their gradients $C'_L = \frac{dC_L}{d\alpha}$ and $C'_D = \frac{dC_D}{d\alpha}$ are evaluated at $\alpha = \alpha_0$. The coefficient in 2.20 corresponds to the damping coefficient of a viscous damping term approximating the aerodynamic forces in the equation of motion for $x(t)$. If this aerodynamic damping coefficient is negative, the aerodynamic forces add energy to vibration of the blade section, whereby its steady state position becomes unstable if the amount of structural damping is insufficient to dissipate this energy.

Several fundamental statements can be deduced from the aerodynamic damping coefficient (2.20) which characterizes the instability mechanism behind stall-induced vibrations:

- The aerodynamic damping is proportional to the relative speed of the steady state inflow V_0 , and not to the square of the relative speed as the aerodynamic forces.
- The first term in brackets shows that drag always increases the aerodynamic damping because the coefficient to C_D is always positive $3 + \cos(2\theta - 2\phi_0) \geq 0$. This effect is largest for vibrations parallel to the inflow ($\theta - \phi_0 = 0$) because it is related to variations in relative velocity.
- The second term in brackets shows that a negative lift gradient decreases the aerodynamic damping because the coefficient to C'_L is positive, or zero $1 - \cos(2\theta - 2\phi_0) \geq 0$. This destabilizing effect is largest for vibrations perpendicular to the inflow ($\theta - \phi_0 = \pm\frac{\pi}{2}$) because it is related to variations in AoA.
- The third term in brackets shows that the positive lift and drag gradient of airfoils in normal operation decreases the aerodynamic damping for directions of vibrations in the 2nd and 4th quadrants relative to the inflow ($\frac{\pi}{2} < \theta - \phi_0 < \pi$ and $-\frac{\pi}{2} < \theta - \phi_0 < 0$).

A special case of stall induced vibrations called dynamic stall and is often found by stall regulated windturbines. It happens when a flow over an airfoil is stalled but not fully seperated (not in deep stall) then a dynamic stall effect will cause the lift to momentarily increase after a step change in AoA, whereafter it will decrease to the static value at the new AoA. This dynamic stall effect means that the dynamic lift of an oscillating airfoil will loop around the static lift curve as shown in Figure 2.17 [Han07].


 Figure 2.17: Dynamic stall loops in a C_L - α diagram

2.7 Theodorsen's Theory

Theodorsen's theory forms one root for many of the unsteady aerodynamic solution methods used for rotor blade analysis. The problem of finding the airloads on an oscillating airfoil was first tackled by Glauert (1929), but was properly solved by Theodorsen (1935). Theodorsen's model is based on a harmonically oscillated airfoil in a 2-D, inviscid, incrompressible flow (Figure 2.18). It describes the influence of the shed vortex wake to the loads of the airfoil.

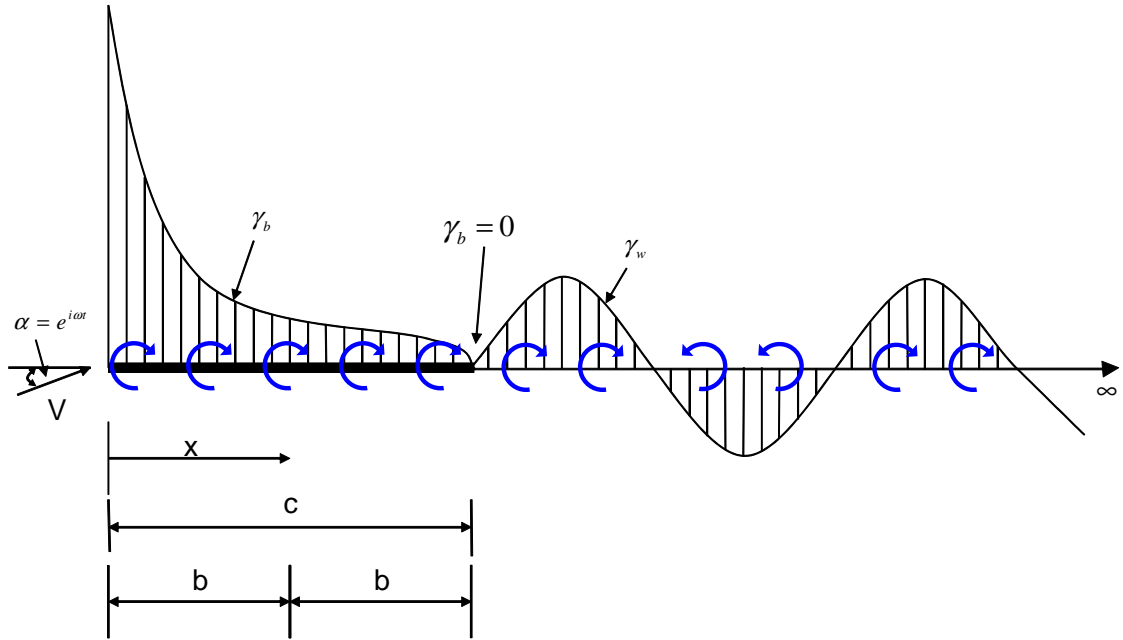


Figure 2.18: Mathematical model used by Theodorsen

For a general motion of pitching ($\alpha, \dot{\alpha}$) and plunging (h) Theodorsen gives for the lift and corresponding moment about the mid chord:

$$L = \pi \rho V^2 b \left[\frac{b}{V^2} \ddot{h} + \frac{b}{V} \dot{\alpha} - \frac{b^2}{V^2} \alpha \ddot{\alpha} \right] + 2\pi \rho V^2 b \left[\frac{\dot{h}}{V} + \alpha + \frac{b \dot{\alpha}}{V} \left(\frac{1}{2} - a \right) \right] C(k)$$

$$M_{\frac{1}{2}} = -\rho b^2 \left[\pi \left(\frac{1}{2} - a \right) V b \dot{\alpha} + \pi b^2 \left(\frac{1}{8} + a^2 \right) \ddot{\alpha} - \alpha \pi b \ddot{h} \right] + 2\rho V b^{2\pi} \left(a + \frac{1}{2} \right) \left[V \alpha + \dot{h} + b \left(\frac{1}{2} - a \right) \dot{\alpha} \right] C(k)$$

a = pitch axis location rel. to the mid-chord

$C(k)$ = Theodorsen's function

The first set of terms in equitation for the lift and the moment results from flow acceleration effects. The second terms arise from the creation of circulation about the airfoil. The Theodorsen function $C(k) = F(k) + iG(k)$ is complex with the reduced frequency k as the argument, which accounts for the effects of the shed wake on the unsteady airloads ([Sne04, Lei06, The34]).

These effects can be divided into four parts:

1. an effective angle of attack resulting from relative motion of the airfoil with respect to an inertial system
2. an induction part, related to the time varying shed vorticity wake of the section
3. Solution of the Laplace equation (incompressible flow) with modified boundary conditions due to 1. and 2. for velocity field
4. Determination of the pressure distribution (and resulting forces) through the unsteady form of the Bernoulli equitation, containing the time derivative of the velocity potential, which is the flow inertia term

Lobitz [Lob04] has investigated the flutter limit of a MW-sized wind turbine blade based on isolated blade stability analysis using quasi-steady and unsteady (Theodorsen) aerodynamics. He showed that the predicted flutter speed of the blade using quasi-steady aerodynamics is lower than the flutter speed obtained using unsteady aerodynamics. This increased flutter speed of the

latter is caused by the decreased effective of the lift curve, when the induced velocities from the shed vorticity are included in the modeling of the unsteady aerodynamic forces (Figure 2.19).

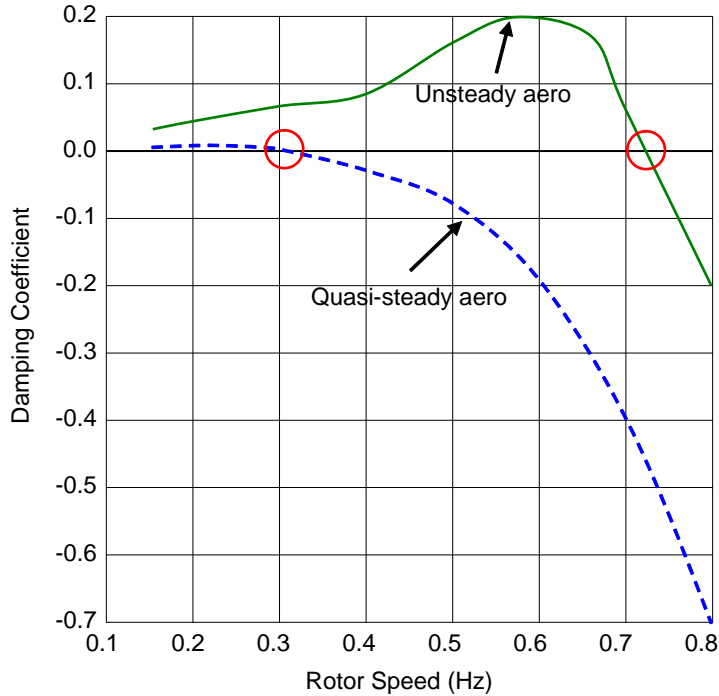


Figure 2.19: Damping coefficient of the flutter mode versus rotor speed for unsteady and quasi-steady aerodynamics [Lob04]

2.8 Simulations Tools

Considering the background of future rising of technology and certification legal requirements concerning the accuracy and the degree of detail of the used programs and models for dynamic simulations of wind turbines, REpower has to find new software solutions in order to meet these increased requirements. With the programs FLEX5® and BLADED®, presently used by REpower, many of the physical phenomena and interactions which have to be considered in the future can not be represented. Besides commercial systems like SAMCEF® for Windturbines, LMS.VirtualLab®, SIMPACK®, to name only a few, there also exists a very promising free OpenSource alternative, called MBDyn, which was developed and published by the aero-space institute at the Polytechnical University of Milan. There the software is used for aero-elastic simulations of helicopters among other applications. REpower wants to supplement his pool of dynamic simulation tools with MBDyn® and will so be prepared for the future challenge.

2.8.1 FLEX5®

In the department Loads and System-Simulation of REpower the multi-body simulation software FLEX5® is used so far for load simulations and certification.

FLEX5® was developed solely for the analysis of wind turbines with 1 to 3 rotor blades. FLEX5® is written by Stig Øye a Danish scientist of the Technical University of Denmark. Whereas FLEX5® does not have any support by Stig Øye, but the user can modify the source code for his purposes individually. Because of the ability of further individual development of the source code FLEX5® is popular in the wind energy sector.

FLEX5® uses a combination of modal analysis and FE modelling. Input data is given in segments for the blades, the tower and the foundation to establish a beam model for the components. The hub and the nacelle are ridged bodies with a certain mass and inertia. The shaft is considered as a flexible rotational body, which is allowed to twist. Inertia can be defined to the generator and any torque and speed characteristic is possible. During the model setup the mass and the stiffness matrices of the windturbine are reduced to modal degree of freedom. A maximum of two mode shapes per direction of motion is used. The reduction is initially applied to the isolated substructures. The used method is the static reduction. The entire mass matrix is fully defined and the stiffness matrix shows a diagonal shape. There are only coupling effects due to the inertias between the single substructures. This kind of modelling a wind turbine automatically yields to a diagonal shaped stiffness matrix. Damping is introduced afterwards as Rayleigh β -damping and therefore the damping matrix obtains a diagonal shape too. In total 28 DOF are used to characterise the wind turbine. They are related to different coordinate systems.

The aerodynamic model of FLEX5® is mainly based on the fast BEMT theory. The accuracy of the results is primary connected to the quality of the 2-dimensional airfoil data. The model is improved with some empirical corrections for the rotor. A dynamic stall effect based on one parameter, a dynamic wake model including dynamic inflow, the yaw correction of Glauert and the tip correction of Prandtl are used to improve the aerodynamic representation. Aerodynamic drag is considered on the hub, the nacelle and the tower. The tower shadow effect is included. This effect cannot be calculated with the BEM model. Therefore the potential flow theory is taken. The effective wind velocity is computed by a combination of mean wind speed, a wind gradient, 3-dimensional turbulences and the deformation speeds of the structure. Furthermore the direction of the wind can be adjusted.

2.8.2 Multibody-Dynamics-Simulation-Software MBDyn

MBDyn is the first and possibly the only free general-purpose MultiBody Dynamics analysis software. It has been developed at the Dipartimento di Ingegneria Aerospaziale of the University "Politecnico di Milano", Italy. MBDyn features the integrated multidisciplinary analysis of multibody, multiphysics systems, including nonlinear mechanics of rigid and flexible constrained

2.8. SIMULATIONS TOOLS

bodies, smart materials, electric networks, active control, hydraulic networks, essential fixed-wing and rotorcraft aerodynamics. MBDyn is especially interesting under cost-specific aspects, as it may be used free and company-wide with an arbitrary number of copies/processes and without any limitation. Compared to the licence costs of commercial systems in the range of 20.000 - 50.000 Euro (depending on the system) for a single full-featured licence and multiplied by the anticipated total amount of licences at REpower, cost-savings in a range of 50.000 - 500.000 Euro seem to be realistic. Gathering and protection of REpower knowledge beyond this, the approach of having a system with an open source code conforms with the philosophy of the Loads and System-Simulation department at REpower as only under this assumption it can be assured that a complete and deep understanding of the software and therefore of the created results will be achieved and only with an OpenSource code implementations of own developments and knowledge can be realized short-timed and in-house and thus preventing the loss of REpower knowhow.

MBDyn has got his own modeling syntax and is an absolute console application, so the output and the input are textual and there is no graphic interface or graphic output. It consists of a comprehensive element library, a collection of linear and nonlinear solvers and comes with an aerodynamic, that bases on the BEMT.

The main differences to FLEX5[®] are:

- Freedom in Model-Creation: Any mechanical / structural model can be designed
 - No longer fixed model topology with DOFs that can be switched ON/OFF and which are fixed in their physical representation inside the model.
 - A model can vary in size (Num of DOFs) and thus the calculation time
- No Modal Approach but MultiBody-System Approach
 - Model build of Nodes + Joints, RigidBodies + Beams, Forces + Couples, etc.
 - More detailed representation of components possible with realistic deformation modes; idealisation or simplifications for deformation not needed but possible.
- Sophisticated Structural Representation
 - 6 x 6 Stiffness Matrix, so that bending-torsion-coupling and other complex effects can be considered
 - TotalMass + 3 x 3 MassInertia Matrix w.r.p.t center of gravity in arbitrarily oriented coordinate system, this allows an exact consideration of all relevant mass effects
- Rigid Body Translations and Rotations are possible
- Integrated aerodynamic, controller, etc. can be replaced

2.8.3 Blender

Blender is an OpenSource program for graphic animations and video productions. It provides a broad spectrum of modeling, texturing, lighting, animation and video post-processing functionality. It is based on the code Phyton and is one of the most popular OpenSource 3D graphics applications in the world. Through its open architecture, Blender provides interoperability, in example for MBDyn. The Loads and System-Simulation department of REpower uses Blender to animate the results from the textural MBDyn output to get a better physically understanding from the rows of number eigenmodes.

2.8.4 ANSYS®

ANSYS is a major product for computer based design and prototyping. It can be used for numerically solving mechanical problems, including static/dynamic structural analysis (both linear and non-linear), heat transfer and fluid problems, as well as acoustic and electro-magnetic problems, to name only a few. Based on its wide circulation in industry and science its a good tool to compare its trusted results with results from a new tool. All models and calculations that where used during this thesis are produced under ANSYS v12, license owned by REpower.

2.8.5 SIMPACK®

SIMPACK is a general nonlinear Multi-Body Simulation Software which is used to aid engineers in the analysis and design of mechanical and mechatronic systems. SIMPACK is primarily used within the automotive, railway, engine, wind turbine, power transmission and aerospace industries. Within all industries SIMPACK is used for single component design and complete system analyses. Besides taking internal dynamics and control into account, SIMPACK can also consider any external influences on the system, e.g. ground disturbances and aerodynamic loading.

Chapter 3

Accomplishment of model validations

3.1 The configuration of a rotor blade in MBDyn

3.1.1 Preprocessing

For the use of MBDyn at REpower Systems it is essential to build up new models or change the existing ones. To speed this up and not to build up a hole new skript each time, the Loads and System-Simulation department designed a preprocessor and a modelgenerator, both based on C#. This allows to create new models of a rotor in a very short time and users do not have to know the exact MBDyn syntax for this.

Multi-Body-Systems (MBS) suits perfectly for simulation of complex systems that are influenced of outer forces. In contrast to FEM-Models the MBS-Models can be reduced further and this saves harddisk-capacity and, much more important, processing power. The goal is to design a MBS-blademodel with less than 10 beams, but with no relevant losts of the original properties. Figure 3.1 shows an example for the assembly of a multi-body-windturbine model.

3.1. THE CONFIGURATION OF A ROTOR BLADE IN MBDYN

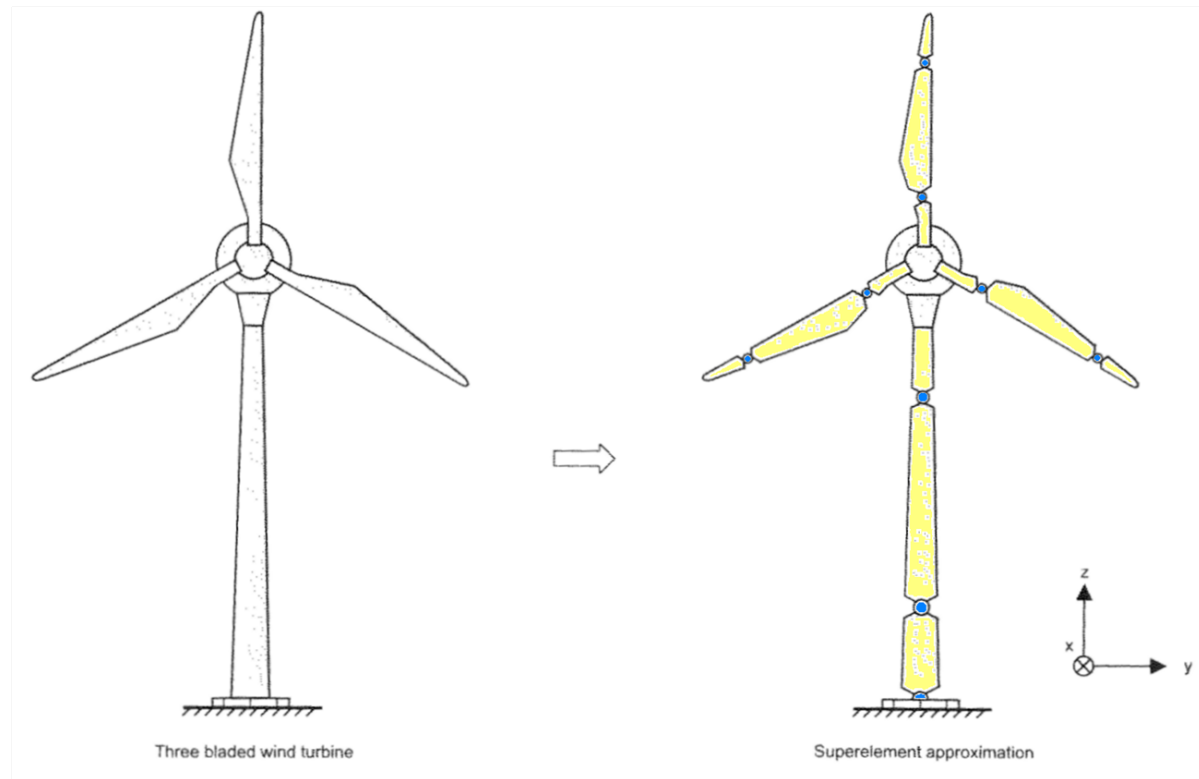


Figure 3.1: Approximation of a windturbine as a MBS

For a rotorblade in MBDyn a finite number of beams are required . The family of finite volume beam elements implemented in MBDyn allows to model slender deformable structural components with a high level of flexibility. The beams are defined by reference lines and by manifolds of orientations attached to the line. The beam elements are defined by their nodes, possible are two or three node beam elements. Each node of the beam is related to a structural node by an offset and an optional relative orientation to provide topological flexibility (Figure 3.2). The beam elements can rigid as well as flexible.

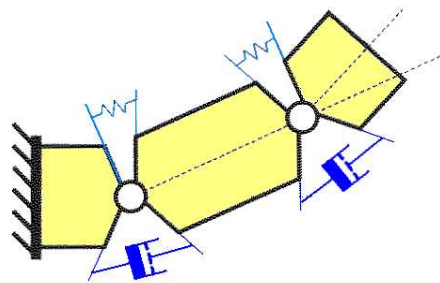


Figure 3.2: Assembly of nodes and beams for MBS

The beam element is modeled by means of an original Finite Volume approach, which computes

3.1. THE CONFIGURATION OF A ROTOR BLADE IN MBDYN

the internal forces as functions of the straining of the reference line and orientation on selected points along the line itself, called Gauss points. In Figure 3.3 the structural assembling of a blade can be schematically seen with four three node beam elements, a totally number of nine nodes (yellow), eight Gauss points (cyan) and the rigid bodies between the Gauss points.

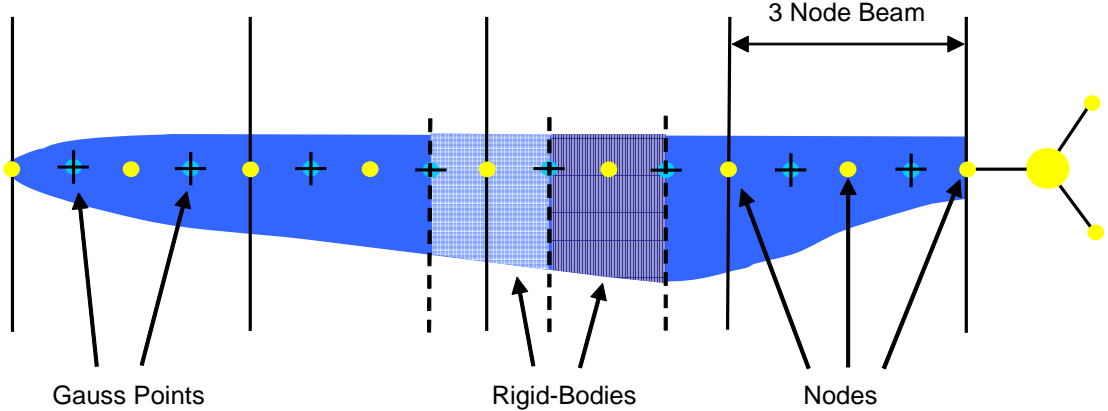


Figure 3.3: Structural assembling of a blade in MBDyn

For the structural assembling constitutive laws have to be set on this Gauss points. At the 3 node beam they are situated between two nodes with a distance of $\frac{L}{2\sqrt{3}}$ where L is the beam length (Figure 3.4).

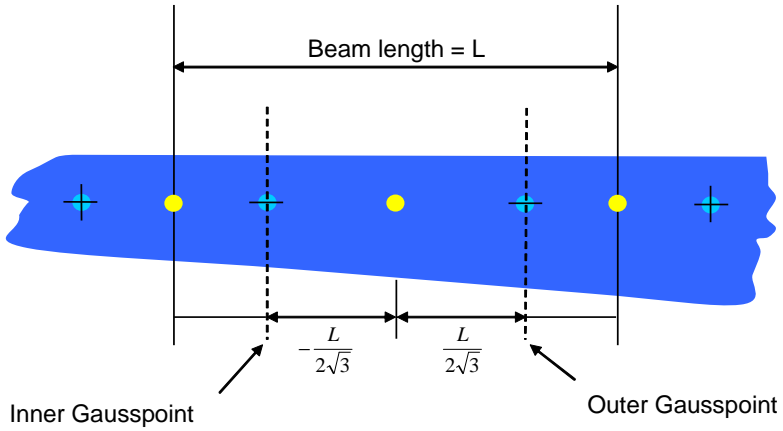


Figure 3.4: Location of the Gausspoints

Once the gauss points position is placed, the necessary parameters can be interpolated to describe the constitutive laws. Rigid bodys respectively the mass parameter, the location of the AC, EC, SC, the stiffnesses, etc.. between two gauss points bonding on the node between them. Joints are set on the root, where the blade is connected with the rotor (Figure 3.1).

The aerodynamic forces and moments are computed with the help of aerodynamic beams. They are comparable with structural beams, because they are attached on the same nodes and are

3.1. THE CONFIGURATION OF A ROTOR BLADE IN MBDYN

three node beams, too. The different airfoil data over the length of the aerodynamic beam is separated into sections with variable length (Figure 3.5). The crossings between two airfoils are approximated with in MBDyn so called shaped-function and the aerodynamic forces calculated by the BEMT are calculated for the 1/4 points of the different airfoils. All aerodynamic forces between two gauss points are related to the respective node lying between.

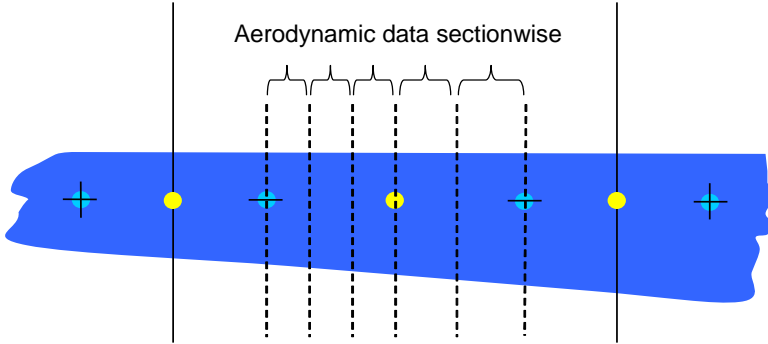


Figure 3.5: Aerodynamic assembling of a blade

The aerodynamic and structural input data is a table sorted by n-section from the root to the tip of the blade. For every section the following parameters are given:

- offset concerning prebending
- chordlength
- thickness
- structural and aerodynamic twist
- airfoildata
- location of centre of mass, shear center
- mass
- moments of inertia

The preprocessor computes the needed parameters for the aerodynamic and structural sections for the MBDyn-model. The modelgenerator then creates the model, consists of many files (Figure 3.6), by use of this parameters and in the following a working blade or rotor model can be used. Attached to this thesis is a CD where the MBDyn NREL-blade model is included for testing purposes or illustration (Appendix: 5.4).

3.1. THE CONFIGURATION OF A ROTOR BLADE IN MBDYN

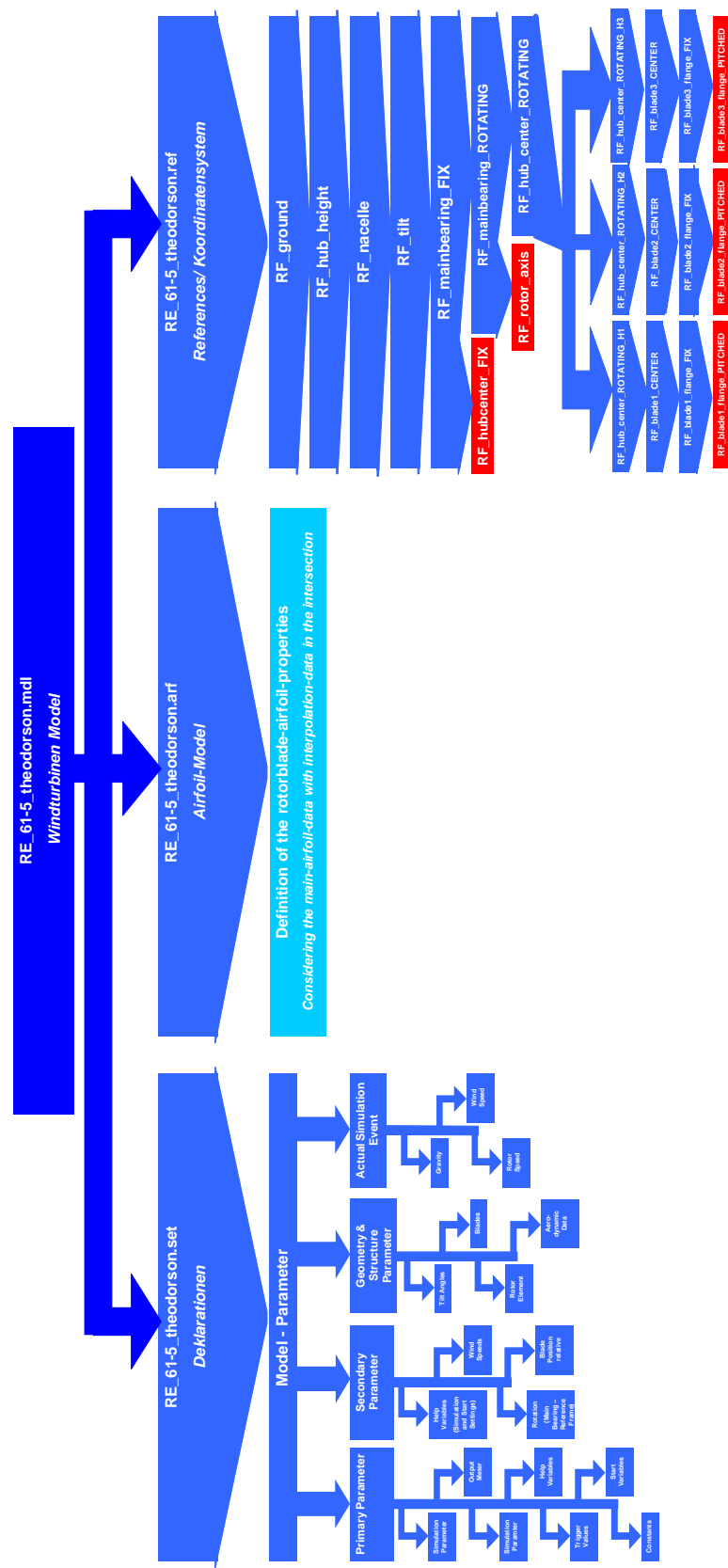


Figure 3.6: Structure of the model created by the preprocessor

3.1. THE CONFIGURATION OF A ROTOR BLADE IN MBDYN

Furthermore it is always attended to change the basic structure of the preprocessor so that the function of building up other elements, like maybe the tower, will not be affected. The main target of MBDyn at REpower is not only studies on the rotor but also studies on a whole windturbine with all its components. For this purpose the preprocessor considers this in its structure and to show how complex it is, it can be seen in Figure 3.7 and Figure 3.8 that many different coordinate-systems have to be taken in consideration to represent later a whole windturbine.

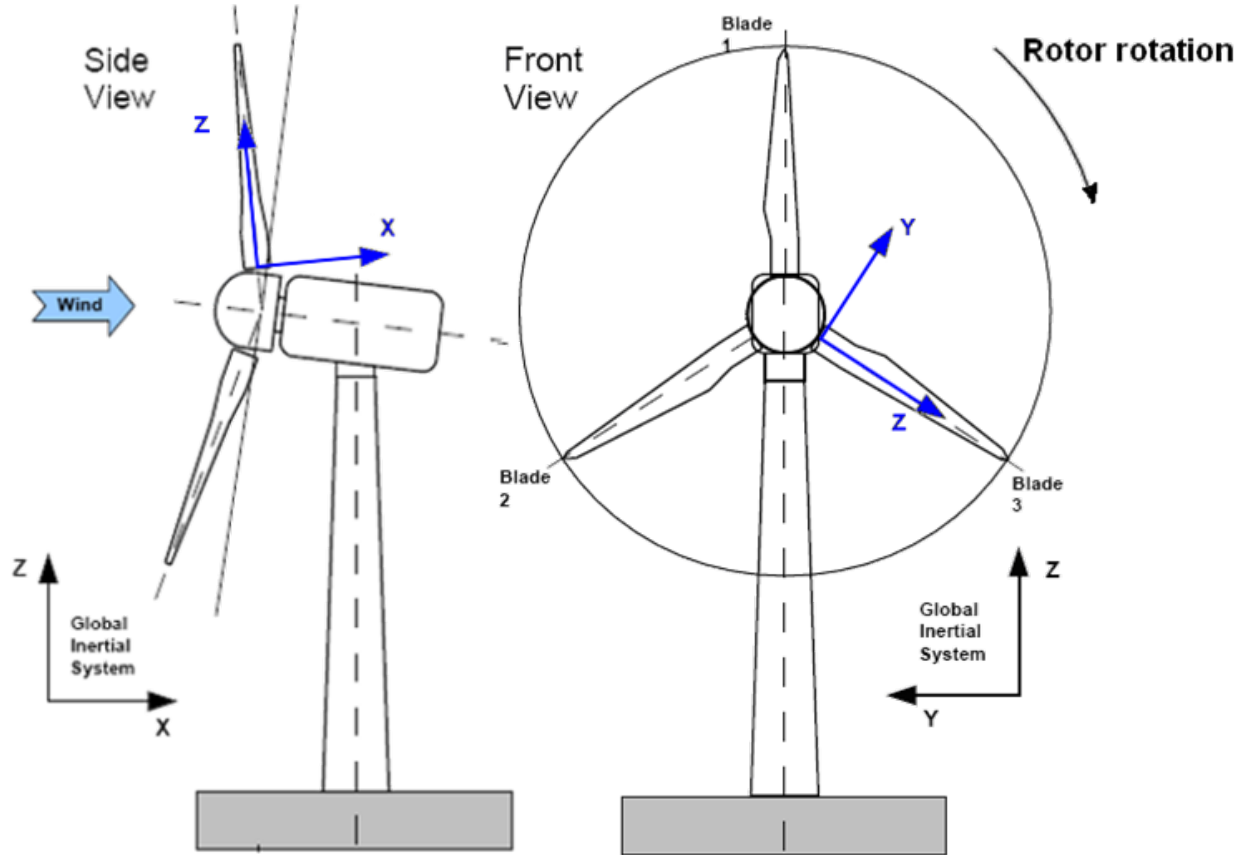


Figure 3.7: Global definition and coordinate system of a windturbine in MBDyn

3.1. THE CONFIGURATION OF A ROTOR BLADE IN MBDYN

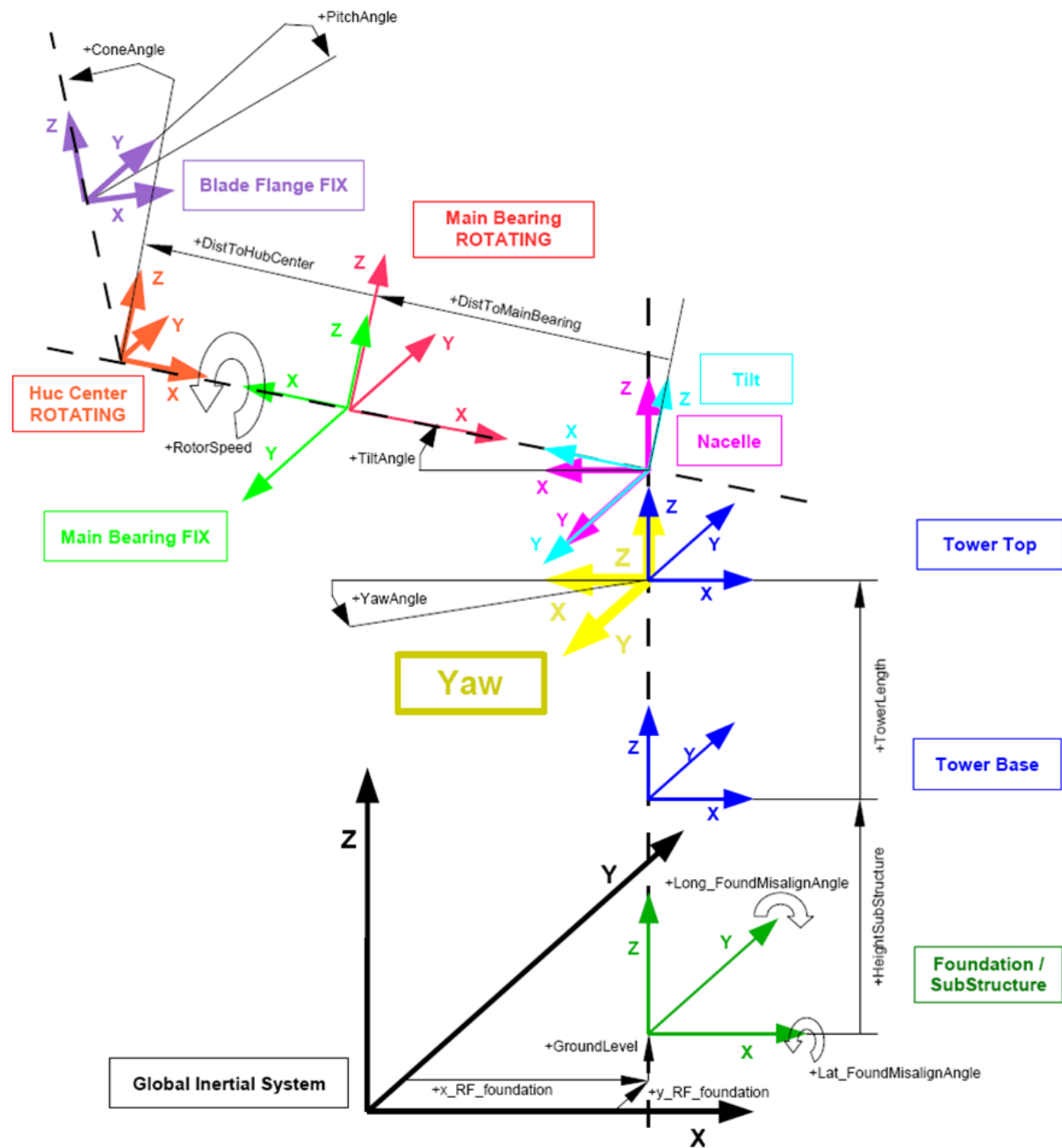


Figure 3.8: The different coordinate systems of a windturbine

3.2 First Simulation

In the first simulations with the whole rotor (all three blades) with a default rotary speed of 18 rpm, a wind speed of 13.2 m/s and without gravity, a physically disagreement has been detected. In Figure 3.9 a section of the flapwise- and torsionmotion of a 61.5m blade is shown. During the postprocessing of this time section a failure in the movement of the blade in the individual directions is noticed.

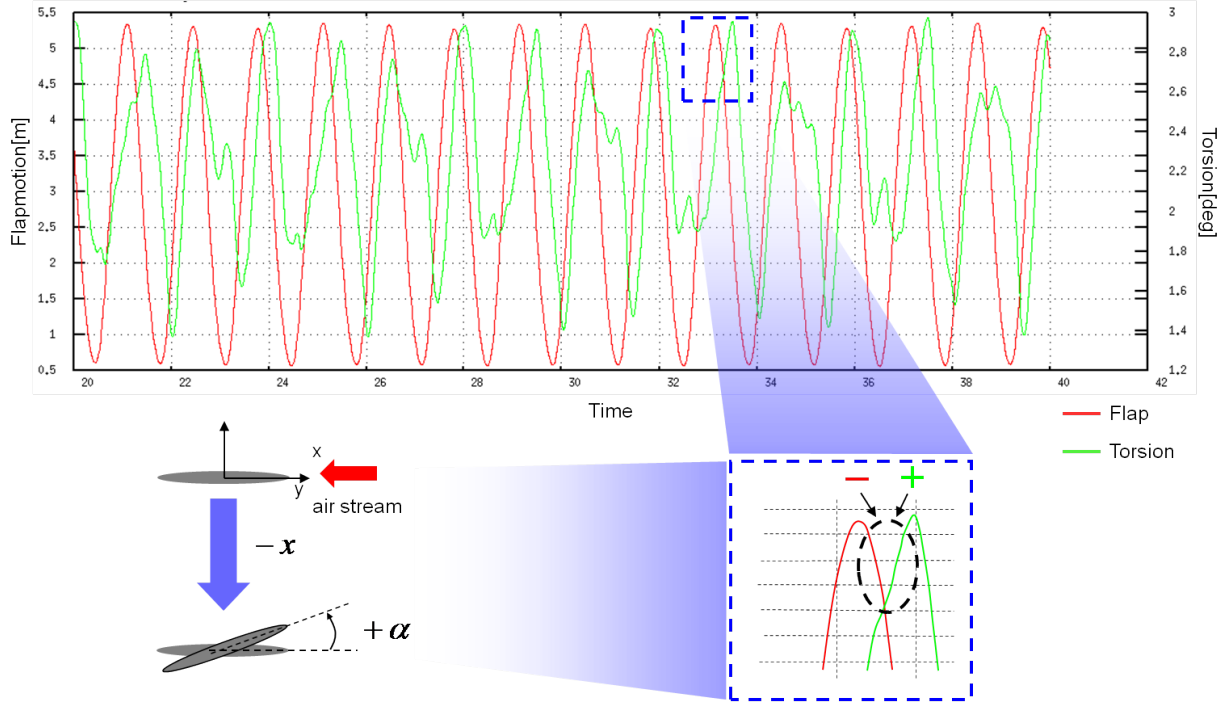


Figure 3.9: Section from the flapwise- and torsionmotion of a 61.5m blade

To specify this: In the blue framed box and in the picture on the lower left side of Figure 3.9 it can be seen that there is something wrong in the correlation between the flapwise- and the torsionmotion, compare Figure 2.13. Everytime when the flapwise-motion is going from a positive to a negative gradient there is the beginning of a negative fall of the flapwise-motion, the torsion gradient keeps positve. But when the torsion gradient is positive there is a rising angle of attack and therefore a higher lift. Therefore should be seen a deformation in positive flapwise-motion, but it is not. The first idea that comes in mind is, that it could have something to do with the calculation of the coupling-coefficients in the matrix of the elements of the blades, because the absolute values of the results of this simulation are not wrong in size but the prefixes are incorrect.

After a few simulations with different values of sh12 and sh23 (the shear components in the upper left corner of the stiffnessmatrix (Chapter 3.3.1)), one discovers, that if sh12 is changed from negative to positive and sh23 from positive to negative the torsionmotion-characteristic

3.3. STRUCTURAL VALIDATION

is mirrored , from the characteristic in Figure 3.9 and this seems much better. Therefore it is clear that the failure has to be somewhere in the calculation of the components of the stiffness matrix. To find the failure and to be sure that the models, the preprocessor creates, are correct, a structural and aerodynamic validation of simple structures created by the preprocessor is done next to the point of new simulations of the rotor.

3.3 Structural validation

Based on the fact that the forming and the blades behaviour seem not false in all terms, the static deformation in flapwise direction agrees to only a little deviation from results of FLEX5®, it is suspected a failure of the calculation of the couple-components in the stiffness matrices. In this matter it has to be said that even today there is no adequate solution for the computation of the stiffnesses between two integration points/gauss points, used in a MBS-Tool, which represents a beam or a blade element of a specific length with different stiffnesses over the length.

Even ANSYS derived an abberation around two percent considering on the one hand a straight beam and on the other the same beam consisting of two beams. Certainly this abberation depends on things like material, cross sections and so on, but attending to that, this abberation sums up, if many beams are considered.

These different stiffnesses accrue from things like unequal materials, mass properties or different orientations of the fiber mats. The preprocessor approximates the stiffness by an integration between the stiffnesses that are effective on their respective position in the considered structure, i.e. the blade.

Adapted from the knowledge that the failure has to be somewhere at couple coefficents, a validation of those couple-coefficents can be started . This is done by calculation of MBDyn in comparison with ANSYS. As models are taken an one meter beam with a retangle cross section, with a U-profile cross section and with a L-profile cross section.

The validation of the beam with the retangle cross section 20x20x1mm (L,B,H) offers no surprises if the results of both tools are compared. Based on the fact that by a retangle cross section beam the elastic and shear center is situated on the same position there are no couple-coefficents in use. Therefore the static deformation does not show big meandering between ANSYS and MBDyn. The validation of the U-profile and the L-profile is displayed in more detail in the following sections.

The different models in MBDyn for the structural validation are all generated with the preprocessor, which is developed to established the rotor blades. All models used beams based on the Timoshenko theory, meaning that the shear deformations of a cross section are respected. In ANSYS Beam188 elements are used (this elements are based on Timoshenko beam theory; shear deformation effects are included.). The elasticity modul is set to $2.1 * 10^{11} \frac{N}{m^2}$ and the major

3.3. STRUCTURAL VALIDATION

Poisson's ratio is set to 0.3 and the beams are always isotropic or solid. All following simulations in the next subsections are done without the influence of gravitation.

3.3.1 The U-profile and L-profile validation with ANSYS

An U-profile is elected by the fact as it is semi-asymmetric. This means that an U-profile is symmetric in the one direction (reflectable on x-axis) and asymmetric in the other (non reflectable on y-axis) and not like a L-profile, which is in both directions asymmetric. A standard U-profile (30x15x4mm) is taken for the one meter beam as cross section (Figure 3.10).

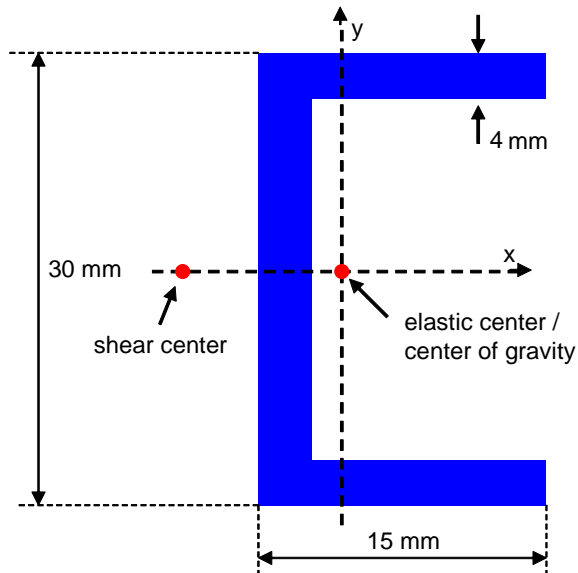


Figure 3.10: U-profile parameters

For the validation the load cases consist of six different kinds. Three different loads, a force in x-direction, a force in y-direction and a moment consecutively applied to the elastic center (EC) then on the shear center (SC) (Figure 3.13). The forces have an amount of 1000N, the moments of 100Nm. The values for the deformation or rotation that are less than $1.0e^{-6}$ can be set to zero. Two different methods are used for the ANSYS calculation, a nonlinear calculation and a linear one. Later it turns out, that for the loads with a moment the comparison between the results of the linear ANSYS computation are better than with the nonlinear ones. It is the exact reverse when the loads are forces. In Figure 3.13 the first computation with the unmodified preprocessor can be seen. The loads are displayed in red.

3.3. STRUCTURAL VALIDATION

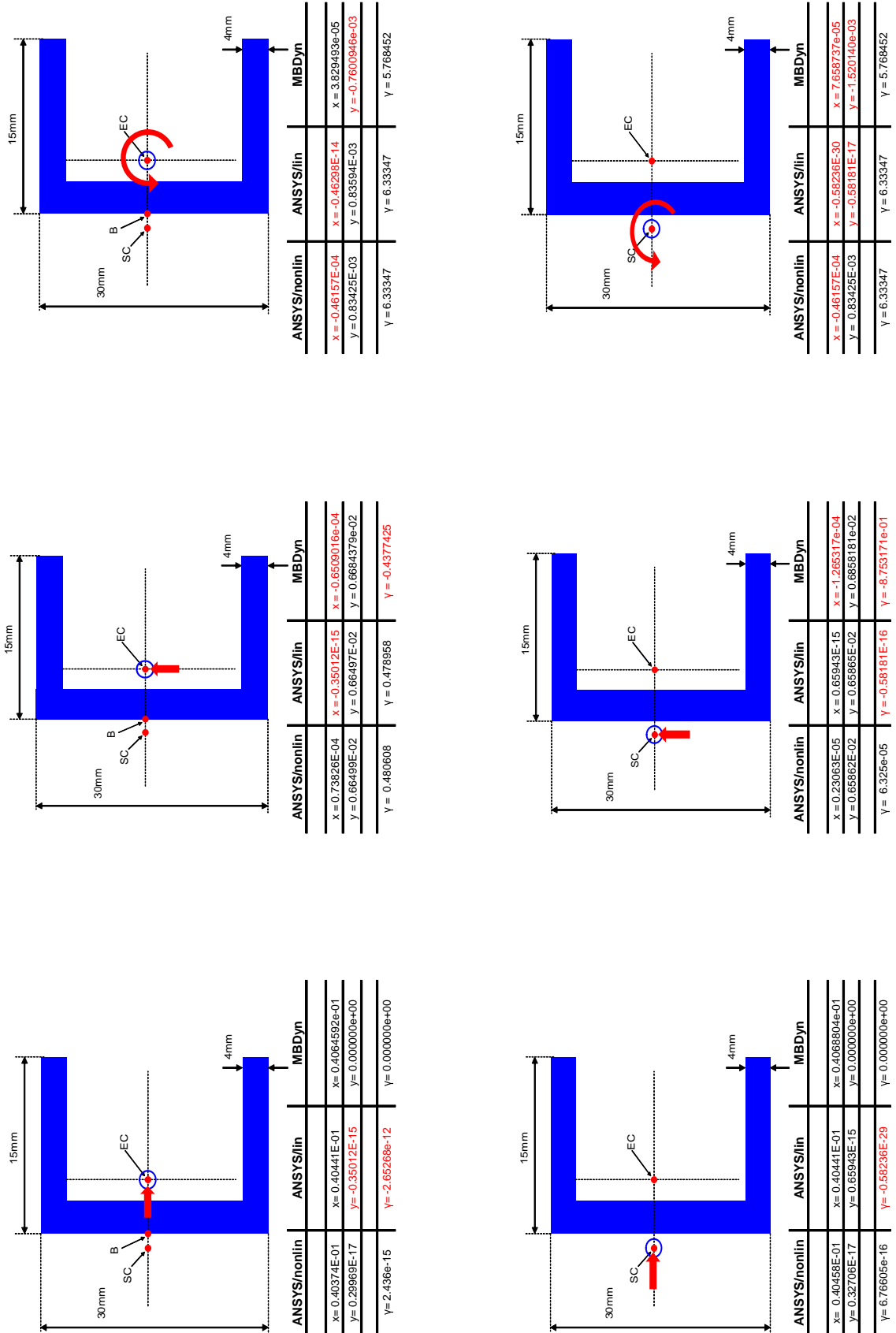


Figure 3.11: Loads on an U-profile (unmodified preprocessor)

3.3. STRUCTURAL VALIDATION

As expected if loading on an axis through the SC, here the x-axis, there is only a deformation in the direction of this force and the meanderings keep within a small limit. For a force in y-direction the deformation in x-direction of the MBDyn results and the rotation about z is showing differences. The same can be noticed by the loading with a moment, here the x- and y-deformation are not matching with the ANSYS results. Consequently it is approved of this results that something is wrong with the coupling between a force in y-direction and the resulting deformation in x-direction. Also the coupling between a moment and the resulting x- and y-deformations is wrong. After exclusion of other possible sources errors, i.e. the position of the nodes in relation to the profile or position of applied forces, the stiffness matrix has to be the only possible error source.

The stiffness matrix with the couple-coefficents that MBDyn uses for calculations is build up like this [Mas10, Mas09]:

$$\begin{bmatrix} F_x \\ F_y \\ F_z \\ M_x \\ M_y \\ M_z \end{bmatrix} = \begin{bmatrix} S_{11} & S_{12} & & S_{13} \\ & S_{22} & & S_{23} \\ & & A_{33} & A_{13} & A_{23} \\ & & A_{13} & A_{11} & A_{12} \\ & & A_{23} & A_{12} & A_{22} \\ S_{13} & S_{23} & & S_{33} \end{bmatrix} * \begin{bmatrix} \delta_x \\ \delta_y \\ \delta_z \\ \kappa_x \\ \kappa_y \\ \kappa_z \end{bmatrix}$$

It is a diagonal matrix with axial components (A) and with shear components (S). The components on the diagonal line are the uncoupled ones and all others are coupled. The axial components can be calculated by this formulas:

$$\begin{aligned} A_{11} &= EI_{xx}\cos^2\alpha + EI_{yy}\sin^2\alpha + y^2EA \\ A_{12} &= \cos\alpha \cdot \sin^2\alpha(EI_x - EI_y) - xyEA \\ A_{22} &= EI_{yy}\cos^2\alpha + EI_{xx}\sin^2\alpha + x^2EA \\ A_{13} &= -yEA \\ A_{23} &= xEA \\ A_{33} &= EA \end{aligned}$$

The shear components are:

$$\begin{aligned} S_{11} &= GA_x\cos^2\beta + GA_y\sin^2\beta \\ S_{12} &= (GA_y - GA_x)\cos\beta \cdot \sin\beta \\ S_{11} &= GA_y\cos^2\beta + GA_x\sin^2\beta \\ S_{13} &= -yGA_x\cos\beta + xGA_y\sin\beta \\ S_{23} &= yGA_x\sin\beta + xGA_y\cos\beta \end{aligned}$$

3.3. STRUCTURAL VALIDATION

$$S_{33} = GI + y^2GA_x + x^2GA_y$$

Responsible for this wrong coupling at the U-profile are the couple-coefficients from the stiffness-matrix, more precisely the non diagonal shear components (S). Next to GA_x and GA_y the angle β is playing a role in the computation of this factor. The value of x and y cannot be the failure, because the axial components seem to be right, here the calculated values matched between the two tools.

The angles α and β are needed to transform the properties into the common reference frame of the beam section (Figure 3.12).

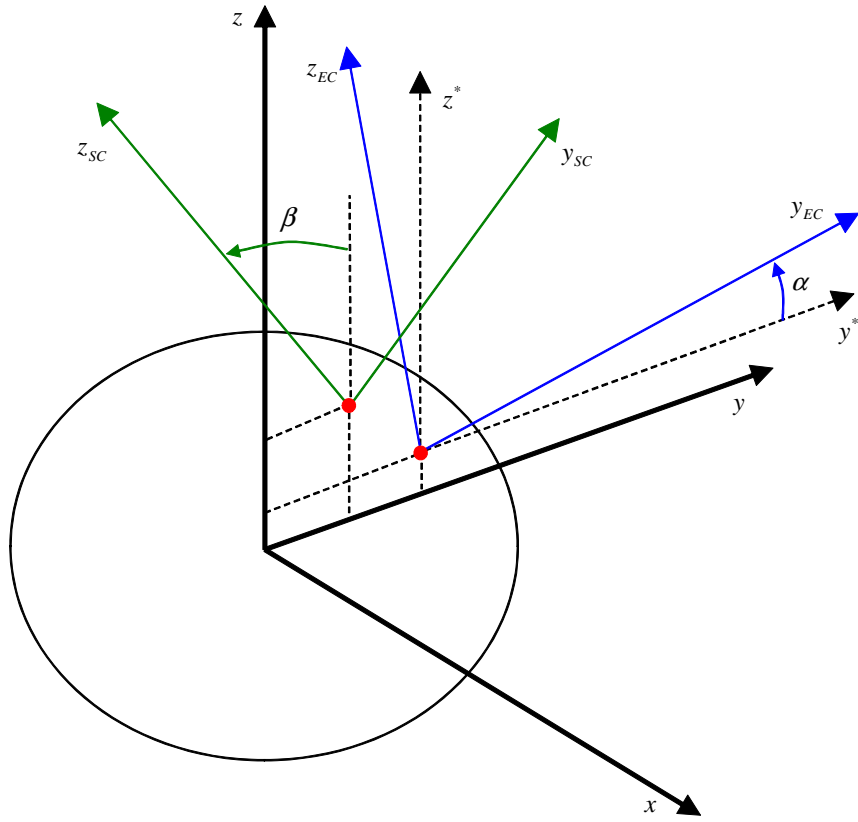


Figure 3.12: Beam Section

On re-examination of the preprocessor and comparison by the theory of the MBDyn input it exposes that a wrong assumption is taken for the calculation of the angle β . The angle $\beta = t(E) - t(S)$, where $t(E)$ is the angle between the base system and the elastic system and $t(S)$ is the angle between the base and the shear system. Different from the theory manual of MBDyn in the case of our preprocessor the shear angle $t(S)$ has been set to 0, so that the shear system is orientated the same as the base system. If this is considered the prefixes of the values are turned around in comparison to the unmodified model and are now the same like the prefixes in ANSYS (Figure 3.13).

3.3. STRUCTURAL VALIDATION

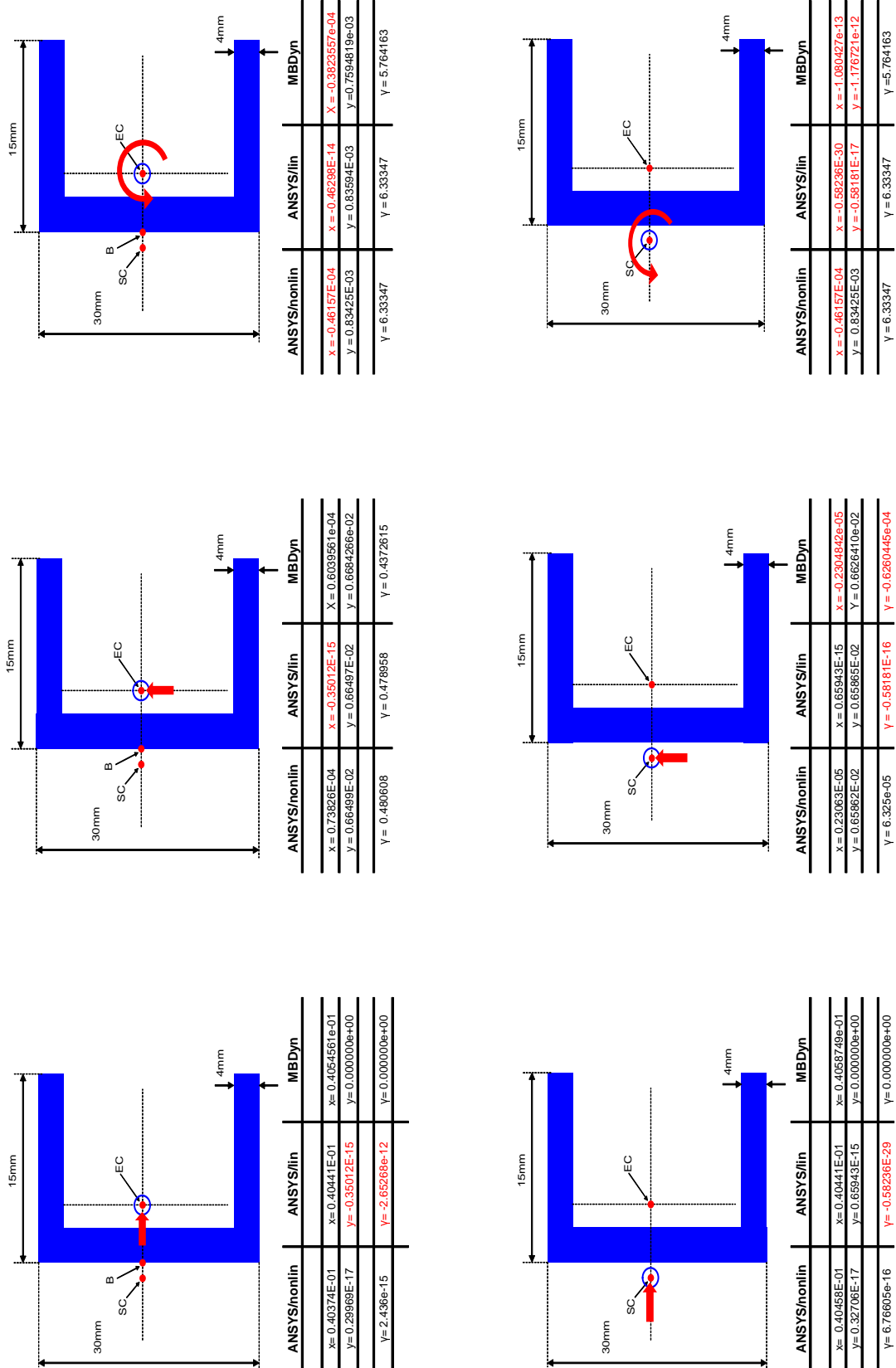


Figure 3.13: Loads on an U-profile (modified preprocessor)

3.3. STRUCTURAL VALIDATION

For the comparison to the L-profile an 1m in length beam is taken with a 30x20x3mm L-profile (Figure 3.14) .

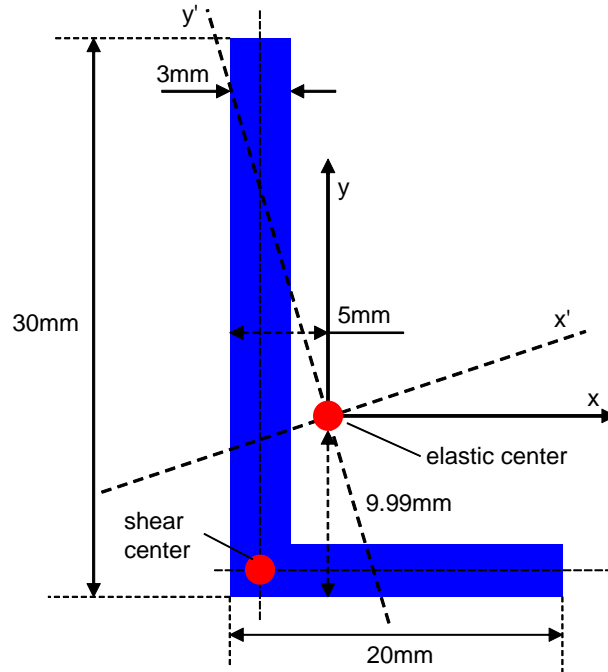


Figure 3.14: L-profile parameters

The load cases are the same as the U-profile load cases. In Figure 3.16 are shown the results of the computation with the model of the modified preprocessor. Here all the prefixes are correct in comparison to ANSYS and there are only minor changes by checking the results from ANSYS to the results from MBDyn.

To get closer to the geometrical structure of a rotorblade it is meaningful to compute with this relative simple L-profile a L-profile beam that is twisted over its length (Figure 3.15).

3.3. STRUCTURAL VALIDATION

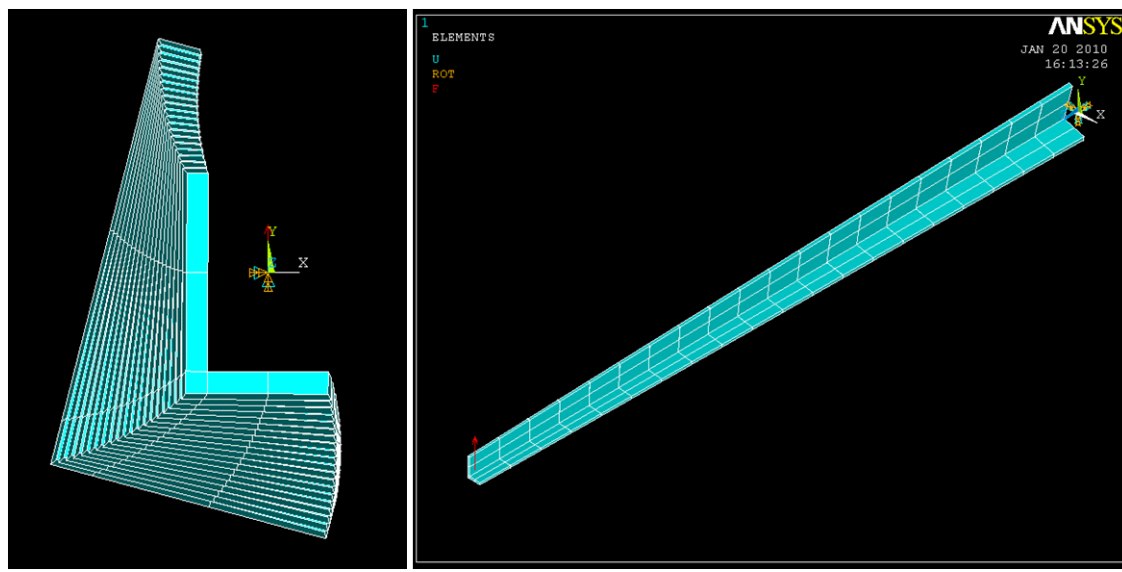


Figure 3.15: L-profile beam with a twist of 15 degree in ANSYS(2.8.4)

The results of this L-profile beam with a twist angle of 15 degrees of the root compared to the tip are shown among others in the Appendix 5.3.

3.3. STRUCTURAL VALIDATION

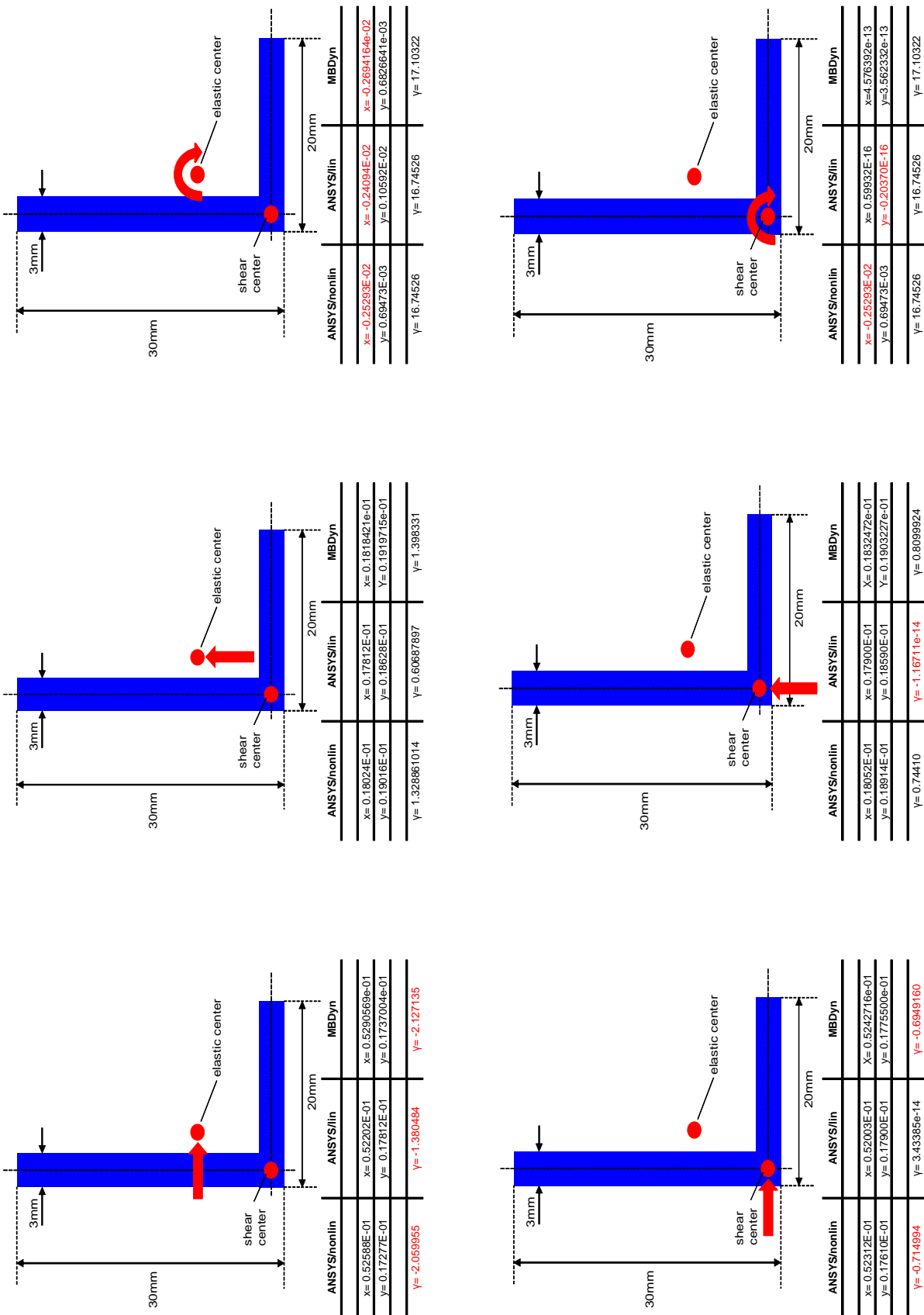


Figure 3.16: Loads on a L-profile (modified preprocessor)

3.3. STRUCTURAL VALIDATION

3.3.2 Structural analysis of the rotor blade

After the validation of simple profiles and confirmation of achieved reliable results in the different load cases it is the next thing to start a structural check of the blade.

To validate the structural properties of the rotor blade an ANSYS model is taken as reference. This ANSYS model (Figure 3.18) is constructed by the Rotorblade department and is validated by structural tests in reality. The results of this ANSYS model can be trusted on. It considers the same input table for the section properties like MBDyn. In Figure 3.17 the data from the table 3.2 are shown .

For the structural comparison forces on different locations are applied to the blade model on both tools, MBDyn and ANSYS. After every simulation with the same stresses the results are compared.

First five forces are applied to x-direction (Figure 3.18). In ANSYS all nodes of a x-y-layer on a certain z-level are selected and connected with a new node by a MPC184 element. So, if a force will act on the one new node, it will affect all connected nodes in this layer.

MBDyn Node	ANSYS Node	z-Position	Forces/moment applied
7101	61	1.64	-
7102	60	3.64	-
7103	59	7.79	-
7104	58	10.865	-
7105	57	13.94	-
7106	56	17.015	-
7107	55	20.09	-
7108	54	22.892	-
7109	53	26.24	-
7110	52	29.315	-
7111	51	32.39	-
7112	50	35.465	-
7113	49	38.54	-
7114	48	41.615	-
7115	47	44.69	-
7116	46	47.765	25000N/250000Nm
7117	45	50.84	25000N/250000Nm
7118	44	53.915	25000N/250000Nm
7119	43	56.99	25000N/250000Nm
7120	42	60.065	25000N/250000Nm
7121	41	63.14	-

Table 3.2: Position of the nodes in MBDyn and ANSYS and the applied forces

3.3. STRUCTURAL VALIDATION

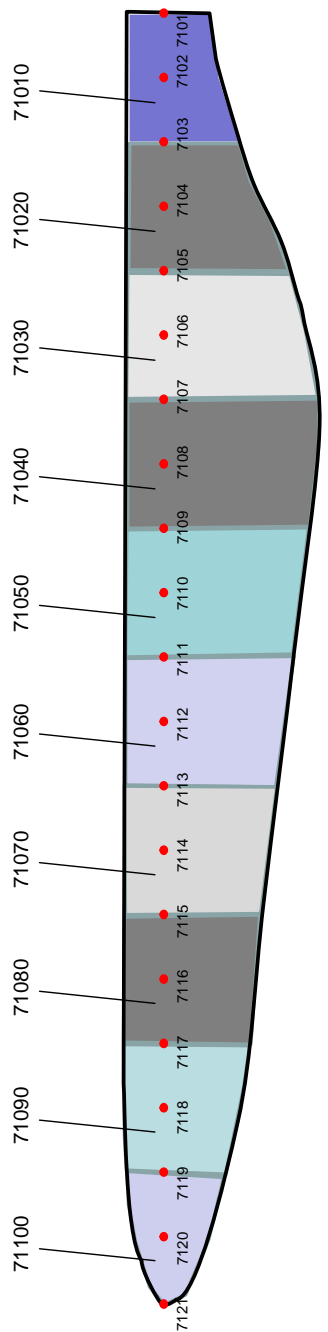


Figure 3.17: Blade assembling, with nodes and elements

In Figure 3.19 is shown in red the applied force on the new node, in light blue the connections between the new node and the nodes, lying on the profile. The profiles in ANSYS are constructed like in reality with a strut trailing edge and with several bars.

3.3. STRUCTURAL VALIDATION

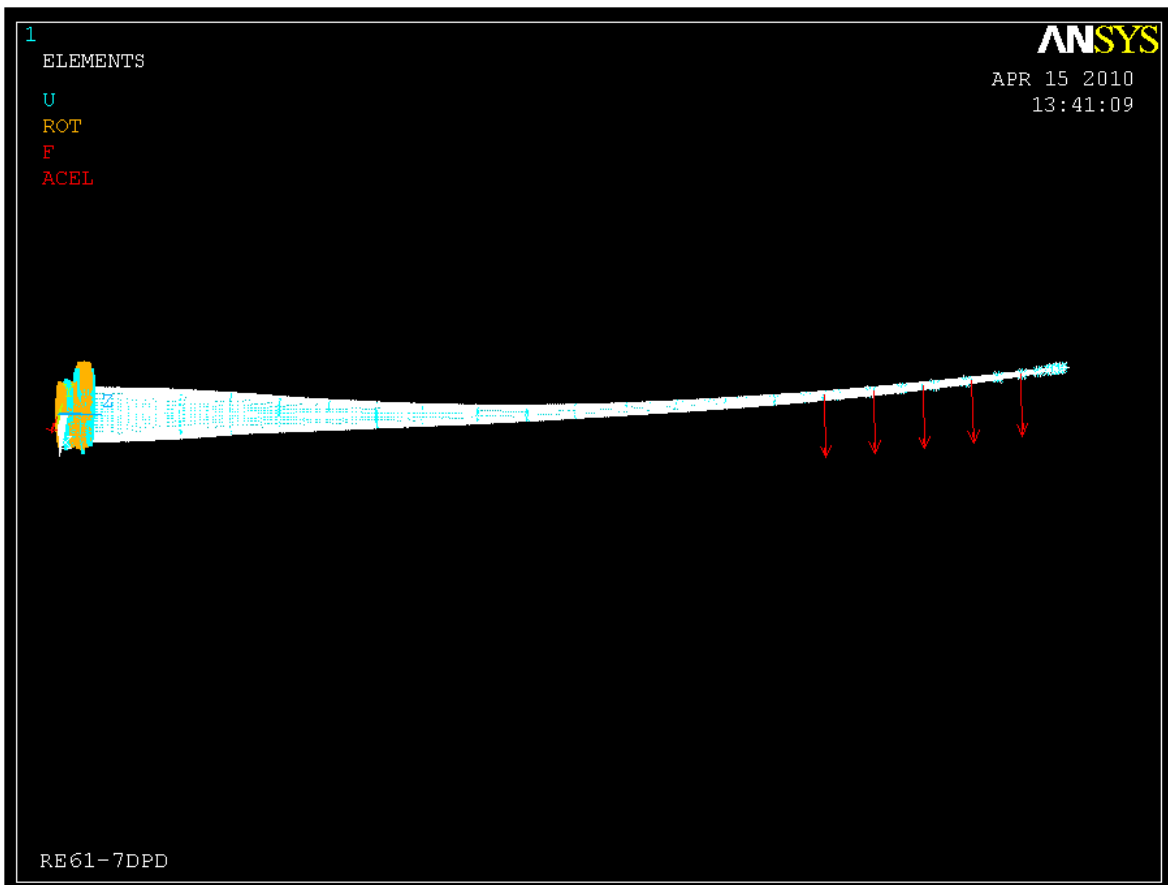


Figure 3.18: Blade with applied Forces on five nodes in ANSYS(2.8.4)

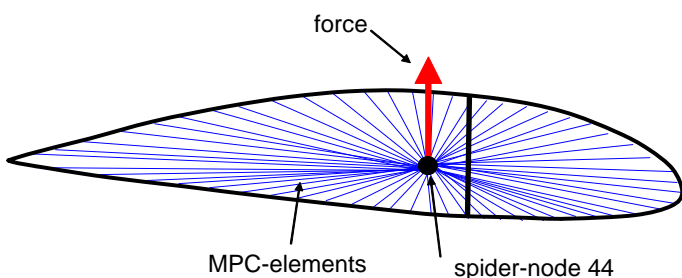


Figure 3.19: Cut-out with spider-node 44

It is easier in MBDyn, caused on the fact that MBDyn is not an FEM-Tool like ANSYS. Here a force will be directly applied to a node. To simplify it the z-levels in ANSYS are on the same z-level like the nodes in the MBDyn model.

In the next Figure (3.20) an evaluation in MBDyn for loads in x-direction is shown. The y scale is reduced by the conviction of the terms of REpower Systems and shows only the zero and the max. The x-axis displays the 18 nodes, from node 42 to 59.

3.3. STRUCTURAL VALIDATION

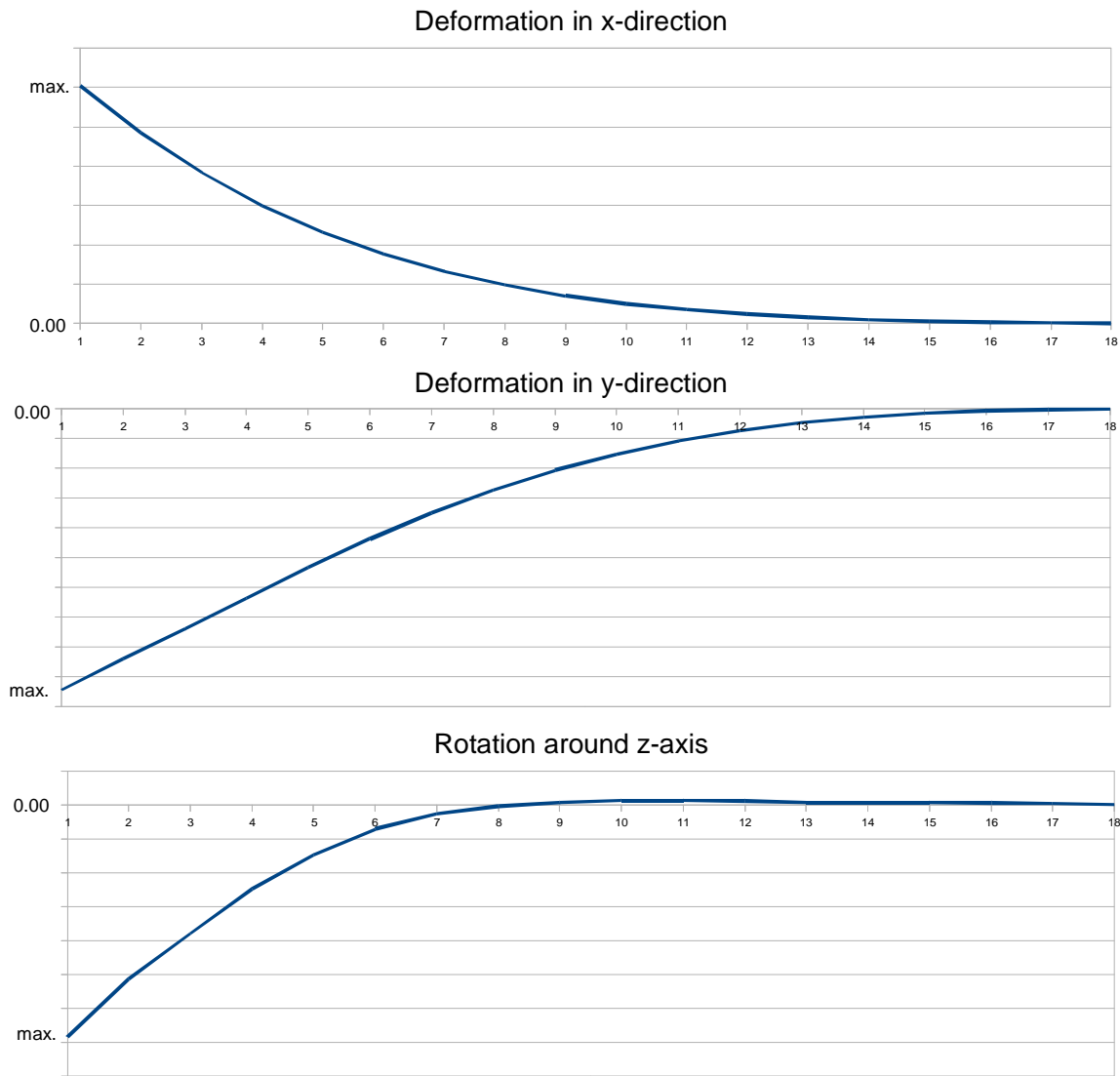


Figure 3.20: Diagram of the deformation in MBDyn

For the load in x-direction the compared results are given in the next diagramms (Figure 3.21)

The left scale of the diagramms is for the deformation of the nodes. The scale relates to the maximal bending of the ANSYS model, that means on the scale $1.0 \equiv 100\%$ stands for the maximal deformation of the tip node of the ANSYS model (red lines). The yellow lines represent the deviation from the ANSYS and MBDyn (blue line). The deformation in x- and y-direction fits very good together. Only at the rotation around z the failure is bigger.

By applying loads to y-direction the results are shown in the following diagramms (Figure 3.23).

For applying moments to the five nodes with a strength of 250.000Nm each, the deformations are shown in Figure 3.23

3.3. STRUCTURAL VALIDATION

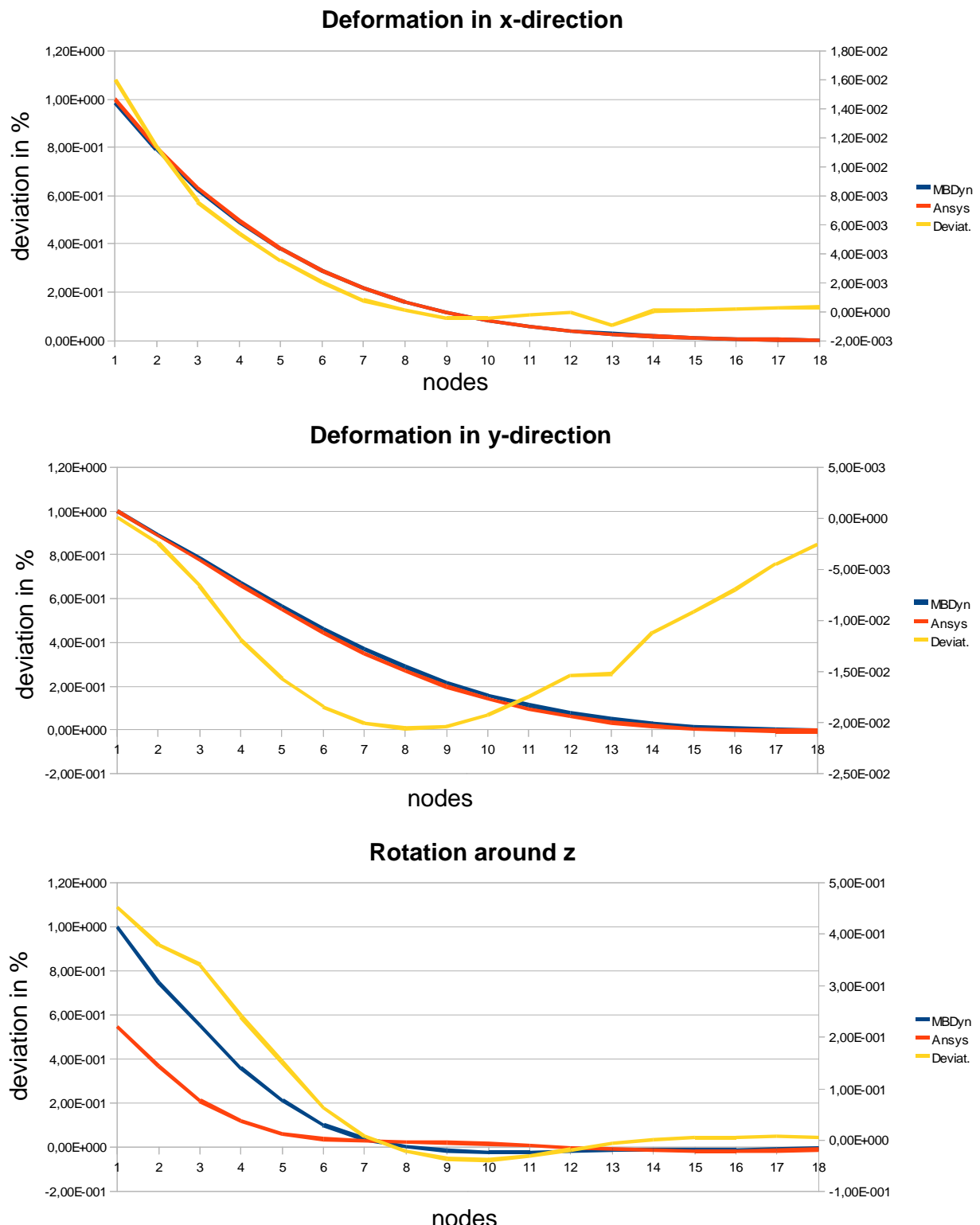


Figure 3.21: Deviation from results(ANSYS/MBDyn) of applied loads in x-direction

3.3. STRUCTURAL VALIDATION

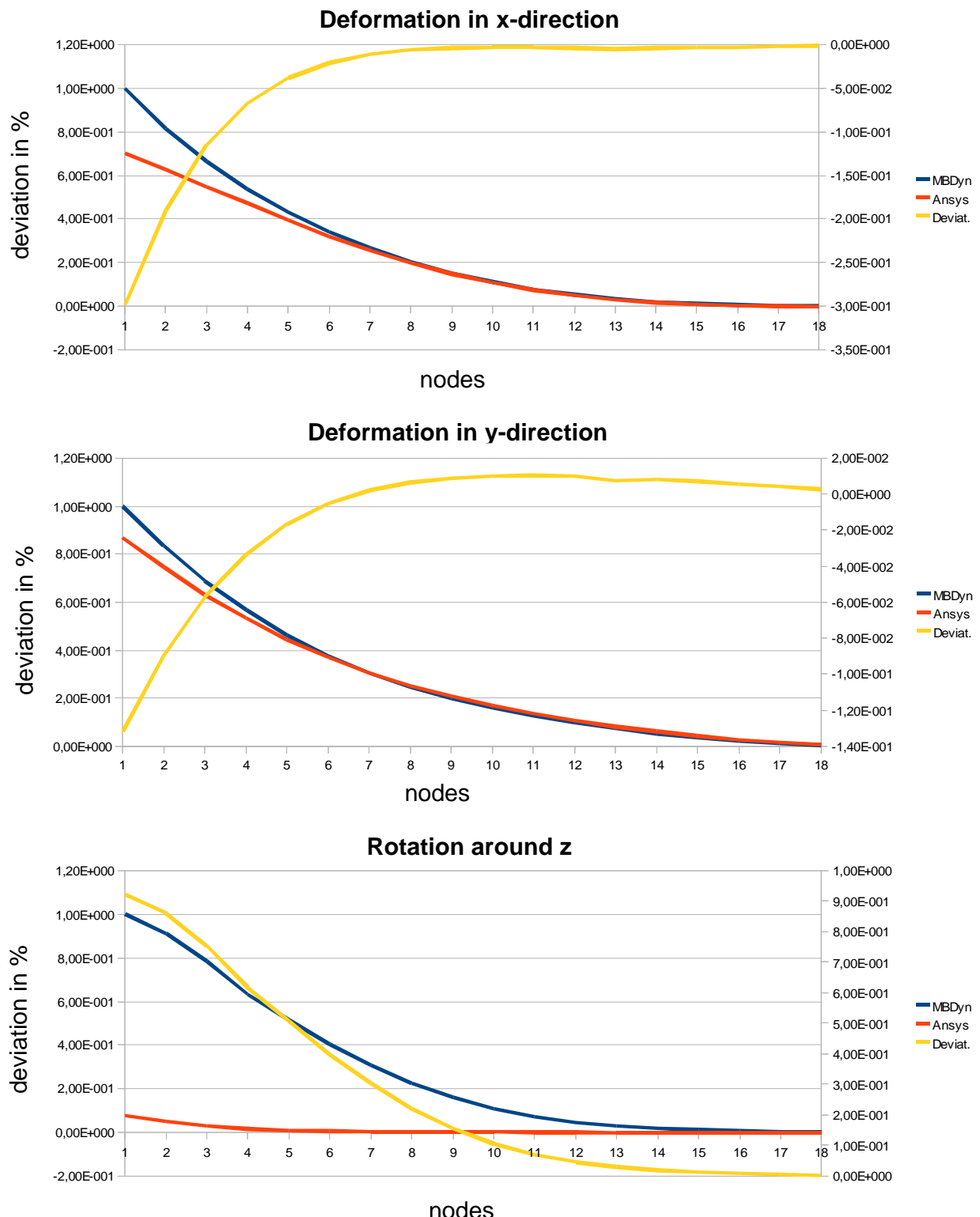


Figure 3.22: Deviation from results (ANSYS/MBDyn) of applied loads in y-direction

3.3. STRUCTURAL VALIDATION

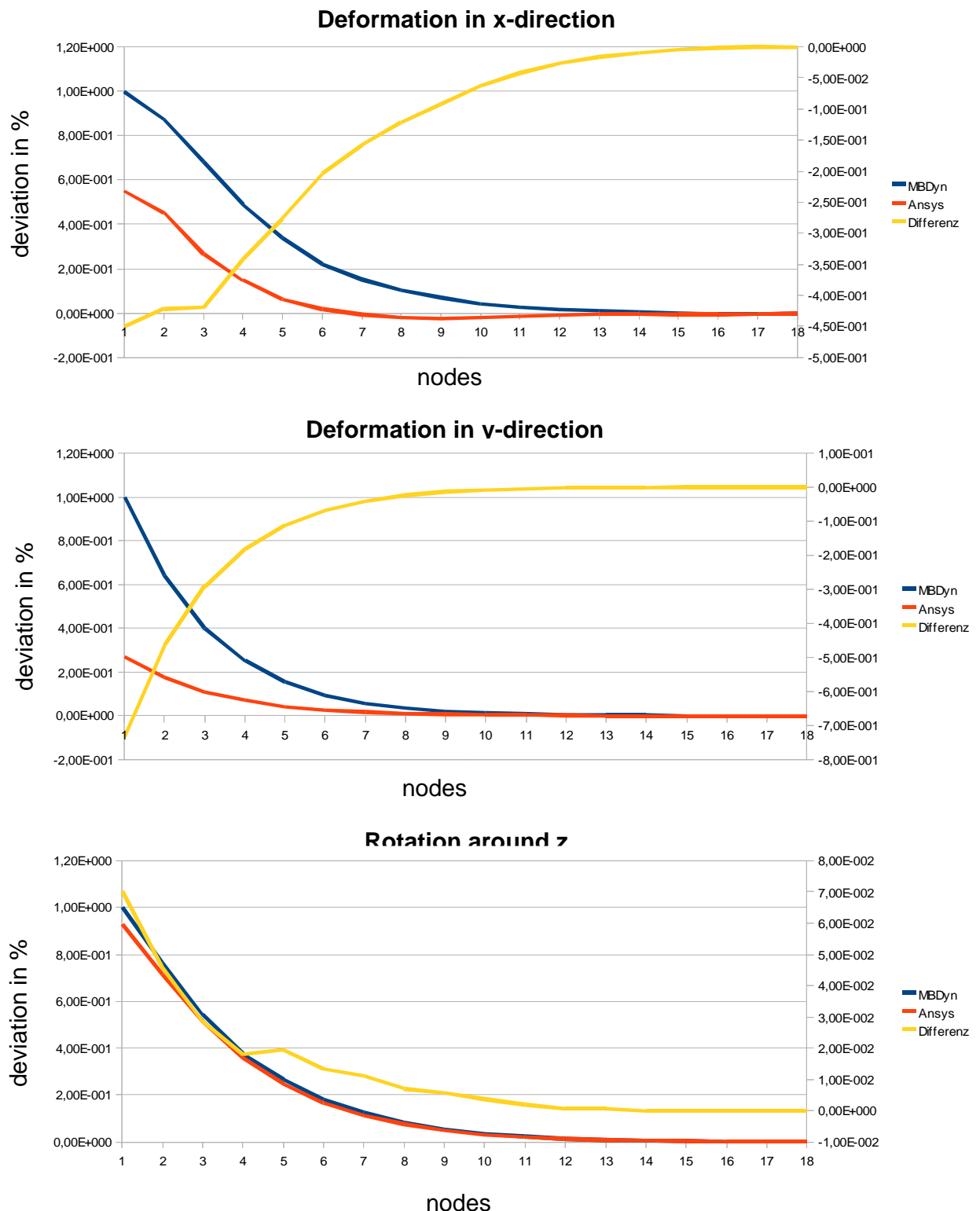


Figure 3.23: Deviation from results(ANSYS/MBDyn) of applied moments around z-axis

3.3. STRUCTURAL VALIDATION

A modal analysis on the blade model in MBDyn is executed if the designation of the dynamic properties of the blade is needed . These parameters are then compared with the parameters out of FLEX5® and other MBS-Tools which are calculated for the same blade model.

The goal of a modal analysis is to determine the natural mode shapes, structural damping and frequencies of a structure during free vibration. These factors are important for models that are subjected to cyclic or vibration loads.

The results of a modal analysis in MBDyn from the blade and the comparison to the results of ADAMS is shown in table 3.3.

Eigenfrequency	MBDyn	ADAMS
1.Flap	0.640	0.665
2.Flap	1.765	1.805
3.Flap	3.690	-
1.Edge	0.990	1.081
2.Edge	2.991	-
1.Torsion	5.20	-

Table 3.3: NREL-eigenfrequencies on comparison

3.3.3 Research on the influence on the centrifugal force with the eigenfrequencies

In this subsection a research is done on the influence over the eigenfrequencies done by the centrifugal force in running simulations by different rotation speeds. Therefore a rotor model is taken and the eigenfrequencies are compared with one another after each run. The first results come from a rotor without any rotation speed. The modal-analyses computes the eigenfrequency of this rotor without any centrifugal force. Then this modal-analysis is repeated for different rotation speeds, considering the gravitation, the air density and the wind set to zero/setting off and the pitch angle to zero degrees. The results of this experimental series are displayed in Figure 3.24.

3.4. AERODYNAMIC VALIDATIONS

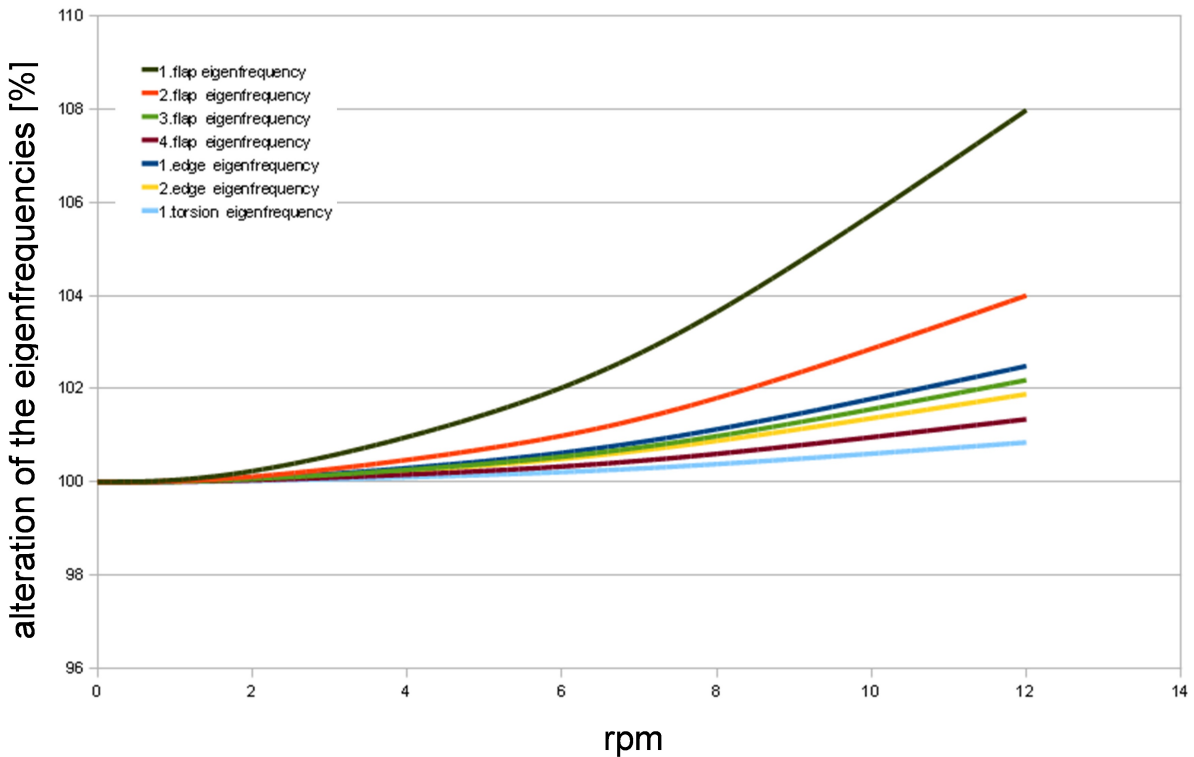


Figure 3.24: Alteration of the eigenfrequencies over rpm corresponding to a standstill rotor

Significantly all eigenfrequencies of the eigenmodes are going up by increased rotation speed. This bases on the rising loads conviction under the centrifugal force that proportional is increasing with the rotation speed. Furthermore can be established that the centrifugal force at higher rotation speeds does not advantage the effect of flutter. This causes on the diversification based on the different gradients of the eigenfrequencies (Chapter 2.3.1; Point 3).

3.4 Aerodynamic validations

The validations of static validations are realized like that: a model of a blade element with a chordline and span of each one meter is clamped on the elastic center with a spring and a damper to the ground (Figure 3.25). The degrees of freedom of the motion of the blade element can be set free or be blocked, so that it is possible to set the system to a single- or to a multiple-degree-of-freedom-system. Detail data of the profile are listed in table 3.4.

3.4. AERODYNAMIC VALIDATIONS

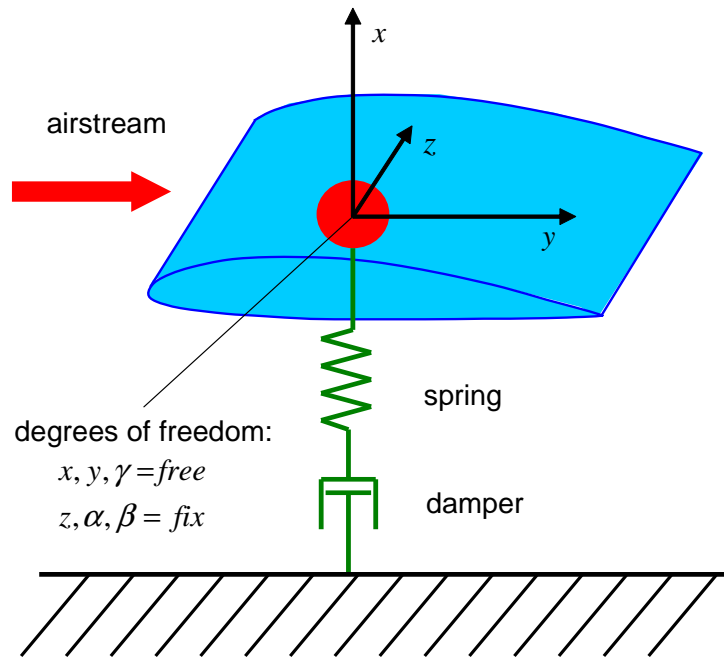


Figure 3.25: Bladeelement for static aerodynamic validations

Profil	NACA5515
Span[m]	1
Chordlength[m]	1
Position AC[m]	0.00,-0.028,0.00(x,y,z)
Mass[kg]	44.00
Distance CG -SC[m]	0.035,0.085,0.00 (x,y,z)
$I_{xx}[\text{kgm}^2]$	3.48020
$I_{yy}[\text{kgm}^2]$	0.15542
$I_p[\text{kgm}^2]$	3.51410
air density [kg/m^3]	1.22500

Table 3.4: Detail information about the profile

To check if the profile allocates the right lift, for different angle of attacks α the resulting lifts are computed for the bladeelement with only one degree of freedom, namely in x-direction. The velocity V of the wind computed of conversion of $L = \frac{1}{2}\rho V^2 S C_L(\alpha)$ and $\frac{L}{C_L(\alpha)} = 1$. $C_L(\alpha)$ is taken from the polar diagram of the profile (Figure 3.26).

3.4. AERODYNAMIC VALIDATIONS

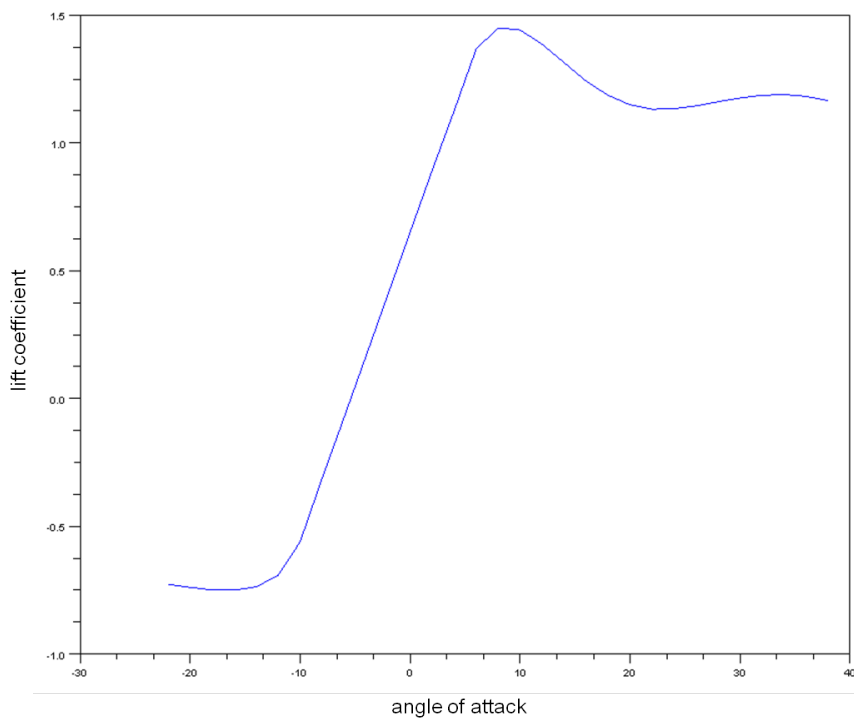


Figure 3.26: Exemplary $C_L(\alpha)$ -diagram

Simulation results can be seen in table 3.5. The results have a maximum deviation of ca. two percent.

Angle of attack α [deg]	Lift by formula	Lift by MBDyn
4	1.125	1.127
6	1.364	1.370

Table 3.5: Results of aerodynamic comparison

By using a sweep test the spring and damper parameter are defined with the goal of the approximation of this parameter to be the same as they are on the outer radius of the blade. Therefore the blade is coupled with springs and dampers in flap, edge and torsion direction. The aerodynamic and the gravitation is off and one after another the direction switched from fix to free, so that always one degree of freedom is possible. Then for every case the bladeelement is charged with an impulse in the respective direction. Through the analysis of the test readings it is possible to assign the eigenfrequency and the damping factor. The damping factor d is assigned by the logarithmic decrement λ :

$$D = \frac{\lambda}{\sqrt{(2\pi)^2 + \lambda^2}} \text{ and } \lambda = \ln \frac{x_m}{x_n} ; \delta = \omega_0 D = \frac{d}{2m}$$

where x_m = amplitude of first peak, x_n = amplitude of second peak, δ =decay constant, d = damping constant, D = damping ratio, m =mass and ω_0 =eigenfrequency of undamped system.

3.4. AERODYNAMIC VALIDATIONS

Following parameters consist for the researched bladeelement (table 3.6):

Direction	Flap	Edge	Torsion
Eigenfrequency	3.4655	3.4615	8.2417
Springstiffness[N/m,N/rad]	$2.10e^{+04}$	$2.10e^{+04}$	$1.10e^{+04}$
Dampingfactor	0.0028	0.003	0.0013

Table 3.6: Dynamic structure properties of the blade element

Some researches are done with this parameterized bladeelement . A research of the effect of the distance between AC and SC by an airspeed of $53.5 \frac{m}{s}$ is done and a research of the effect of the Theodorsen theory on the aeroelastic instabilities, too. The SC and the EC are lying on the same position and the nodes of the MBDyn model are also positioned there, so that the structural forces apply to this position (Figure 3.27).

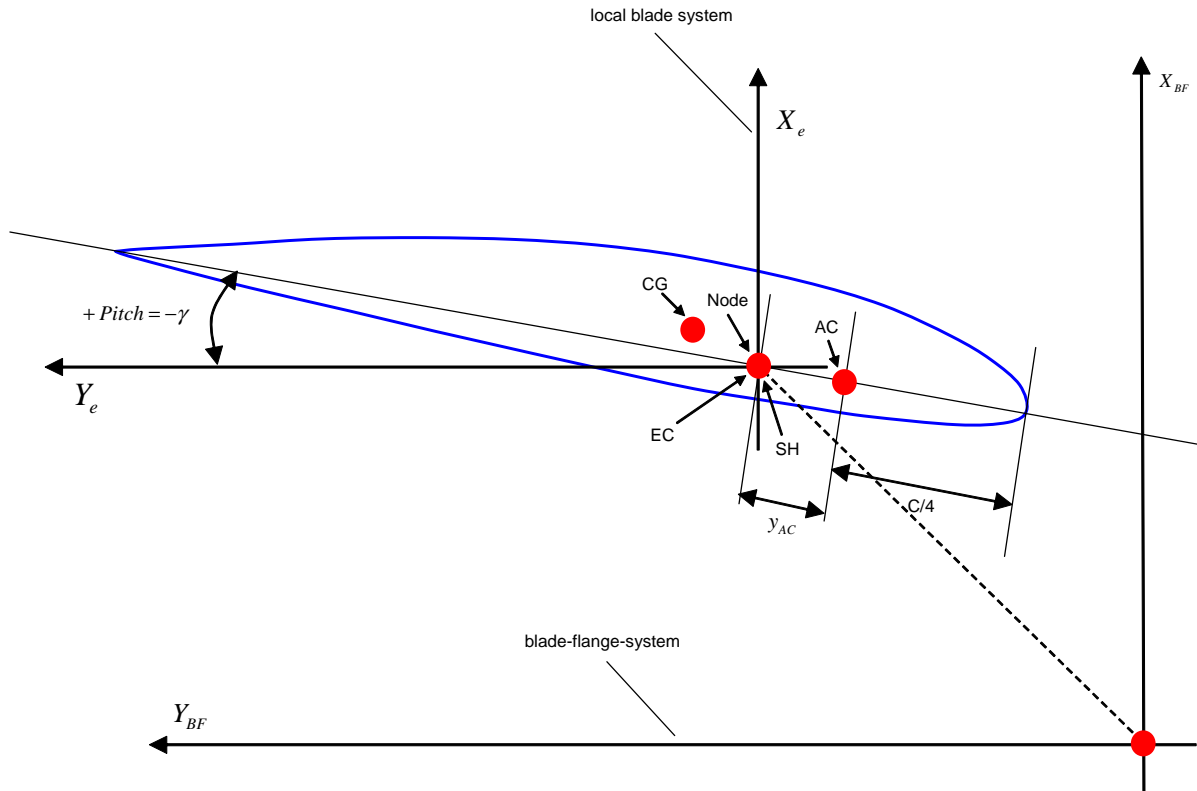


Figure 3.27: Arrangement of AC, SC, CG, EC and node position on a profile

The examination of three simulations with different distances between AC and SC shows a behavior that is well known for the theory of longitudinal stability, concerning the position of the CG related to AC . The theory of the longitudinal stability of an airfoil says that there are three category groups:

1. CG ahead AC: The additional lift adds a top-heavy/backing moment => stable behavior

3.4. AERODYNAMIC VALIDATIONS

2. CG in AC: The additional lift generates no moment, a disturbance will be preserved => indifferent behavior
3. CG aft AC: The additional lift adds a back heavy moment => instable behavior

In Figure 3.29 all three simulations are done with the same wind velocity ($53.5 \frac{m}{s}$) and with no other outer stimulation. The wind velocity of $53.5 \frac{m}{s}$ is choosen because here the profile is at its stability limit. The first row shows the results of the flap, edge and torsion motion with the original position of the SC. In the next row the distance is enhanced and in the last row it is reduced. It is nice to see that if the distance is enhanced the profile is much more instable, compared to the original distance. Contrary to this a reduction of the distance gives the profile much more stability. In the instability regions the flapwise and torsion signals are both oszilatting with ca. 7.8 Hz. This frequency lies between the flap and torsion eigenfrequency.

Furthermore the influence of aerodynamics based on the Theodorsen theory is investigated. Therefore in comparison to static aerodynamic the goal is to find the wind velocity where the blade element is getting instable. It turns out that the flutter-velocity with Theodorsen aerodynamic is round about $116 \frac{m}{s}$ (Figure 3.28). This observation fits to the theory, known by Theodorsen (2.7).

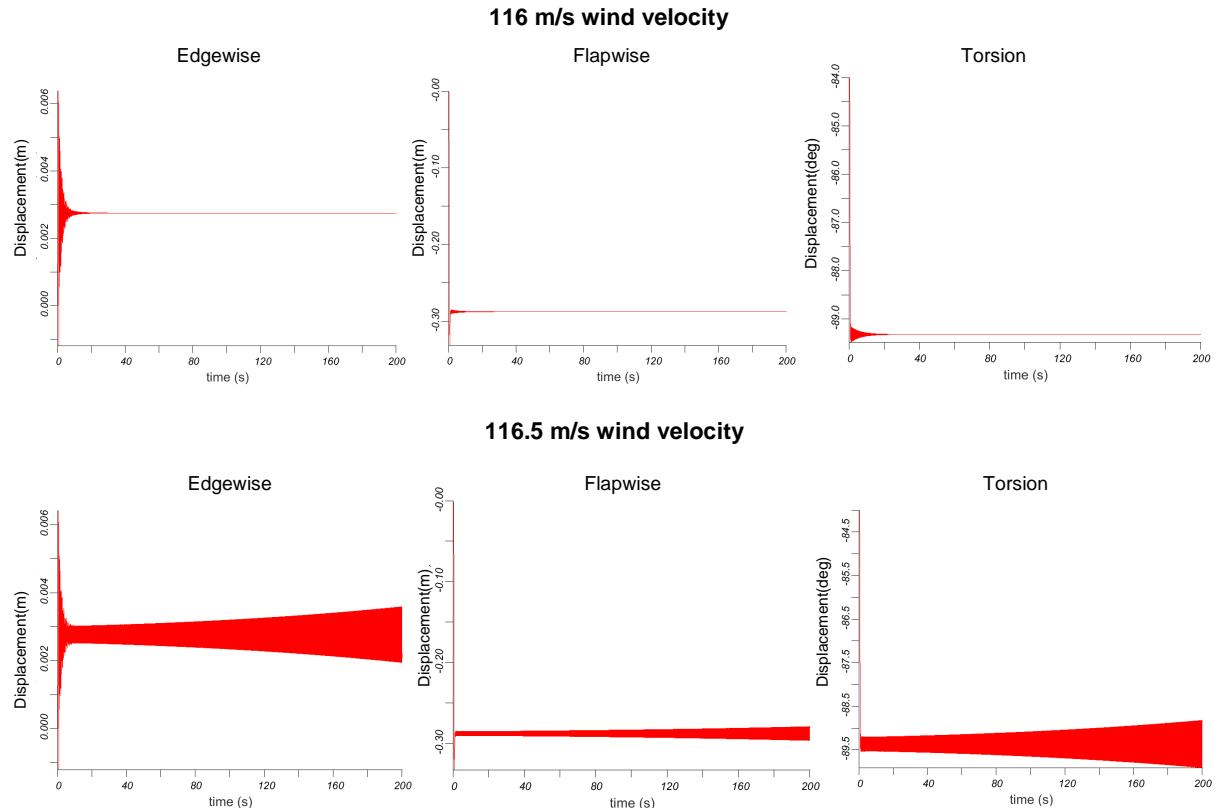


Figure 3.28: Influence of Theodorsens aerodynamic on an blade element

3.4. AERODYNAMIC VALIDATIONS

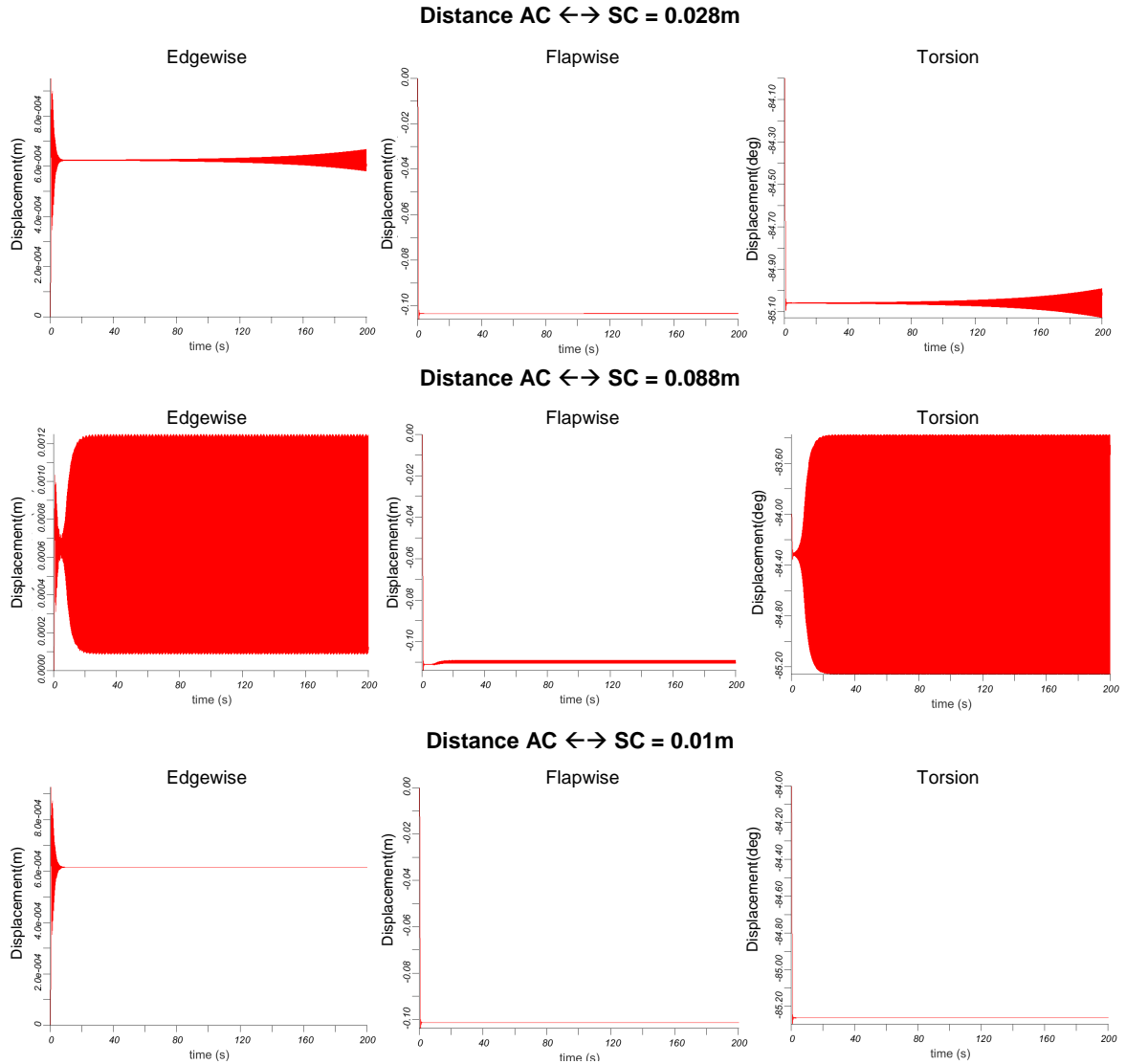


Figure 3.29: Examination of the effect of the distance between SC and AC

3.4.1 Aerodynamic load on windturbine rotorblades

In Figure 3.30 the forces in flapwise direction for four different loadcases are displayed : fixed rotor and wind (no windshear) with a velocity of 60m/s (black), no wind and a rotorspeed of 12 rpm (magenta), 12 m/s wind and 12 rpm (green) and 20 m/s wind and 12 rpm rotorspeed. In comparison to the cases were the rotorspeed is not zero the black curve shows a more flat characteristic. This bases in the fact that the 60 m/s constant affect all over the blade and the caused one on the blade design, the profiles with a relative big area/long chordline create a massive force. If the rotor rotates the maximum loads concentrate more near the tip because then the highest airstream velocities appear here and therefore the lift. The dramatic fall after node 20 is the result of the beam consideration. The forces on node 21 only consider the profilelength

3.5. RESEARCHES ON AEROELASTIC INSTABILITIES/FLUTTER IN RUNNING SIMULATIONS

of round about 1.5 meter, the other nodes consider ca. 3 meters.

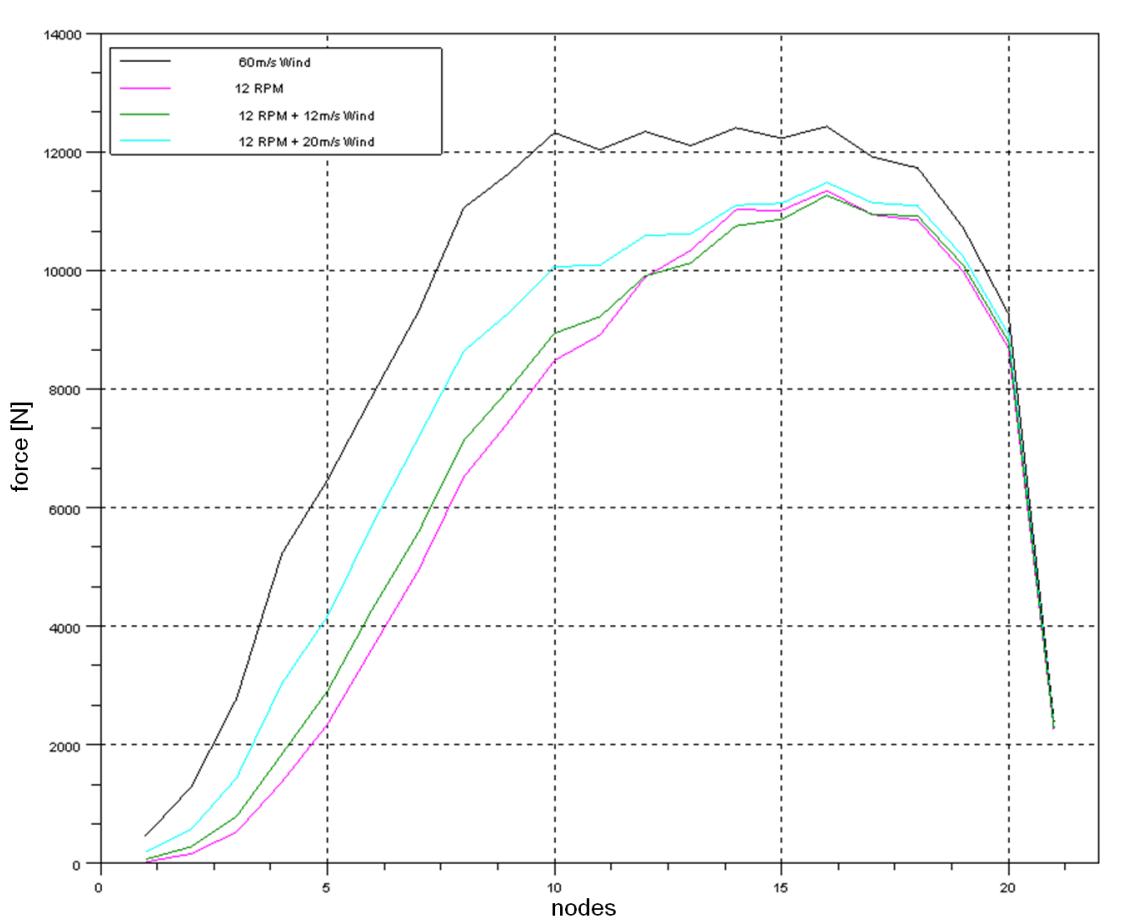


Figure 3.30: Different loadcases on a windturbine rotorblade

The difference of the magenta (only rotorspeed) and green (rotorspeed + windspeed) curve has to accent, too. It can be recognized, that the green curve lies in the outer half of the blade under the magenta one. This is caused by the alteration of the AoA, based on the influence of the incoming windspeed (Figure 3.38).

3.5 Researches on aeroelastic instabilities/flutter in running simulations

In the following chapter different simulations with full rotor and three blades will be executed. First blades are considered to be clamped fix at the rotor and the rotor is clamped fix, too. No vibrations and forces can be transmitted from one blade to the other structurally, but caused on the BEMT there is an involvement in the aerodynamic between the blades. Taking the focus on the structural and aerodynamic context in addition the influence of the gravity is neglected.

3.5. RESEARCHES ON AEROELASTIC INSTABILITIES/FLUTTER IN RUNNING SIMULATIONS

Furthermore the researches concentrate on the tip of the blades above all, caused by getting here the highest velocities and the most movement. The difference between the last five nodes is tested and can be neglected, so it suffice to look at the tip node.

There are different tools to be used for postprocessing, depending on the results people are interested in. For the animation of the deformations EasyAnim is available. This is a small OpenSource tool that can display graphically the information of the simulation. To use Blender (2.8.3) is more to recommend. Here you have also the opportunity to let the modes plot, to make movies and to get more discretion. For the numerical postprocesing there are a lot of tools written by my tutor Patrick Rix and his workmate Philippe-Emmanuel Ascar.

3.5.1 Looking on instabilities Region I

The aeroelastic instability between 100 and 200 seconds of simulation data in attachment 5.1 is shown by motion of Node 7120.

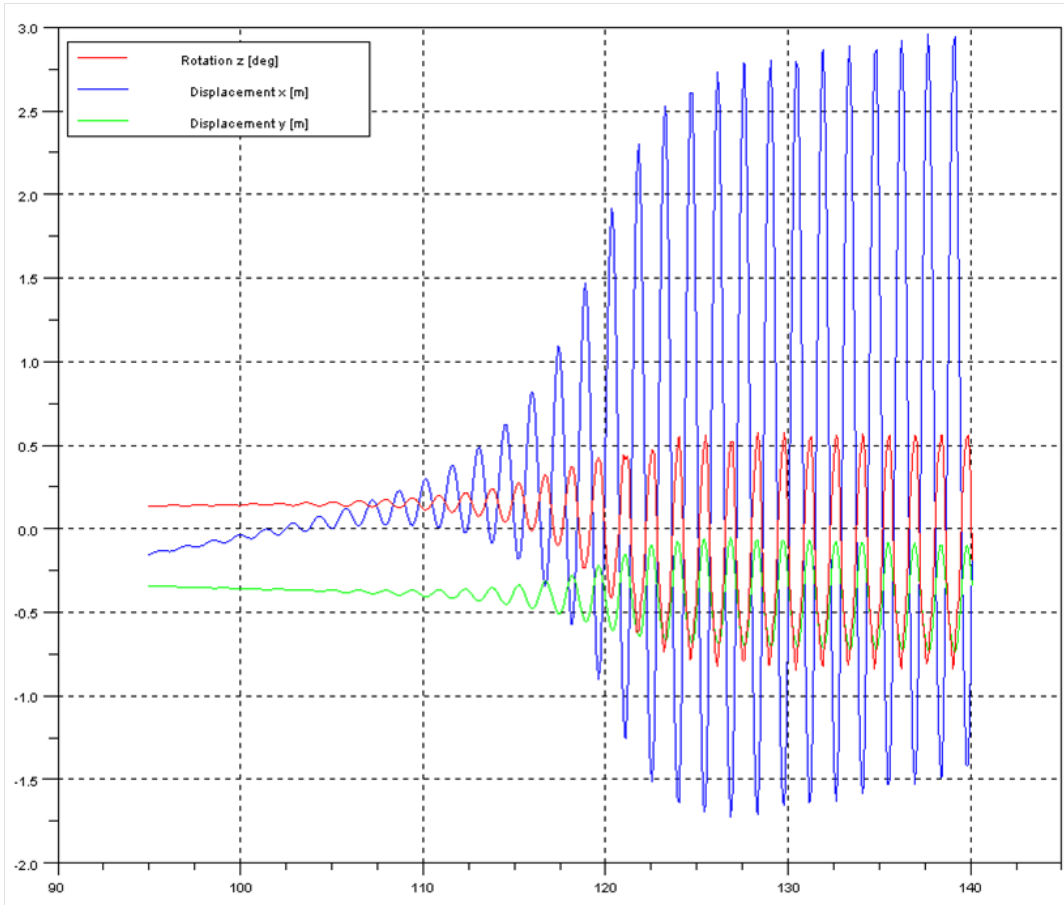


Figure 3.31: Time serie 95 - 140sec of simulation no.1

In Figure 3.31 the time serie 95 - 140 sec is plotted, where the instability emerges by a rising

3.5. RESEARCHES ON AEROELASTIC INSTABILITIES/FLUTTER IN RUNNING SIMULATIONS

amplitude of all three signals, flapwise (blue), edgewise (green) and torsion (red). The flapwise amplitude is rising from a few centimeters to more than 4 meters of deflection.

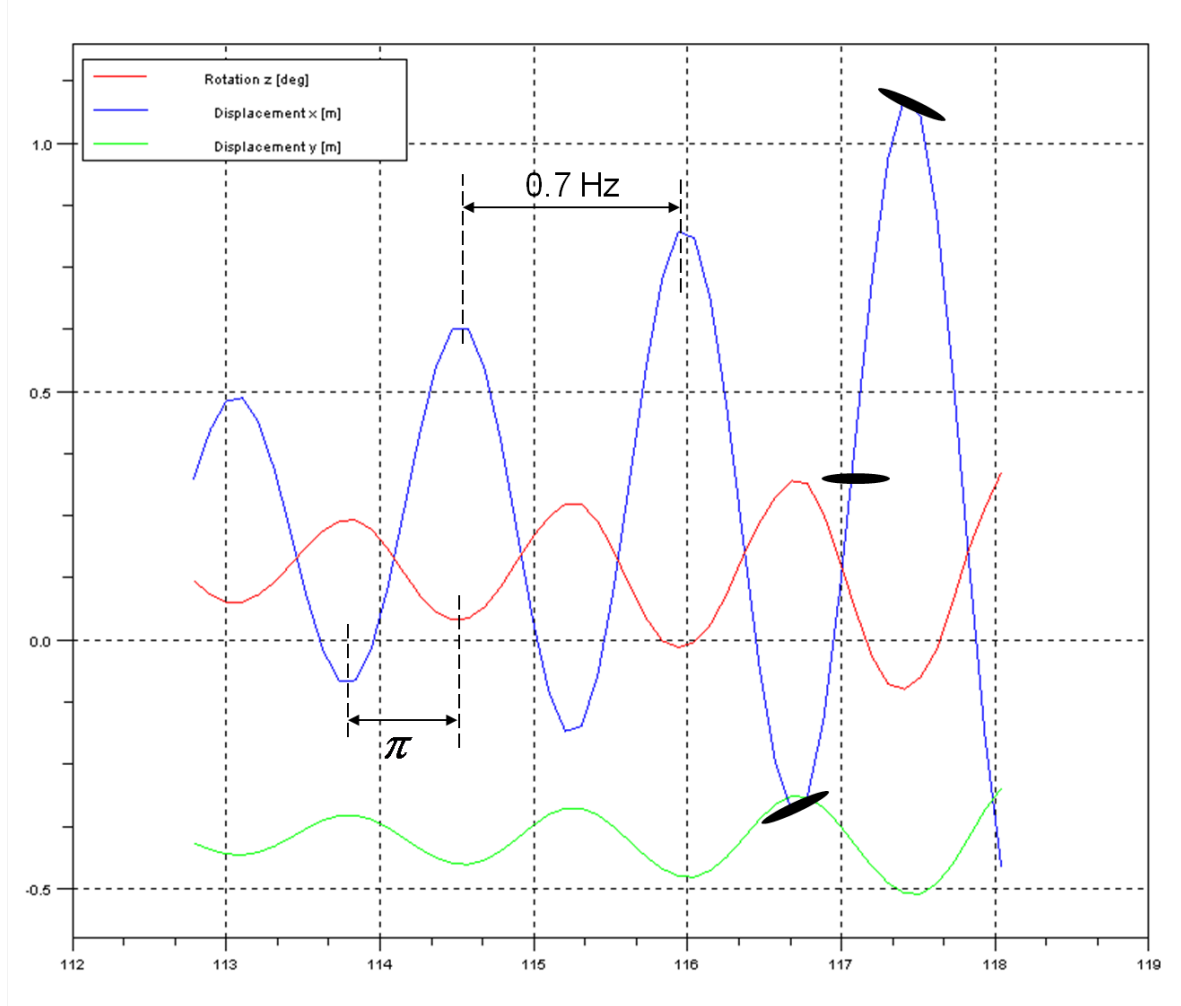


Figure 3.32: Detailed time serie

The torsion and the edgewise deflection oscillated in phase can be seen in Figure 3.32. The flapwise deflection oscillates with a gap of π in front of the torsion/edge deflection. This gap remains of the relations between the deformations based on the couple-coefficents in the stiffness matrix. Figure 3.20 shows for a load in x-direction the main component of the lift force directs in x-direction, if the blade is doing a deformation in x the torsion and the edge deformation is negative. Therefore the conclusion can be given for this observed time serie, the torsion and edge displacement occur from the deformation in flapwise direction. Another thing is good to observe in Figure 3.32. The picture shows a simplified profile (black on the last oscillation) with its

3.5. RESEARCHES ON AEROELASTIC INSTABILITIES/FLUTTER IN RUNNING SIMULATIONS

current position (flap and torsion). It is another confirmation for the results of MBDyn, because the positions show the self-stabilized properties the blade has to be developed for, contrariwise the blade would bend over and break.

To explain the excitation for the x-direction a look should be made at the forces that act over the time serie. Therefore an approach to assing the aerodynamic forces on the blade has to be done. MBDyn calculates the aerodynamic forces and moments of an aerodynamic beam for every node at every single timestep. For an energy consideration over the whole blade the nodes one and three of every aerodynamic beam have to become one node, because i.e. node three of beam 1 and node 3 of beam 2 lie on the same position and both are connected to the original node at this position (Figure 3.3).

The next step is an euler-transformation of the aerodynamic forces from the absolute (rotating) system into the relative (fixed) system. Do this by multiplication the absolute force/moment with the transformation matrix R :

$$F_r = R \times F_a$$

$$M_r = R \times M_a$$

$$R = \begin{bmatrix} \cos\beta\cos\gamma & -\cos\beta\sin\gamma & \sin\beta \\ \cos\alpha\sin\gamma + \sin\alpha\sin\beta\cos\gamma & \cos\alpha\cos\gamma - \sin\alpha\sin\beta\sin\gamma & -\sin\alpha\cos\beta \\ \sin\alpha\sin\gamma - \cos\alpha\sin\beta\cos\gamma & \sin\alpha\cos\gamma + \cos\alpha\sin\beta\sin\gamma & \cos\alpha\cos\beta \end{bmatrix}$$

After doing this the exact aerodynamic forces on every node are common and can be displayed (Figure 3.33).

The hacky characteristic annoys and has to be getting smoother. The characteristic occurs through the gauss points that are taken from the interpolation function to compute the forces. As in Figure 3.4 illustrated the gausspoints are lying at position $\pm \frac{L}{2\sqrt{3}}$ seen from the middle node of the three node beams. This signifies that the area around the middle node is by a scale of 0.268% bigger than the area around the outer points (Figure 3.34).

3.5. RESEARCHES ON AEROELASTIC INSTABILITIES/FLUTTER IN RUNNING SIMULATIONS

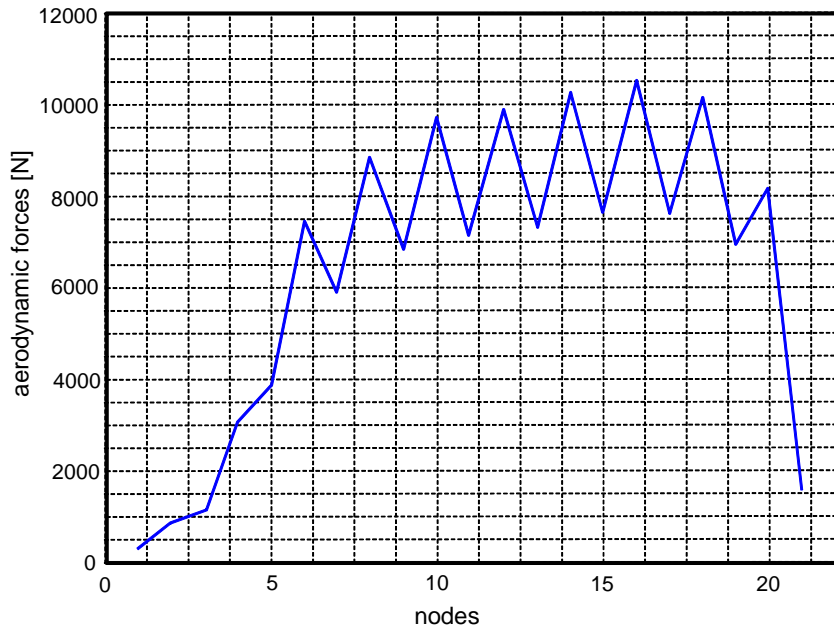


Figure 3.33: Aerodynamic forces over the blade

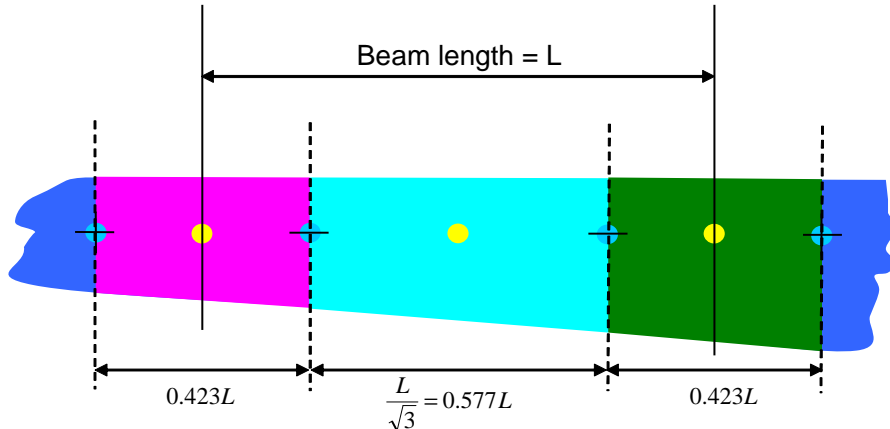


Figure 3.34: Interpolation areas on the blade

This is proved by a simple test, where a blade with a constant chord and profile simulates under constant terms. The computed aerodynamic forces, as seen in Figure 3.36 lie exactly in the same range if the force of the middle node (red) is multiplied with $1 - 0.268 = 0.732\%$ and compared with the sum of the forces (black, blue) of one of the outer nodes.

3.5. RESEARCHES ON AEROELASTIC INSTABILITIES/FLUTTER IN RUNNING SIMULATIONS

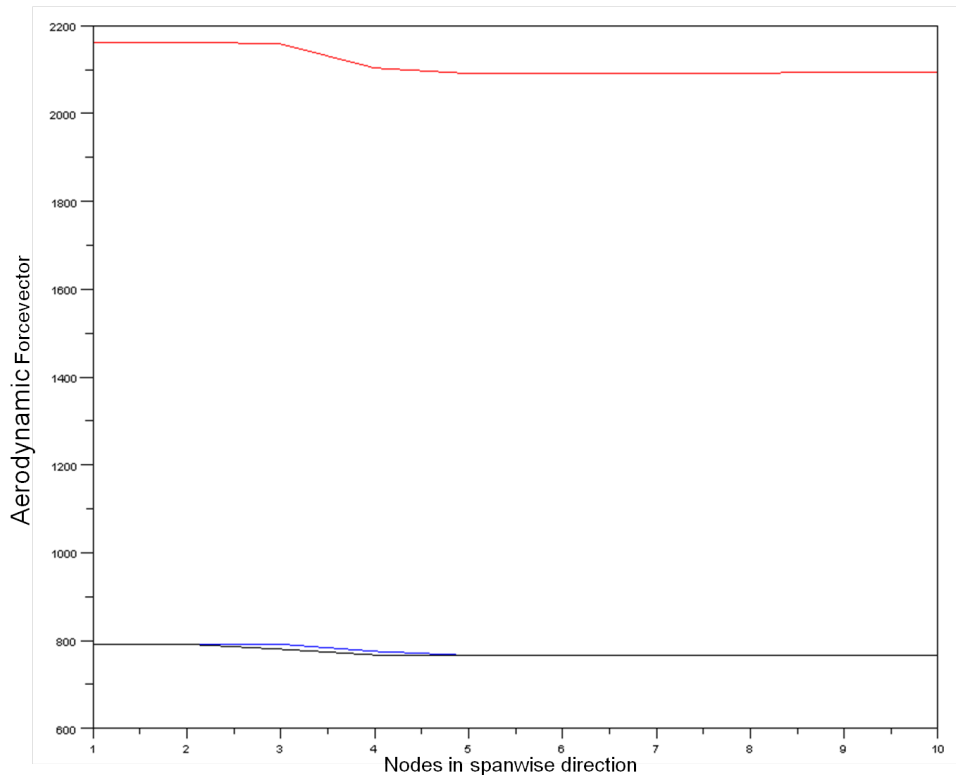


Figure 3.35: Aerodynamic forces of a constant profile in spanwise direction

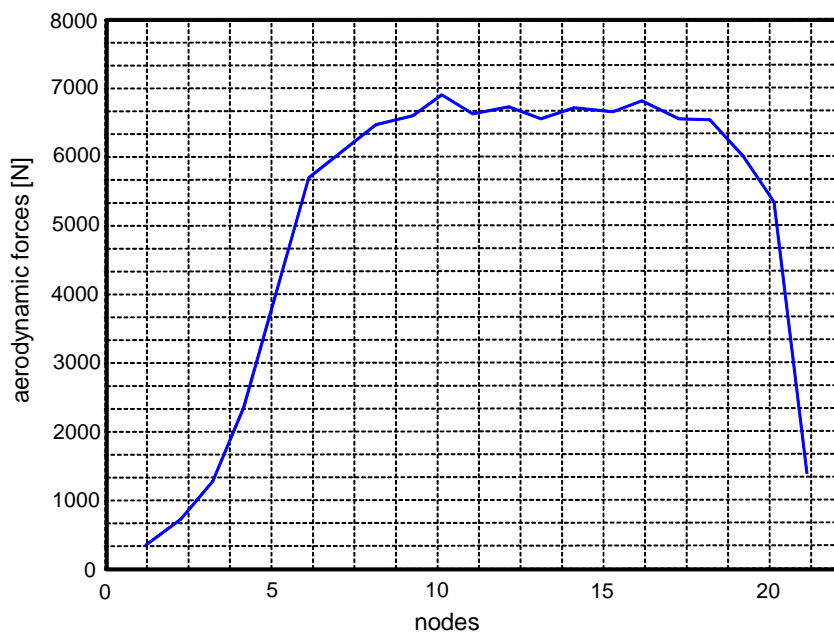


Figure 3.36: Aerodynamic forces of a constant profile in spanwise direction in consideration of gauss points positions

3.5. RESEARCHES ON AEROELASTIC INSTABILITIES/FLUTTER IN RUNNING SIMULATIONS

The force trend over the blade in spanwise direction is much more accurate (Figure 3.36) in comparison to Figure 3.33.

The force characteristic is picked out in the considered time region of 110 and 125 sec between 112 and 119 sec of node 7120 (Figure 3.37). Notice here the force is oscillating with nearly exactly the same frequency, around 0.7 Hz, the blade is oscillating in flapwise direction. This means the aerodynamic forces initiate the blade to vibrate in its first flap eigenmode (Table 3.3).

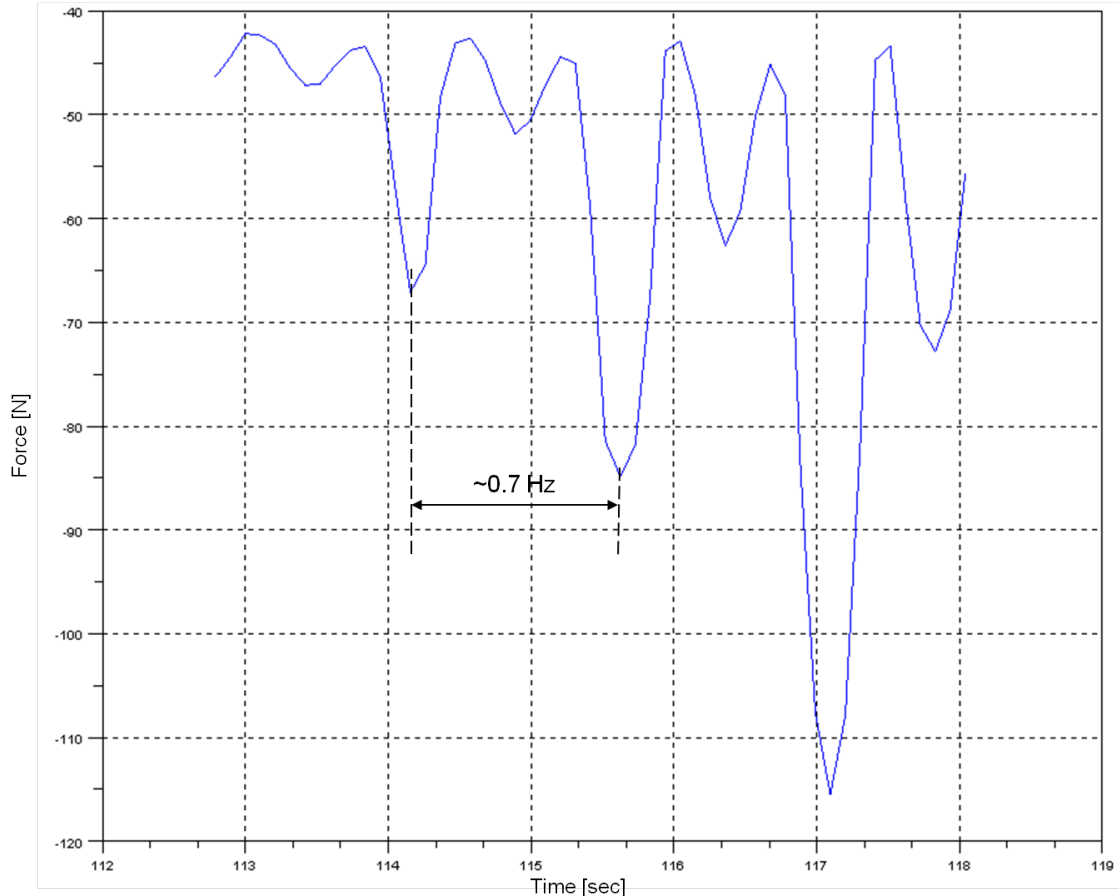


Figure 3.37: Force-characteristic 112-119sec of node 7120

The scraggy curve of the force characteristic results from the effect called stall induced vibrations. The instability emerges at a rpm of 7 and a wind speed of 13.2m/s. Here the rotation speed of the node is:

$$v_t = 2 \times \Pi \times f \times L = 43.98 \frac{m}{s}$$

f = rotation frequency

L = radial distance of the node from the center

This is a very low track speed and therefore the angle of attack is very high, here 16.7 degrees

3.5. RESEARCHES ON AEROELASTIC INSTABILITIES/FLUTTER IN RUNNING SIMULATIONS

(Figure 3.38). Notice that with a pitch of zero degrees in reality a windturbine does never a start-up, because then there have to be put rotation energy into the system.

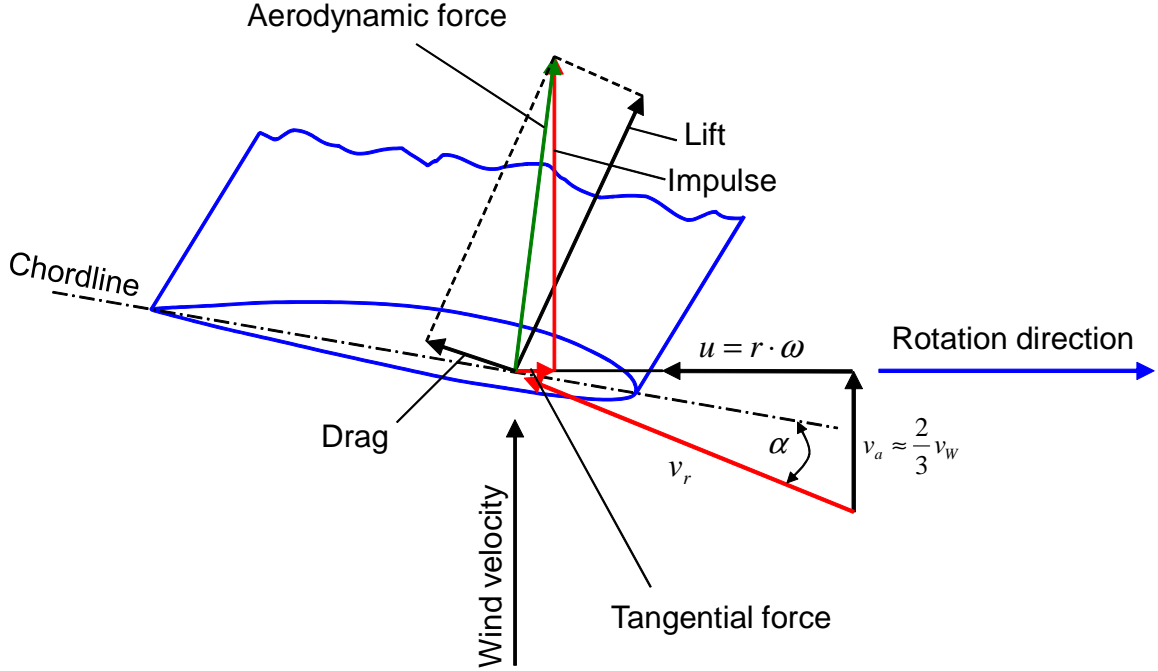


Figure 3.38: Angle of Attack

As the rpm-speed is rising the track speed gets higher and the AoA goes down. This means the $C_L-\alpha$ -diagramm comes up the other way round.

As seen in the appendix the instability caused by the stall disappears after some time and with a higher rpm. To take a closer view on the region where the instability disappears, Figure 3.39 is helpfully. The disappearance of the oscillation bases on the fact that with the rising rpm, the speed is increasing and the AoA is going down, so the CL-alpha is in a more stable region.

3.5. RESEARCHES ON AEROELASTIC INSTABILITIES/FLUTTER IN RUNNING SIMULATIONS

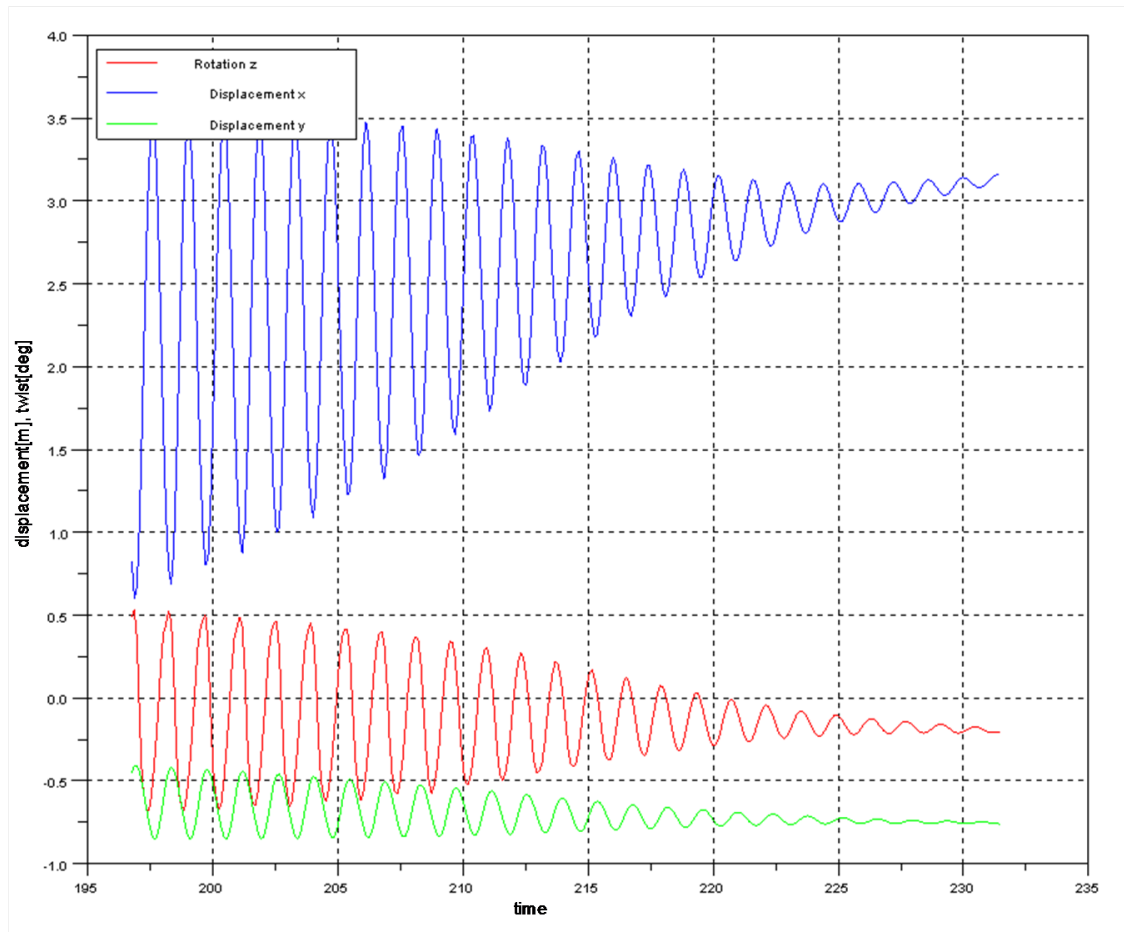


Figure 3.39: Time serie 195 - 230 sec

3.5.2 Looking on instabilities Region II

The next region where an instability arises is in the diagramm of Appendix 5.1 after 400 seconds. Surprisingly MBDyn runs into and behind this instability, while other simulation tools brake up when coming near this area.

In Figure 3.40 the flapwise signal shows a big back swing about a distance over two meters. The signal of the torsion about the Z-axis is also significant that shows relatively big oscillations with amplitudes round about 20 degrees.

3.5. RESEARCHES ON AEROELASTIC INSTABILITIES/FLUTTER IN RUNNING SIMULATIONS

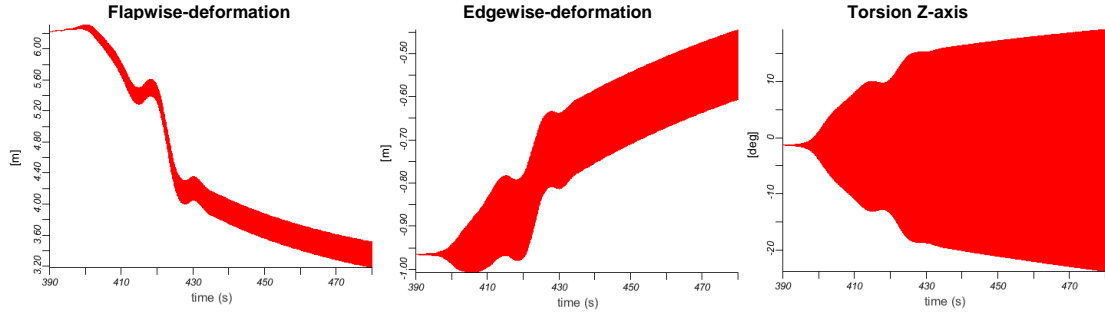


Figure 3.40: RegionII

The next Figure (Figure 3.41) displays three cuttings from region No.II in the range from 410 to 450 sec. It shows that the oscillation of the deformations in the three directions (flap, edge and torsion) have the same frequency, that is a little bit more than ~ 7 Hz over the whole time range of this instability. This ~ 7 Hz is made up of the first torsion eigenfrequency together with the fourth flap eigenfrequency of the blade. The torsion eigenfrequency is higher than the ~ 7 Hz and the fourth flap is lower than this, so coupled together they can give as a result the ~ 7 Hz.

The phase displacement of the flapwise and torsion oscillation lies between 25 and 50 degrees (Figure 3.42). The flapwise motion runs in front of the torsion with this absolute phase and therefore the theory of classical flutter is approved. It is not the 90 degree or $\frac{\pi}{2}$ of phase displacement here that the theory described, but this is only the perfect and extreme case of classical flutter. The phase displacement suffices to stimulate and hold the strong oscillation of the blade. The characteristics of the curves of the individual deformations come out of the interaction by structural and aerodynamic forces.

3.5. RESEARCHES ON AEROELASTIC INSTABILITIES/FLUTTER IN RUNNING SIMULATIONS

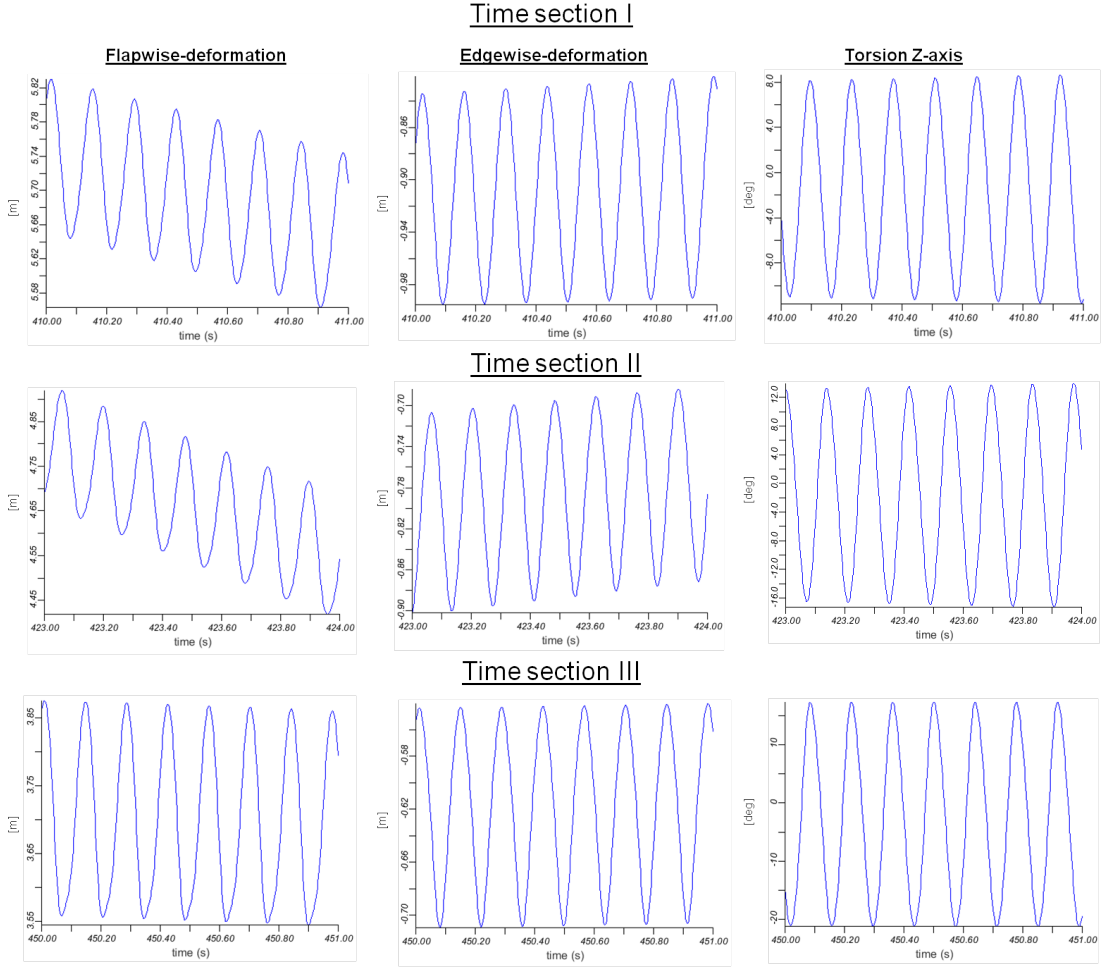


Figure 3.41: Three time sections of Region No.II

The aerodynamic forces are strongly up with the AoA and the $C_L(\alpha)$. So around 450 sec the simulation has reached a value of 20.5 rpm in its rpm ramp. This means the rotor rotation has a frequency of nearly 0.34 Hz. The characteristics of Figure 3.42 show the deformations on the tip node 7121. This means with:

$$v_t = 2 * \Pi * f * L$$

$$f = \text{rotation frequency} = 0.34 \text{ Hz}$$

$$L = \text{radial distance of the node from the center} = 63.14 \text{ m}$$

the airstream velocity is accordingly 135 m/s. The windvelocity in rotorplane is with respect to the BEMT $v_{wi} = \frac{2}{3} * 13.2 \frac{m}{s} = 8.8 \frac{m}{s}$ and with $\arctan \frac{v_{wi}}{v_t} = 3.7^\circ$ the incoming angle of the air velocity is defined. The average torsion-angle of the oscillation in Figure 3.42 is -1.9° . Therefore the profile in the sketch has an AoA of 1.8° in its neutral position.

3.5. RESEARCHES ON AEROELASTIC INSTABILITIES/FLUTTER IN RUNNING SIMULATIONS

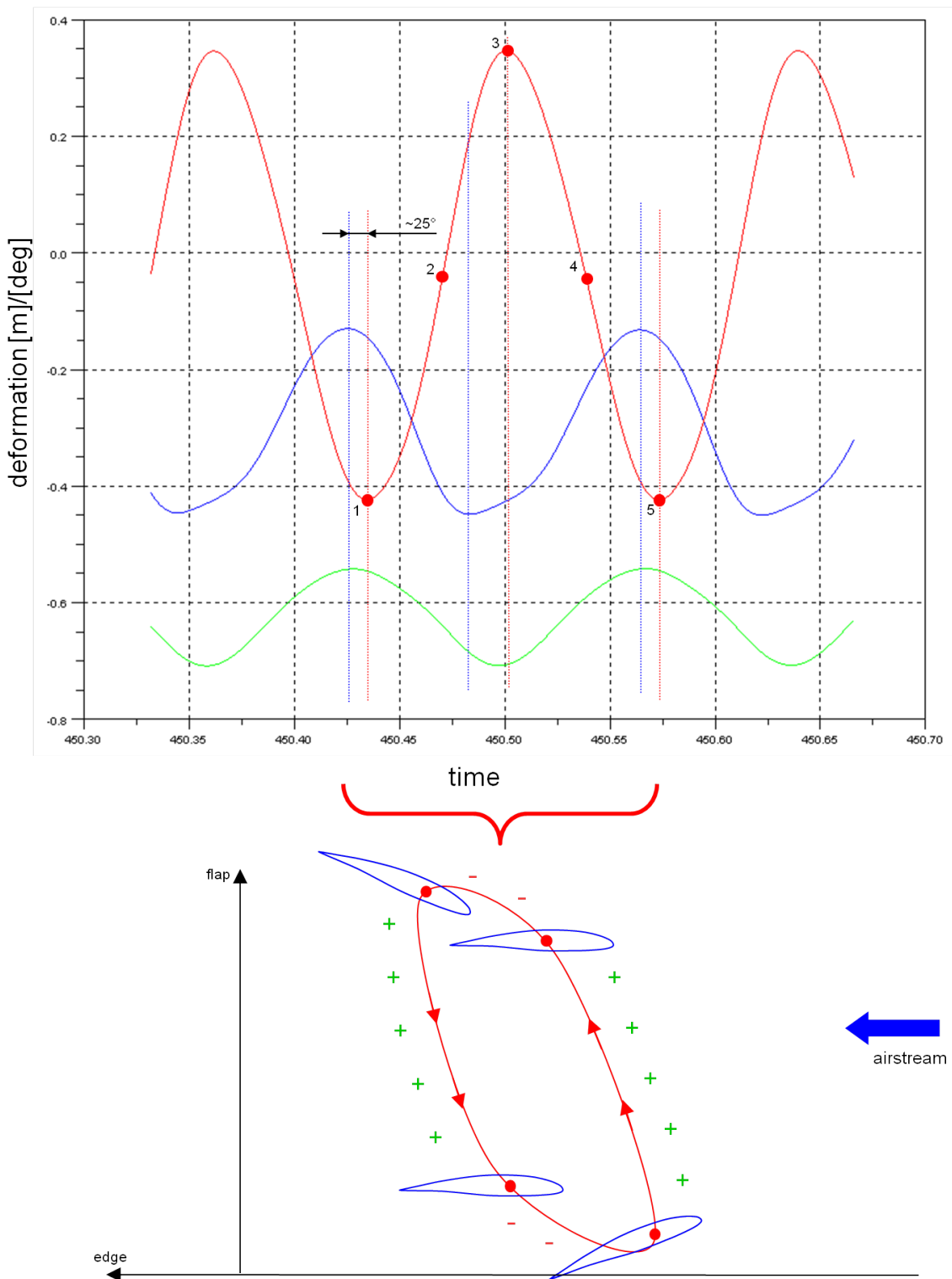


Figure 3.42: Detailed characteristics, torsion scaled by 1/50 and the middle value of flap charged with minus four, torsion (red), flap (blue), edge (green)

From this neutral position the torsion angle oscillates with an amplitude of $\sim 20^\circ$. So in both,

3.5. RESEARCHES ON AEROELASTIC INSTABILITIES/FLUTTER IN RUNNING SIMULATIONS

amplitudes of the torsion, the maximum and the minimum, the tip is provided or was provided in a stall region.

As it can be seen in Figure 3.42 with the help of the green pluses and the red minuses, the way is longer where energy is put in from the aerodynamic forces than the way where the energy acts negative on the movement.

Another question however is how the big swing back flapwise of the blade can be explained between the time range of 400 - 430 sec. This deformation bases on the characteristic of the torsion, therefore compare the two characteristics (flapwise and torsionwise) in Figure 3.43.

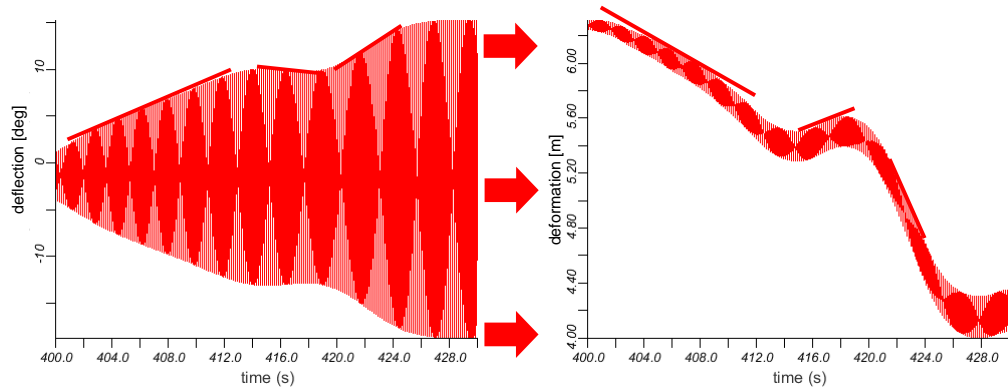


Figure 3.43: flapwise and torsionwise displacement

The gradient of the fall of the flapwise signal is addicted to the gradient of the amplitude of the torsion signal. The more the amplitude of the torsionwise oscillation is, the more the middle bending of the blade goes back. This bases on the fact that with the rise of the amplitude together with the high frequency the aerodynamic loads flapwise decrease, with higher amplitudes also the stall effect decrease the lift. This connection is shown in Figure 3.43 with help of the red bars.

As a result of this section can be retained that on the RE61.5 - blade with stationary aerodynamics fluttereffects occur at a higher rotary speed than the NREL - blade. Comparison with other simulation tools show that this result is not wrong at all. The nominal rotation speed with this blade is 12 rpm, the maximum permissible rotary speed is about 15.2 rpm. Fluttereffects occur with the assumption of stationary aerodynamics with a sufficient reserve at higher rotation speeds. In reality the appearance of this instability will be additionally retarded to higher rotation speeds through the adaptation of more realistic aerodynamics (Theodorsen, tip losses, etc...).

The conclusions of this chapter obtain in the present case from the results from the structure and aerodynamic. It is possible that based on missing local aerodynamic informations at this time other mechanism guides as well to the instability.

3.5. RESEARCHES ON AEROELASTIC INSTABILITIES/FLUTTER IN RUNNING SIMULATIONS

3.5.3 Influence of Theodorsen on the instabilities

In this section the influence of the aerodynamic based on the theory of Theodorsen will be researched. Many troubles appeared by the stability of the simulations during this research. This arise from the fact, that the aerodynamic Theodorsen model in MBDyn is still experimental [Mas10]. Therefore the following results have to be thought over.

It was very difficult to find a simulation configuration that gives useable results. In table 3.7 the configurations of different simulations are listed that were tested with the RE61.5-blade. The simulations should be run with the instability discussed in 3.5.2..

Blade	Beams	TimeStep	Wind		Density		rpm		Solver	Tolerance	Other	Status
			Time from - to	Value [m/s]	Time from - to	Value [kg/m3]	Time from - to	Value [1/s]				
RE 61.5	10	0.01	1 - 3	0 - 13.2	0 - 9.5	0 - 1.225	0 - 15 / 55 - end	0 - 12 / 12 - 40	ms = 0.6	0.001		break during run-up
RE 61.5	10	0.02	1 - 3	0 - 13.2	0 - 9.5	0 - 1.225	0 - 15 / 55 - end	0 - 12 / 12 - 40	ms = 0.6	0.001		break during run-up
RE 61.5	10	0.005	1 - 3	0 - 13.2	0 - 9.5	0 - 1.225	0 - 15 / 55 - end	0 - 12 / 12 - 40	ms = 0.6	0.001		break during run-up
RE 61.5	10	0.01	1 - 3	0 - 13.2	0 - 9.5	0 - 1.225	0 - 15 / 55 - end	0 - 14 / 14 - 40	ms = 0.6	0.001		break during run-up
RE 61.5	10	0.01	1 - 3	0 - 13.2	0 - 9.5	0 - 1.225	0 - 15 / 55 - end	0 - 16 / 16 - 40	ms = 0.6	0.001		break during run-up
RE 61.5	10	0.01	1 - 3	0 - 13.2	0 - 9.5	0 - 1.225	0 - 10 / 55 - end	0 - 18 / 18 - 40	ms = 0.6	0.001		break at 18.68 rpm
RE 61.5	10	0.01	1 - 3	0 - 13.2	0 - 9.5	0 - 1.225	0 - 20 / 55 - end	0 - 18 / 18 - 25	ms = 0.6	0.001		break at 18.68 rpm
RE 61.5	10	0.01	1 - 3	0 - 10	0 - 9.5	0 - 1.225	0 - 15 / 55 - end	0 - 12 / 12 - 25	ms = 0.6	0.001		break during run-up
RE 61.5	10	0.01	1 - 3	0 - 20	0 - 9.5	0 - 1.225	0 - 15 / 55 - end	0 - 12 / 12 - 40	ms = 0.6	0.001		break during run-up
RE 61.5	10	0.01	1 - 3 / 27 - 50	0 - 13.2 / 13.2 - 25	0 - 9.5	0 - 1.225	0 - 15 / 55 - end	0 - 12 / 12 - 40	ms = 0.6	0.001		break during run-up
RE 61.5	10	variable	1 - 3	0 - 13.2	0 - 9.5	0 - 1.225	0 - 15	0 - 12	ms = 0.6	0.001		break during run-up
RE 61.5	10	0.01	1 - 3	0 - 13.2	0 - 9.5	0 - 1.225	0 - 15	0 - 12	ms = 0.5	0.001		break after run-up
RE 61.5	10	0.01	1 - 3	0 - 13.2	0 - 9.5	0 - 1.225	0 - 15	0 - 12	ms = 0.4	0.001		break after run-up
RE 61.5	10	0.01	1 - 3	0 - 13.2	0 - 9.5	0 - 1.225	0 - 15	0 - 12	ms = 0.3	0.001		break after run-up
RE 61.5	10	0.01	1 - 3	0 - 13.2	0 - 9.5	0 - 1.225	0 - 15	0 - 12	ms = 0.6	0.01		break during run-up
RE 61.5	10	0.01	1 - 3	0 - 13.2	0 - 9.5	0 - 1.225	0 - 15	0 - 12	ms = 0.6	0.001	sh33+10%	break after run-up
RE 61.5	10	0.01	1 - 3	0 - 13.2	0 - 9.5	0 - 1.225	0 - 15	0 - 12	ms = 0.6	0.001	sh33+20%	break after run-up
RE 61.5	10	0.01	1 - 3	0 - 13.2	0 - 9.5	0 - 1.225	0 - 15	0 - 12	ms = 0.4	0.001	sh33+10%	break after run-up
RE 61.5	10	0.01	1 - 3	0 - 13.2	0 - 9.5	0 - 1.225	0 - 15	0 - 12	ms = 0.4	0.001	sh33+20%	break after run-up
RE 61.5	10	0.005	1 - 3	0 - 13.2	0 - 9.5	0 - 1.225	0 - 15	0 - 12	ms = 0.4	0.001		break after run-up
RE 61.5	10	0.002	1 - 3	0 - 13.2	0 - 9.5	0 - 1.225	0 - 15	0 - 12	ms = 0.4	0.001		break during run-up
RE 61.5	10	0.02	1 - 3	0 - 13.2	0 - 9.5	0 - 1.225	0 - 15	0 - 12	ms = 0.4	0.001		break during run-up

Table 3.7: Example list of test-simulations-paramaters

With the ten beams models none of the simulations ran as wanted. They even brake up in the run-up phase or some seconds after that. The output always lokked like Figure 3.44.

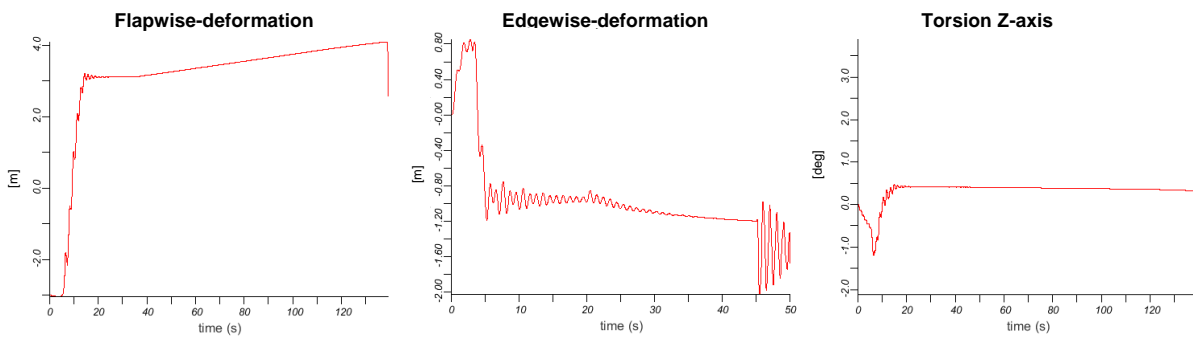


Figure 3.44: Failure during Theodorsen Simulation

There you can see a slightly fall of the flapwise bending and then the simulations stop with the cause the maximum interation number was reached. In another following test the NREL - model of a 61.5 meter blade was taken and the same simulation as with the RE61.5 - blade repeated. The NREL - blade is an older concept than the RE61.5 - blade and bases on the structural

3.5. RESEARCHES ON AEROELASTIC INSTABILITIES/FLUTTER IN RUNNING SIMULATIONS

properties of a LM -Glasfiber blade. This blade has no sensible data and can therefore be send without any trouble or problems to other institutions if help is needed. More about the NREL - blade can be read in source [Jon09] and detailed blade data can be found in the Appendix 5.2. The torsional stiffness of the NREL - Blade is the major difference in comparison to the RE61.5 - blade. It is much softer and thererfore the torsional eigenfrequency is much lower, around 5 Hz, and though closer to the other eigenfrequencies, of maybe flapwise or edgewise. Hence the flutter effect is based on this fact it is former expected than by the RE61.5 - blade.

Looking at the simulation results there are no big differences. First good progress is made by taking lesser beams on the NREL - model. With a five beam NREL - model of a 61.5 meter blade the biggest advantage is the reduction of 20 - 30 % of the calculation time of the simulation. This is a big plus when a lot of test simulations have to be done. The next step is to find an almost solid simulation of the Theodorsen aerodynamic which can be compared to the stationary aerodynamic under equal terms . After several test simulations the terms of this one stable simulation (Figure 3.45 and Figure 3.46) are

- Wind and density ramped up on an cosinus-ramp to their final value ($\rho = 1.225 \frac{kg}{m^3}$, $v_w = 13.2 \frac{m}{s}$) inside of five seconds from zero .
- RPM ramped up on a cosinus-ramp from 0-10 rpm in 0-5 seconds, then be constant until 20 seconds, and then be ramped up with a gradient of 0.167 rpm/sec
- Time step has to be set by a value of 0.02sec

During the multiple simulations it exposes that the major indicators for a simulation that runs over instability is the adjusted time step and the gradient of the time ramp. Already little changes of one of this values make the simulation to break up further. So for example, if the time step was changed from 0.02 sec to 0.01 sec, that is a higher time discretisation of the problem, it tends to no passable results.

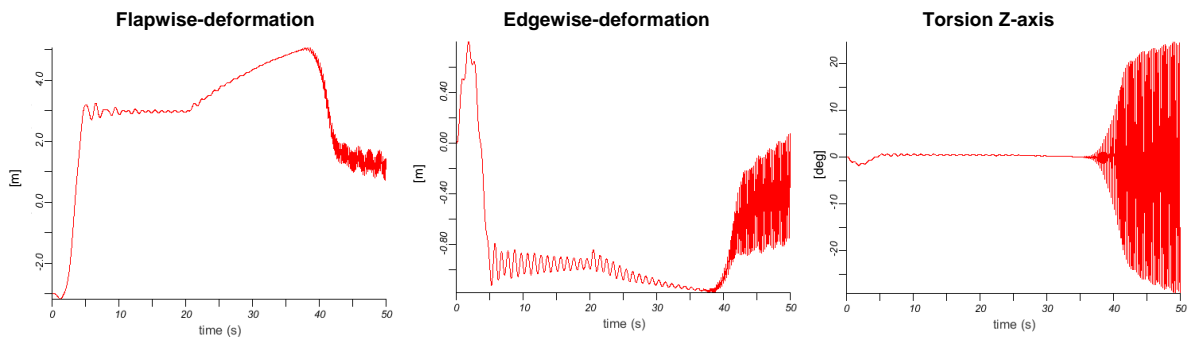


Figure 3.45: C81 Aerodynamic

3.5. RESEARCHES ON AEROELASTIC INSTABILITIES/FLUTTER IN RUNNING SIMULATIONS

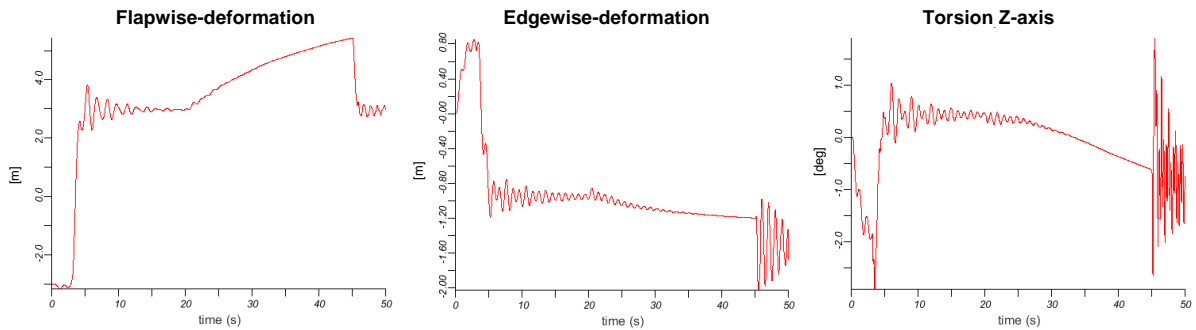


Figure 3.46: Theodorsen Aerodynamic

In comparison to the two Figures 3.45 and 3.46, both simulations realised under further described parameters, it stands out that the characteristic of the Theodorsen simulation has not the high frequencies in oscillation. The maximum amplitude of the torsion signal is also only $\frac{1}{10}$ of the torsion signal with stationary (C81) aerodynamics. The flap- and edgewise signals are in the same range of deformation in both simulations.

If this inconsistencies (the Theodorsen aerodynamics are still experimental) are ignored it can be clearly seen that the instability in both simulations arise at different times. The instability at the stationary aerodynamic arise at ~ 38.5 sec or ~ 13 rpm and the other one with the Theodorsen aerodynamic arise at ~ 44 sec or 14.2 rpm. So it succeeds to demonstrate here the theory of Theodorsen and former studies with MBDyn [Lob04, Lob05]. With the help of deceleration of the airstream caused by turbulences behind the blade the appereance of instabilities can be delayed and be pulled to higher rotary speeds.

Unfortunately this comparison is actually not possible with a RE61.5 - blade. With a five beam RE61.5 - blade model and the simulation parameter above and with other changed parameters it is not possible at this time to get a simulation with both aerodynamic models which can be compared with one another. This bases presumably on the fact, that the RE - model stiffnesses are not that uniform like the stiffnesses of the NREL - model. For example the torsion stiffness of the RE61.5 - blade is considerably stiffer in the first half of the blade compared to NREL, but on the way to the tip the stiffness strongly decreased. This produce, looking on the higher torsion eigenfrequency of the RE61.5 - blade, a torsion stiffer RE61.5 - blade in comparison to the NREL.

The Theodorsen aerodynamic model will also cause an adjustment to higher rotary speed on the RE61.5 - blade . But in comparison to the NREL blade, where the difference in rotary speed between stationary and theodorsen aerodynamics placed by ~ 1.2 rpm, the difference between the rotary speeds by the RE61.5 - blade will be higher. This perception is obtained from the knowledge that the torsion-eigenfrequency is substantial higher in dimension than the torsion-eigenfrequency of the NREL-blade.

Seen in other simulations, that the instability with the same characteristics, as seen here by the

3.5. RESEARCHES ON AEROELASTIC INSTABILITIES/FLUTTER IN RUNNING SIMULATIONS

NREL - blade, are therefore occurred at higher driving speeds of the rotor. Higher driving speeds of the rotor means higher velocity of approach for the airfoils and caused by the dependency of the Theory of Theodorsen by the reduced frequency the influence of the deceleration of the airstream increases with higher velocities. So the distance of the appearance of the instability between the two aerodynamic models is bigger than the ~1.2 rpm at the NREL- model, where the instability occurs around 14 rpm. The instability at the RE61.5 - blade occur with stationary aerodynamic primary at an essential higher rotation speed.

In the last passage the instability in Figure 3.45 and 3.46 that arises around 40 sec is talked about. A section of the instability region of the stationary aerodynamic simulation can be seen in the next Figure 3.47. Only in the simulation with the stationary aerodynamic about it can be said something about the origin of the instability. The characteristic of the Theodorsen aerodynamic simulation is unfortunately too erratic.

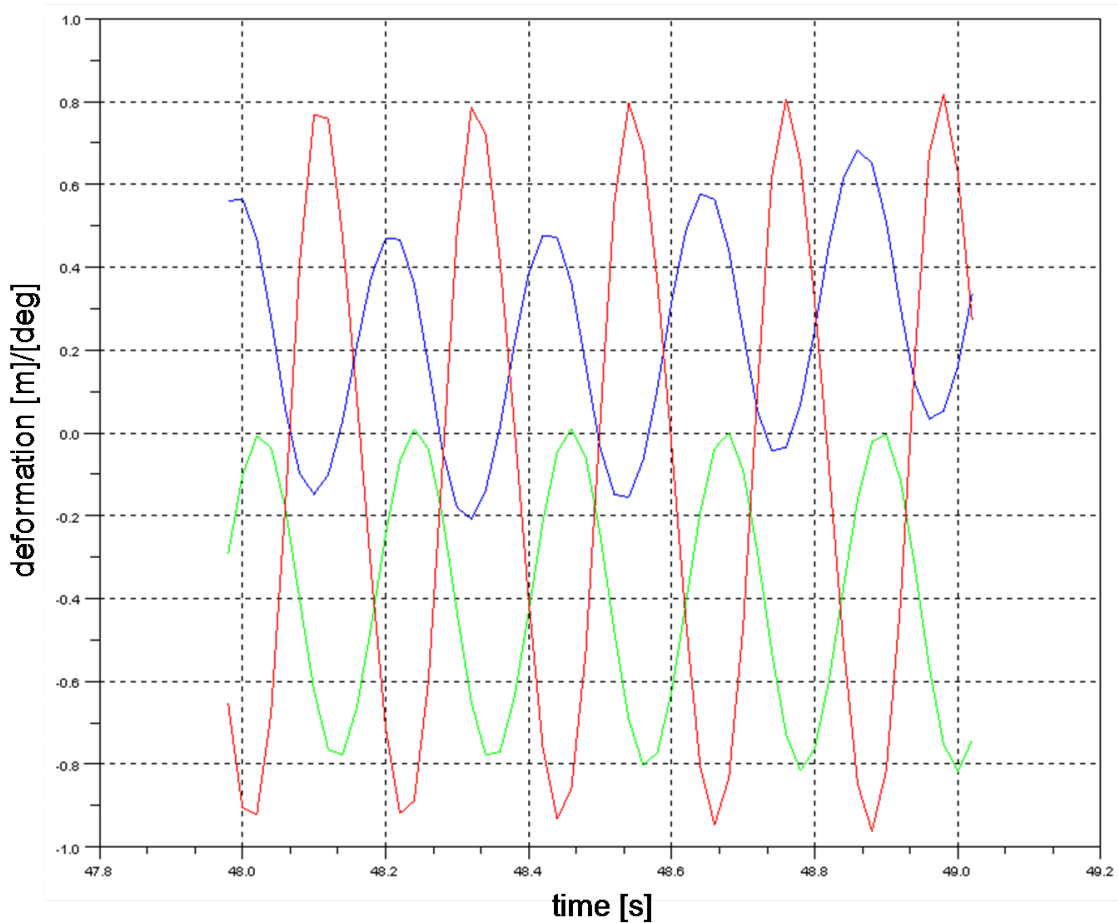


Figure 3.47: Time section around 40sec

If neglected the scraggy characteristic based on the relative high time step of 0.02 sec of the simulation, it can be noticed that here it is the same characteristic to be found as in subsection

3.5. RESEARCHES ON AEROELASTIC INSTABILITIES/FLUTTER IN RUNNING SIMULATIONS

3.5.2. Again the blade is oscillating in a flutter mode, but this time with a higher amplitude flapwise, about one meter. This higher amplitude bases among other things, that on here the NREL - blade oscillates with a frequency around 4.8 Hz, so less than the 7 Hz of the RE61.5 - blade. Therefore the movement of the blade flapwise has more time to form farther to higher amplitudes. Another thing can be that the NREL-blade correlates with another flapwise eigenmode than the RE61.5 - blade, because with a first flap eigenmode higher amplitudes at the tip are significant possible than with i.e. the fourth flap eigenmode.

After the simulation with this defined parameter runs “well” and the first simulation with the five beams model did not run as wanted and are showing the same characteristic like the ten beam model, it is tested if with this defined parameter maybe the ten beam model runs, too as well. The experiment worked. In Figure 3.48 is displayed two simulations, one with the five beam model, one with the ten beam model, both with the same parameters.

Compared to the ten beam model is remarkable that the five beam model records higher amplitudes in the high-frequency oscillation and the instability region starts after 45 sec and not like the ten beam model does. This can be explained by the fact that on the five beam model all beams are 100% longer than the beams of the ten beam model. Comparing a long beam with a shorter beam, both with the same cross section and the same properties, the longer beam will act more softer in torsion than the short beam if applying a load at the end. Therefore the five beam model has a lost in torsion stiffness counterpart to the ten beam model. This has to be considered when changing the number of beams of a model among other things.

3.5. RESEARCHES ON AEROELASTIC INSTABILITIES/FLUTTER IN RUNNING SIMULATIONS

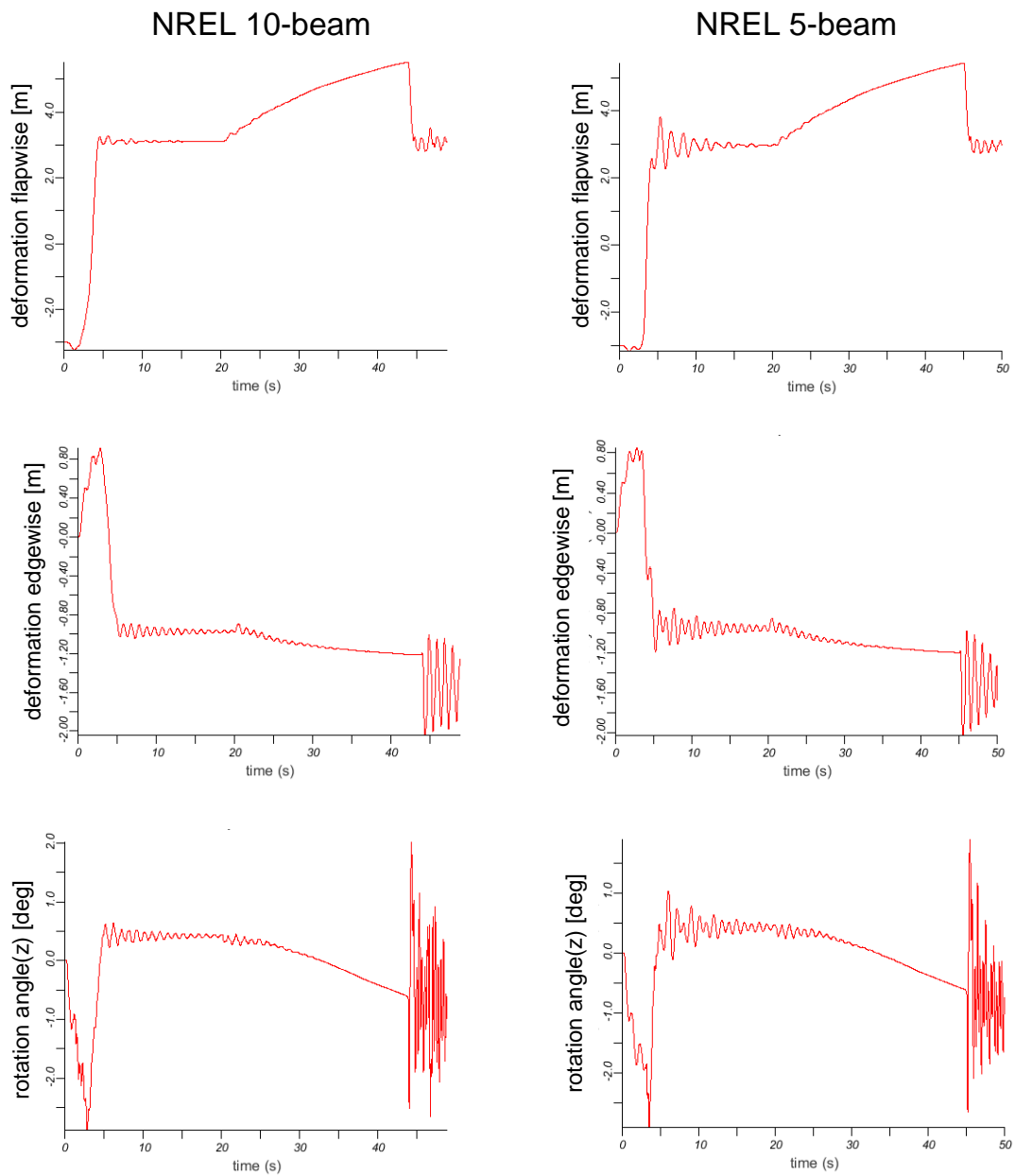


Figure 3.48: Comparison between NREL 5 beam and 10 beam model

Chapter 4

Conclusion and outlook

The validation of models from the modelgenerator is successfully finished as planned. During this process failures are solved and important systemparameters are determined. The validation also demonstrates that in the modelling of simplified beam models there is still a big improvement possible. The approximation of stiffnesses over a specific length, for example a section of a blade as a beam, is nowadays under research by different institutes. A better solution than the integration methods used today, can bring a lot more accuracy and the differences to an FEM- model are declined. Nevertheless the results of this validation under consideration of a less tolerance illustrate physically reliable movements of a rotorblade under loads. Displacements, eigenmodes and eigenforms are nearly equal to other simulation tools.

During the conducted flutter analysis both used blades, the RE61.5 - blade and the NREL-blade, showed an insertion of flutter with stationary aerodynamics at relatively low rotation speed. It is also demonstrate that with non stationary aerodynamics, like Theodorsen aerodynamics, the appearance of flutter occur at higher rotation speeds. By reason of time other effects like tip losses, influence of gravity, gust wind, etc. could not be considered, but other studies show that this effects in sum delay the arise of flutter. The simulations in this thesis demonstrate with the illustration of aeroelastic instabilities, like stall induced vibration and flutter, that MBDyn and the generated models have the ability to display the high dynamic oscillations on windturbine rotorblades. Middle-term MBDyn will become accepted to other multi-body simulation tools in the wind energy sector, like FLEX5® where the torsion is calculated by values from static examination based on the limited degrees of freedom.

Next time a research under realistic aerodynamic influences has to be done. Due to the bordered options of the MBDyn intern aerodynamic an integration of the aerodynamic of AERODYN is advisable for the future. Furthermore it is then possible to validate with other internal used software.

A consideration of the local aerodynamics is required for an exact classification of the fluttereffect. But this is only possible with aerodynamic models, which are not dealing with the BEMT.

As soon as a better approximation of different stiffnesses in one beam is possible this should be integrated in the modelgenerator to get better results of the structural side of the rotorblades.

Bibliography

- [Bur01] Tony Burton. *Wind Energy Handbook*. John Wiley & Sons,Ltd, 2001.
- [Dow04] Earl H. Dowell. *A Modern Course in Aeroelasticity*. Springer Science + Buisness Media, 2004.
- [Gas87] Robert Gasch. *Strukturdynamik*. Springer Verlag, 1987.
- [Han01] Martin O.L. Hansen. *Aerodynamics of Wind Turbines*. Earthscan - James & James, 2001.
- [Han06] M.H. Hansen. Improved modal dynamics of wind turbines to avoid stall-induced vibrations, 2006.
- [Han07] Morten Hansen. Aeroelastic instability problems for wind turbines, 2007.
- [Hau03] Erich Hau. *Windkraftanlagen. Grundlagen, Technik, Einsatz, Wirtschaftlichkeit*. Springer Verlag, 2003.
- [Ing05] Grant Ingram. Wind turbine blade analysis using the blade element momentum method, 2005.
- [Ins10] German Wind Energy Institute. <http://www.dewi.de>, 2010.
- [Jon09] J. Jonkman. Definition of a 5-mw reference wind turbine for offshore system development. <http://www.energiasrenovables.ciemat.es/adjuntosdocumentos/NUSA2.pdf>, 2009.
- [Lei06] J.Gordon Leishman. *Principles of Helicopter Aerodynamics*. Cambrigde University Press, 2006.
- [Lob04] D.W. Lobitz. Aeroelastic stability predictions for a mw-sized blade, 2004.
- [Lob05] D.W. Lobitz. Parameter sensitivites affecting the flutter speed of a mw-sized blade., 2005.
- [Mas09] Pierangelo Maserati. *MBDyn Theory and Developer's Manual*. Dipartimento di Ingegneria Aerospaziale Politecnico di Milano, 2009.

BIBLIOGRAPHY

- [Mas10] Pierangelo Maserati. *MBDyn Input File Format, Version 1.3.14.* Dipartimento di Ingegneria Aerospaziale Politecnico di Milano, 2010.
- [Sne04] H. Snel. Application of a modified theodorsen model to the estimation of aerodynamic forces and aeroelastic stability, 2004.
- [The34] Theodore Theodorsen. Gerneral theory of aerodynmaic instability and the mechanism of flutter, 1934.

Chapter 5

Appendix

5.1 Simulation I

The following results of interested sensors are from a Simulation with the RE61.5 - blade with C81 - aerodynamic and ten beams. The wind is ramped from one to three seconds to its then constant value of 13.2 m/s and the air density reaches its value of $1.225 \frac{kg}{m^3}$ at 9.5 sec. The simulation starts with a rpm of zero. It is ramped by a cos-curve to 5 rpm between 0-15 sec and then it is linear rising so that it reaches 40 rpm by 1000sec (~ 0.8 rpm/sec). It is always the defomation of the tipnode (MBDyn node 7121) considered.

The area around 600 sec and behind 780 sec can be disregarded caused by numerical failure.

Simulation results:

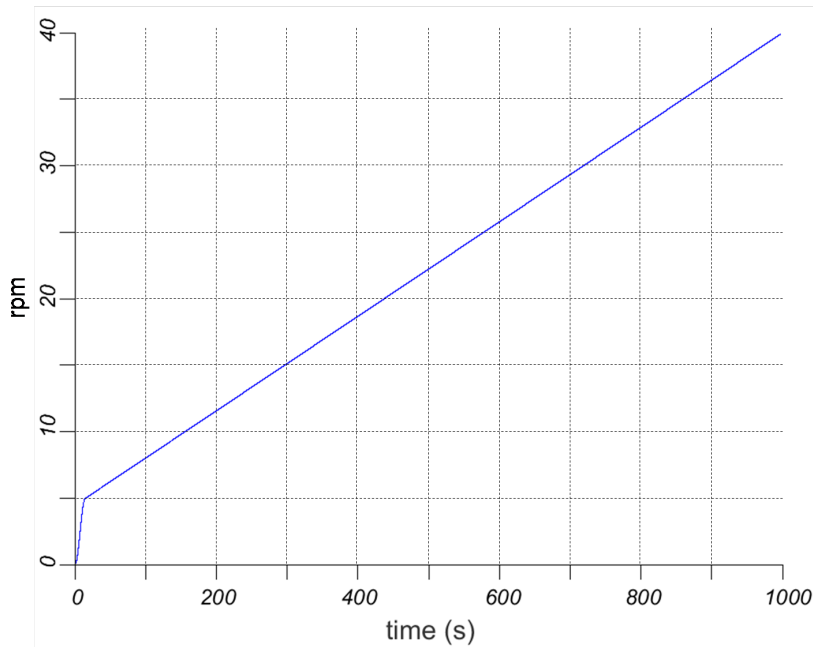


Figure 6.1: RPM-ramp

5.1. SIMULATION I

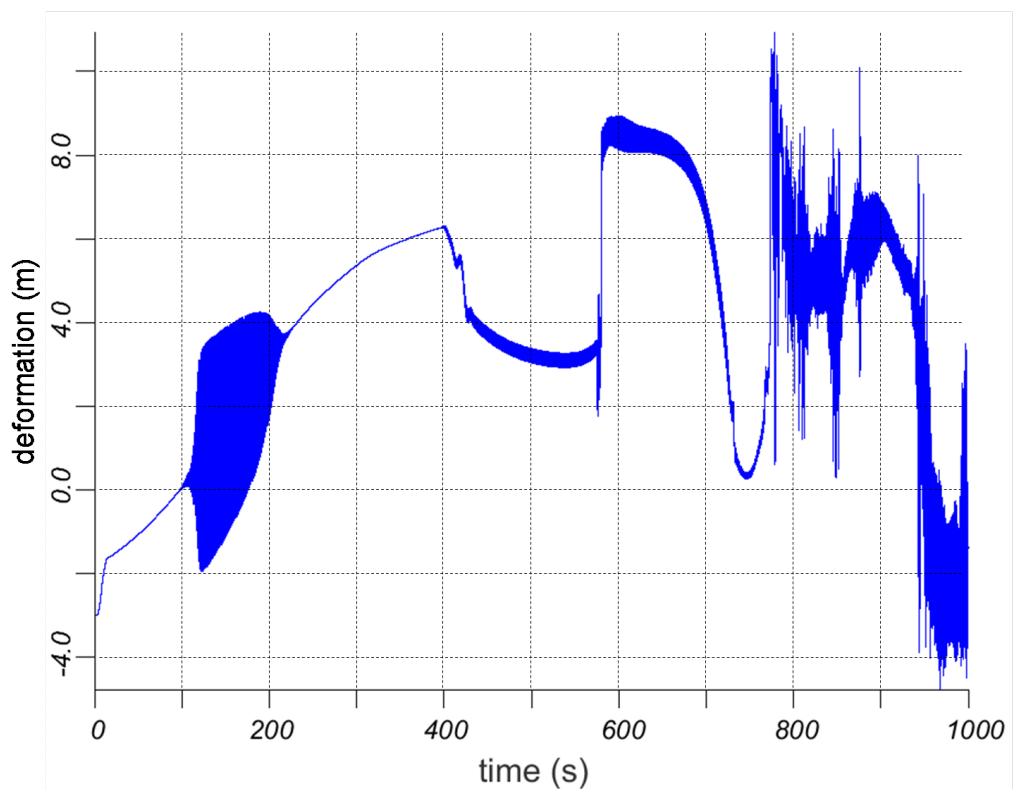


Figure 6.2 : Flapwise deformation

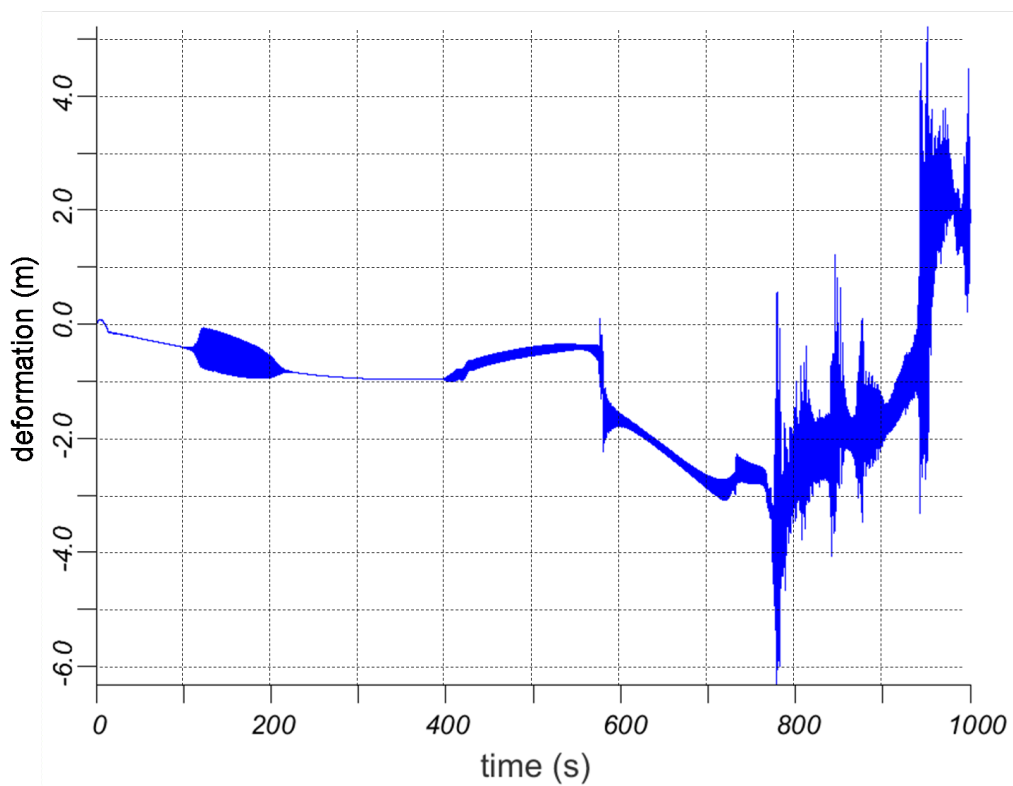


Figure 6.3 : Edgewise deformation

5.1. SIMULATION I

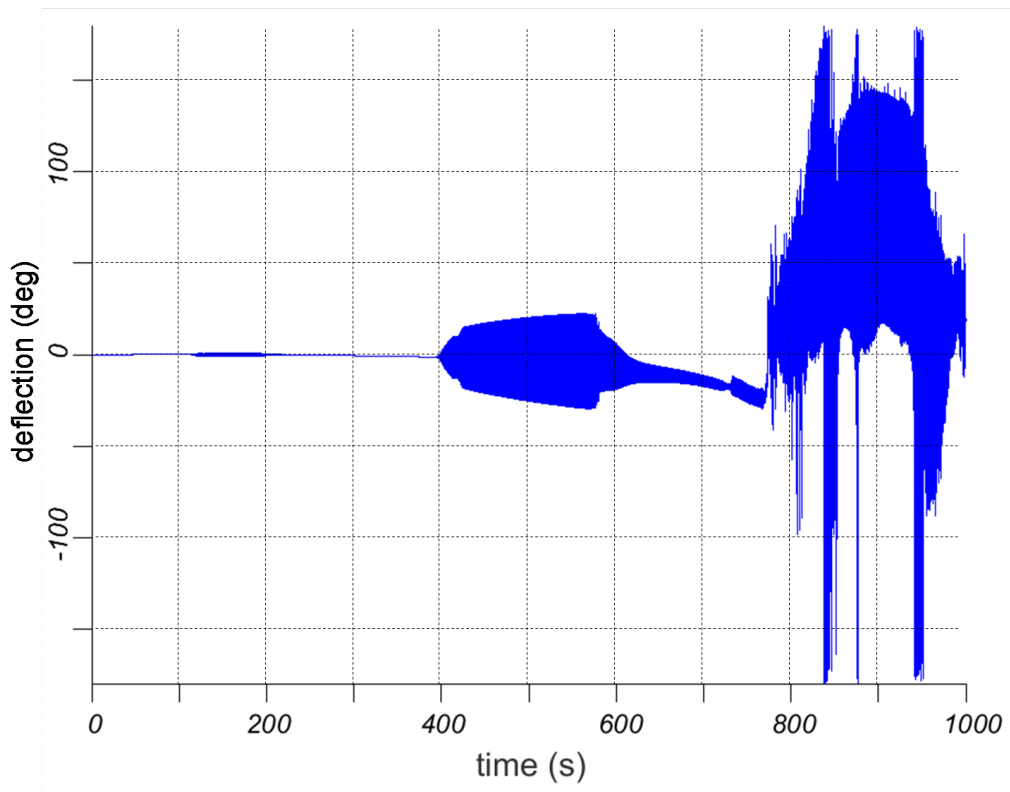


Figure 6.4 : Torsionwise deformation

In another research the windturbine raised up to 15 rpm, to avoid the stall effects. The wind is constant without windshear or any turbulences with a speed of 13.2 m/s. The aerodynamic model is static wind, without windshear, tip losses, Theordorsen, etc.. When 15 rpm is reached, the rpm is slowly increasing with a rate of 0.8 rpm/min.

5.1. SIMULATION I

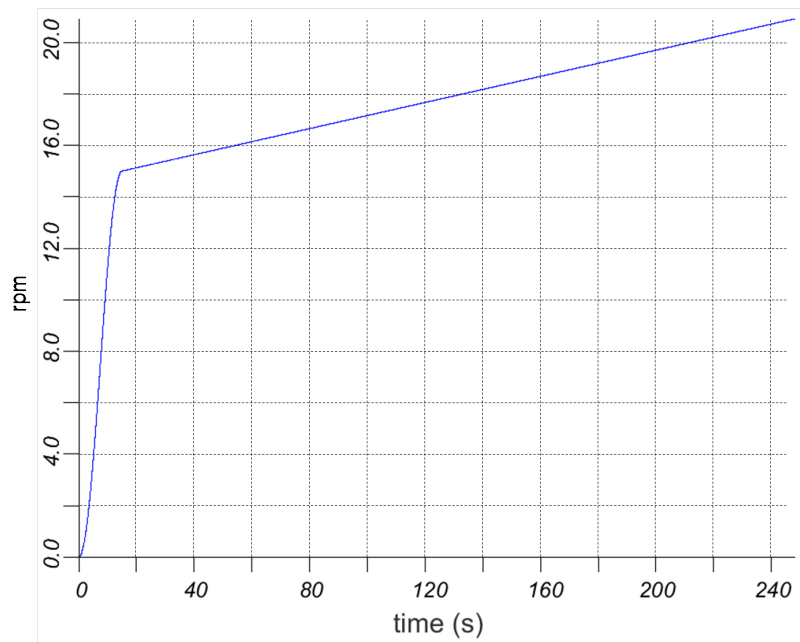


Figure 6.5: RPM-ramp

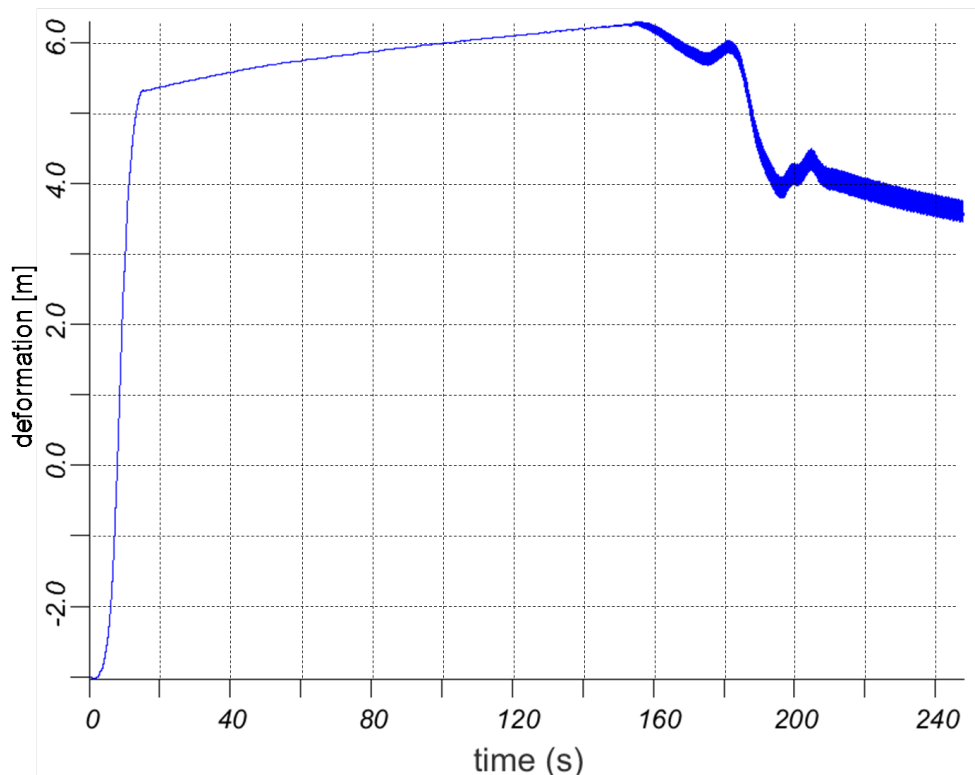


Figure 6.6: Flapwise deformation

5.1. SIMULATION I

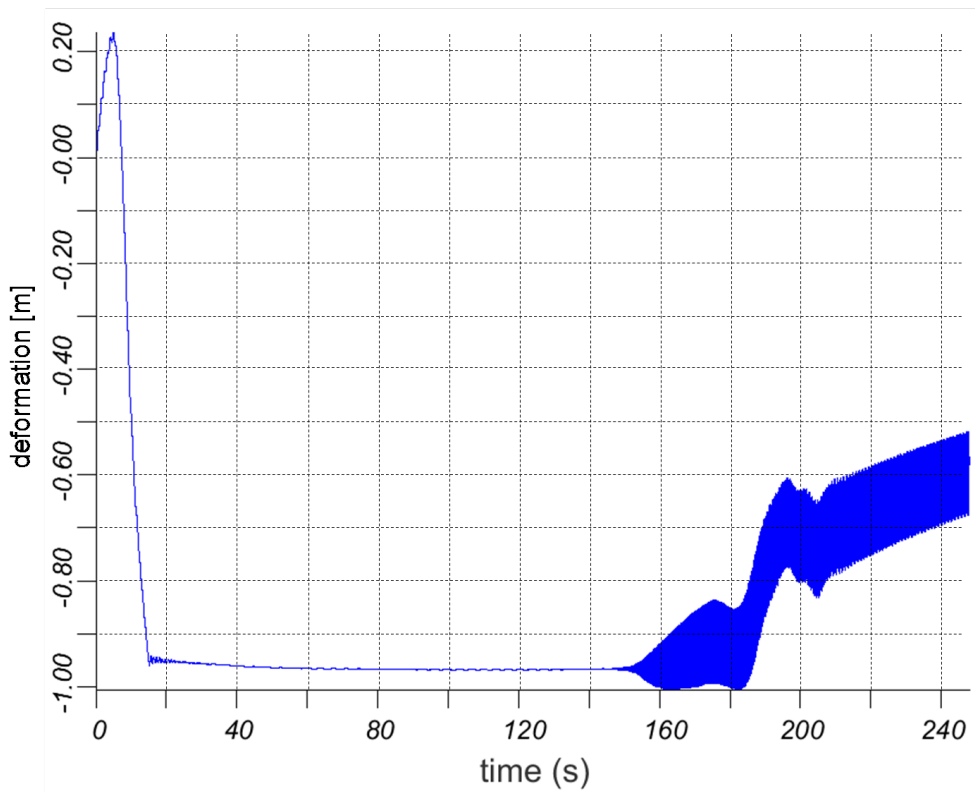


Figure 6.7: Edgewise deformation

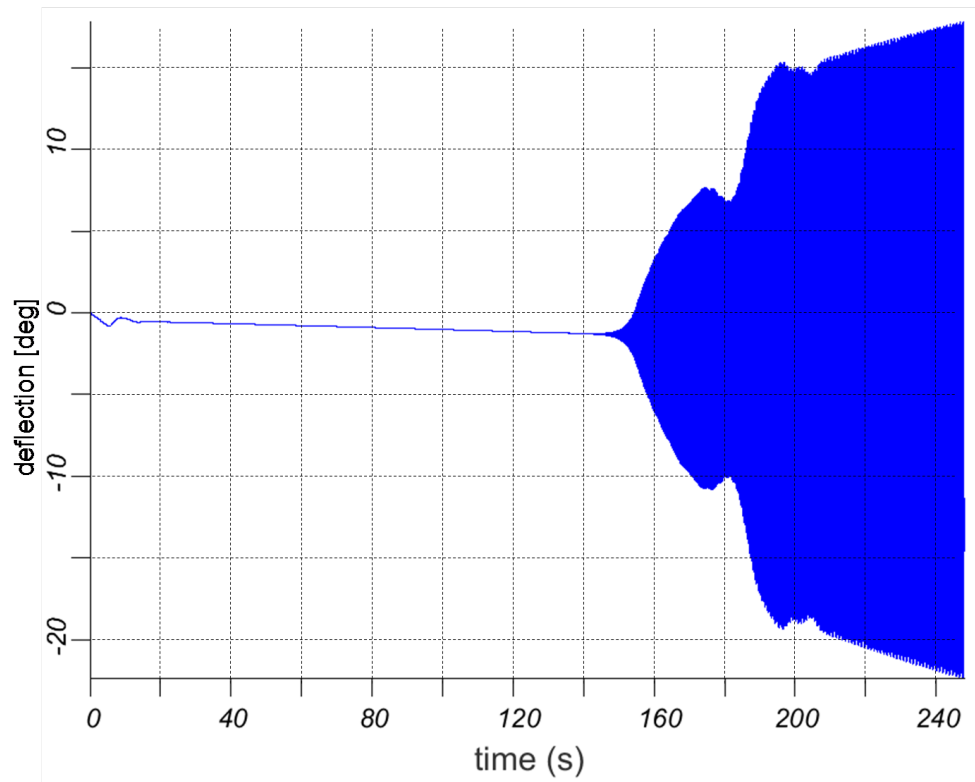


Figure 6.8: Torsionwise deformation

5.2 NREL - Blade - data

Radius (m)	Bifract (-)	AeroCent (-)	Structwst BMassDen (kg/m ³)	FipSff (N-m ⁻¹)	EdgSff (N-m ⁻²)	GJSff (N-m ⁻²)	EASff (N-m ⁻²)	Alpha (-)	Fipiner (kg/m) (-)	Edgliner (kg/m) (-)	FipcgOf (m)	EdgcgOf (m)	FipswRef (m)	EdgswRef (m)	FipEAOf (m)	EdgeAOf (m)	
1.50	0.000000	0.250000	13.305	678.935	18110.00E+6	18113.50E+6	5664.40E+6	6729.48E+6	0.0	972.86	973.04	0.0	0.000117	0.0	0.0	0.0	
1.70	0.003205	0.250000	13.305	678.935	18110.00E+6	18113.60E+6	5664.40E+6	9729.48E+6	0.0	972.86	972.04	0.0	0.000117	0.0	0.0	0.0	
2.70	0.010951	0.24951	13.305	773.363	19452.90E+6	19558.50E+6	5431.60E+6	10788.50E+6	0.0	1061.52	1066.38	0.0	0.0	-0.2303	0.0	0.0	0.0
3.70	0.035777	0.24510	13.305	740.550	17455.90E+6	18449.80E+6	4993.98E+6	10067.23E+6	0.0	966.09	1047.36	0.0	0.0	0.000444	0.0	0.0	0.0
4.70	0.052023	0.232384	13.305	740.042	15287.40E+6	19783.50E+6	4686.60E+6	9867.78E+6	0.0	873.81	1099.75	0.0	0.0	0.04345	0.0	0.0	0.0
5.70	0.068329	0.22059	13.305	652.495	10782.40E+6	14855.50E+6	3474.71E+6	7907.98E+6	0.0	648.55	873.92	0.0	0.0	0.05983	0.0	0.0	0.0
6.70	0.08445	0.20833	13.305	450.275	7229.72E+6	10220.60E+6	2323.54E+6	5491.26E+6	0.0	456.76	641.49	0.0	0.0	0.06494	0.0	0.0	0.0
7.70	0.10081	0.18608	13.305	424.054	6309.50E+6	91447.70E+6	1907.87E+6	4971.30E+6	0.0	400.53	592.73	0.0	0.0	0.07718	0.0	0.0	0.0
8.70	0.111707	0.16382	13.305	400.638	5628.30E+6	60083.16E+6	1570.39E+6	4493.95E+6	0.0	361.61	547.18	0.0	0.0	0.08394	0.0	0.0	0.0
9.70	0.133305	0.17155	13.305	382.082	4980.00E+6	68849.44E+6	1156.29E+6	4034.50E+6	0.0	316.12	490.84	0.0	0.0	0.10174	0.0	0.0	0.0
10.70	0.14989	0.15931	13.305	398.855	4928.84E+6	7009.18E+6	1002.12E+6	4037.29E+6	0.0	303.80	503.86	0.0	0.0	0.10758	0.0	0.0	0.0
11.70	0.165695	0.14706	13.305	426.321	4681.66E+6	7187.68E+6	855.90E+6	4168.72E+6	0.0	289.24	544.70	0.0	0.0	0.16829	0.0	0.0	0.0
12.70	0.18211	0.13461	13.181	416.820	3649.40E+6	7271.66E+6	672.27E+6	4082.35E+6	0.0	248.57	569.90	0.0	0.0	0.22235	0.0	0.0	0.0
13.70	0.19837	0.12500	12.848	406.186	3386.62E+6	7081.70E+6	541.49E+6	4085.97E+6	0.0	215.91	601.28	0.0	0.0	0.37556	0.0	0.0	0.0
14.70	0.21445	0.11500	12.192	361.420	2933.74E+6	6244.53E+6	448.94E+6	3668.34E+6	0.0	187.11	544.56	0.0	0.0	0.33386	0.0	0.0	0.0
15.70	0.23059	0.12500	11.561	372.822	2658.98E+6	6043.98E+6	336.02E+6	3147.92E+6	0.0	180.84	485.71	0.0	0.0	0.26519	0.0	0.0	0.0
16.70	0.247415	0.12500	11.072	349.477	2388.66E+6	4948.49E+6	311.35E+6	3011.58E+6	0.0	148.96	455.76	0.0	0.0	0.26441	0.0	0.0	0.0
17.70	0.263341	0.12500	10.792	316.538	2271.98E+6	4803.02E+6	291.04E+6	2882.93E+6	0.0	140.30	439.22	0.0	0.0	0.26507	0.0	0.0	0.0
18.70	0.28595	0.12500	10.232	319.333	2050.66E+6	4501.40E+6	261.00E+6	2613.97E+6	0.0	136.18	394.18	0.0	0.0	0.2155	0.0	0.0	0.0
21.70	0.32846	0.11500	9.672	330.974	1828.26E+6	4244.07E+6	2288.32E+6	2367.48E+6	0.0	109.42	362.08	0.0	0.0	0.23382	0.0	0.0	0.0
23.70	0.36058	0.11500	9.110	321.990	1598.71E+6	3995.28E+6	200.75E+6	2148.86E+6	0.0	94.36	335.01	0.0	0.0	0.19934	0.0	0.0	0.0
25.70	0.39380	0.12500	8.534	313.820	2650.98E+6	3750.76E+6	174.37E+6	1944.06E+6	0.0	80.24	305.57	0.0	0.0	0.19323	0.0	0.0	0.0
27.70	0.426802	0.12500	7.932	304.734	1021.38E+6	3474.14E+6	144.37E+6	1832.47E+6	0.0	62.67	263.67	0.0	0.0	0.14967	0.0	0.0	0.0
28.70	0.458655	0.12500	7.321	287.120	8176.80E+6	3139.07E+6	119.98E+6	1432.40E+6	0.0	49.42	237.08	0.0	0.0	0.15421	0.0	0.0	0.0
31.70	0.49108	0.12500	6.711	263.343	81.711.30E+6	2734.24E+6	81.19E+6	1168.76E+6	0.0	37.34	196.41	0.0	0.0	0.13252	0.0	0.0	0.0
33.70	0.52338	0.12500	6.122	243.207	534.73E+6	2554.37E+6	69.08E+6	202.40E+6	0.0	28.14	180.34	0.0	0.0	0.13131	0.0	0.0	0.0
35.70	0.55610	0.12500	5.546	241.668	408.00E+6	2334.03E+6	67.45E+6	922.98E+6	0.0	22.43	60.43	0.0	0.0	0.14035	0.0	0.0	0.0
37.70	0.58982	0.12500	4.971	220.633	314.51E+6	1828.73E+6	45.52E+6	760.93E+6	0.0	17.33	34.83	0.0	0.0	0.13353	0.0	0.0	0.0
38.70	0.623115	0.12500	4.401	200.293	283.83E+6	1584.10E+6	35.98E+6	648.03E+6	0.0	13.30	115.00	0.0	0.0	0.15134	0.0	0.0	0.0
41.70	0.65306	0.12500	3.834	179.424	175.88E+6	1323.36E+6	27.44E+6	539.70E+6	0.0	9.86	97.88	0.0	0.0	0.17418	0.0	0.0	0.0
45.70	0.68618	0.11500	3.332	165.094	126.01E+6	1183.58E+6	20.60E+6	531.15E+6	0.0	7.30	98.63	0.0	0.0	0.24222	0.0	0.0	0.0
47.70	0.71870	0.12500	2.890	154.411	107.24E+6	1020.16E+6	18.64E+6	480.01E+6	0.0	6.22	88.78	0.0	0.0	0.26222	0.0	0.0	0.0
49.70	0.75122	0.12500	2.450	138.255	90.88E+6	707.91E+6	16.28E+6	375.57E+6	0.0	6.19	66.96	0.0	0.0	0.25254	0.0	0.0	0.0
51.70	0.78317	0.12500	2.118	129.655	76.3E+6	14.63E+6	14.63E+6	328.98E+6	0.0	4.36	61.41	0.0	0.0	0.22795	0.0	0.0	0.0
53.70	0.824578	0.12500	1.730	107.284	61.05E+6	1584.10E+6	9.07E+6	244.04E+6	0.0	3.36	45.44	0.0	0.0	0.20000	0.0	0.0	0.0
55.70	0.865447	0.12500	1.342	98.770	49.05E+6	454.97E+6	8.08E+6	211.00E+6	0.0	2.75	39.57	0.0	0.0	0.17462	0.0	0.0	0.0
56.70	0.89776	0.12500	1.0173	93.001	34.61E+6	365.72E+6	8.09E+6	181.63E+6	0.0	2.21	34.09	0.0	0.0	0.22784	0.0	0.0	0.0
57.70	0.917362	0.12500	0.760	67.674	30.4E+6	304.73E+6	5.76E+6	160.25E+6	0.0	1.93	30.12	0.0	0.0	0.23124	0.0	0.0	0.0
58.70	0.933008	0.12500	0.404	68.772	28.52E+6	281.42E+6	5.33E+6	109.23E+6	0.0	1.69	20.15	0.0	0.0	0.14826	0.0	0.0	0.0
59.70	0.93821	0.12500	0.319	66.284	23.94E+6	281.71E+6	4.64E+6	92.24E+6	0.0	1.34	17.11	0.0	0.0	0.15349	0.0	0.0	0.0
60.70	0.94636	0.12500	0.253	59.340	19.63E+6	45.97E+6	3.08E+6	21.10E+6	0.0	1.10	11.55	0.0	0.0	0.1682	0.0	0.0	0.0
61.70	0.988150	0.12500	0.218	55.914	16.00E+6	137.68E+6	3.68E+6	53.32E+6	0.0	0.89	9.77	0.0	0.0	0.20018	0.0	0.0	0.0
62.70	0.986290	0.12500	0.173	52.494	12.83E+6	115.79E+6	3.13E+6	44.63E+6	0.0	0.71	8.19	0.0	0.0	0.18861	0.0	0.0	0.0
63.70	0.97073	0.12500	0.140	49.114	10.08E+6	101.63E+6	2.64E+6	36.90E+6	0.0	0.56	6.82	0.0	0.0	0.18035	0.0	0.0	0.0
64.70	0.97866	0.12500	0.101	45.819	7.55E+6	85.07E+6	2.17E+6	29.03E+6	0.0	0.42	5.57	0.0	0.0	0.17098	0.0	0.0	0.0
65.70	0.988698	0.12500	0.062	41.689	4.80E+6	64.26E+6	1.68E+6	21.31E+6	0.0	0.25	4.01	0.0	0.0	0.1624	0.0	0.0	0.0
66.70	0.985612	0.12500	0.023	11.453	0.25E+6	6.61E+6	0.25E+6	4.98E+6	0.0	0.04	0.94	0.0	0.0	0.15387	0.0	0.0	0.0
67.70	0.985000	0.12500	0.000	10.319	0.17E+6	5.01E+6	0.17E+6	3.63E+6	0.0	0.02	0.36	0.0	0.0	0.15181	0.0	0.0	0.0
68.70	1.000000	0.12500	0.000	0.000	0.000	0.000	0.000	0.000	0.0	0.0	0.0	0.0	0.0	0.0	0.0	0.0	0.0

Figure 6.9 : Distributed Blade Structural Properties of NREL-Blade [Jon09]

5.2. NREL - BLADE - DATA

Node (-)	RNodes (m)	AeroTwst (°)	DRNodes (m)	Chord (m)	Airfoil Table (-)
1	2.8667	13.308	2.7333	3.542	Cylinder1.dat
2	5.6000	13.308	2.7333	3.854	Cylinder1.dat
3	8.3333	13.308	2.7333	4.167	Cylinder2.dat
4	11.7500	13.308	4.1000	4.557	DU40_A17.dat
5	15.8500	11.480	4.1000	4.652	DU35_A17.dat
6	19.9500	10.162	4.1000	4.458	DU35_A17.dat
7	24.0500	9.011	4.1000	4.249	DU30_A17.dat
8	28.1500	7.795	4.1000	4.007	DU25_A17.dat
9	32.2500	6.544	4.1000	3.748	DU25_A17.dat
10	36.3500	5.361	4.1000	3.502	DU21_A17.dat
11	40.4500	4.188	4.1000	3.256	DU21_A17.dat
12	44.5500	3.125	4.1000	3.010	NACA64_A17.dat
13	48.6500	2.319	4.1000	2.764	NACA64_A17.dat
14	52.7500	1.526	4.1000	2.518	NACA64_A17.dat
15	56.1667	0.863	2.7333	2.313	NACA64_A17.dat
16	58.9000	0.370	2.7333	2.086	NACA64_A17.dat
17	61.6333	0.106	2.7333	1.419	NACA64_A17.dat

Figure 6.10 : Distributed Blade Aerodynamic Properties

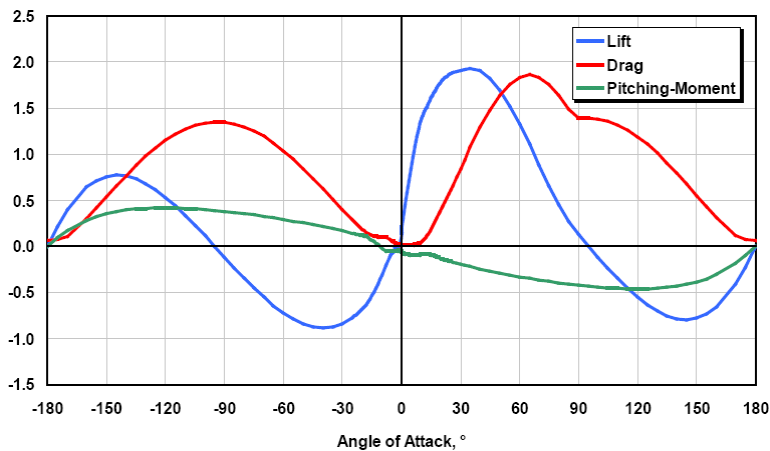


Figure 6.11 : Corrected coefficients of the DU40 airfoil

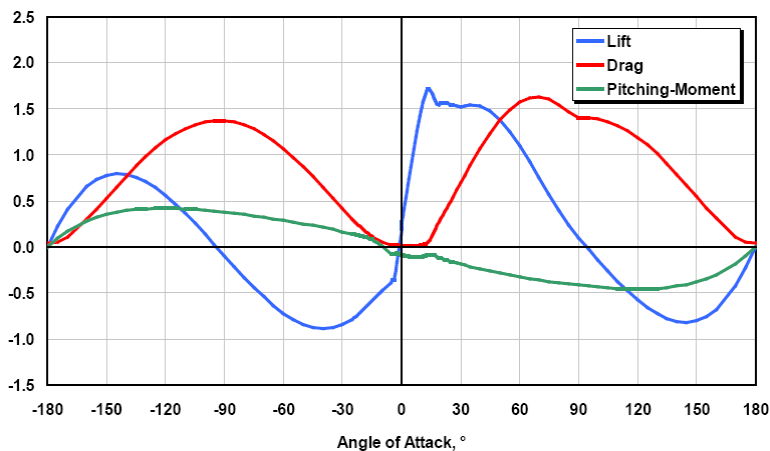


Figure 6.12 : Corrected coefficients of the DU35 airfoil

5.2. NREL - BLADE - DATA

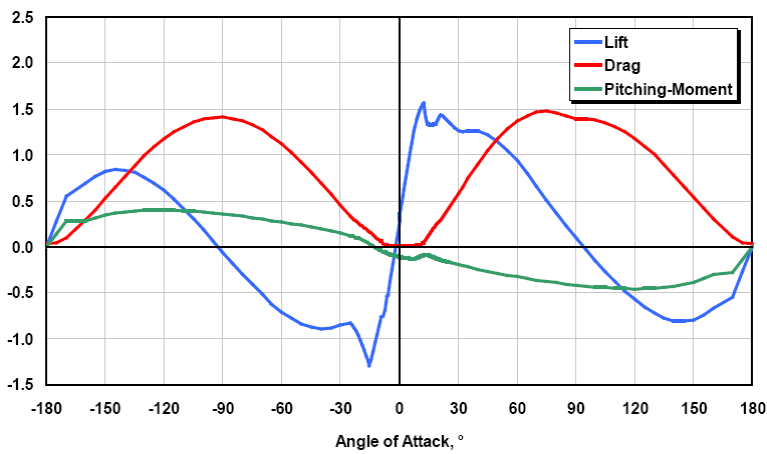


Figure 6.13 : Corrected coefficients of the DU30 airfoil

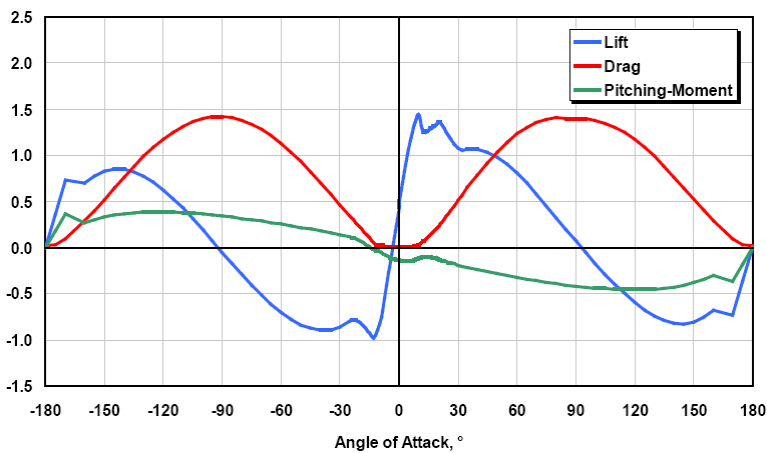


Figure 6.14 : Corrected coefficients of the DU25 airfoil

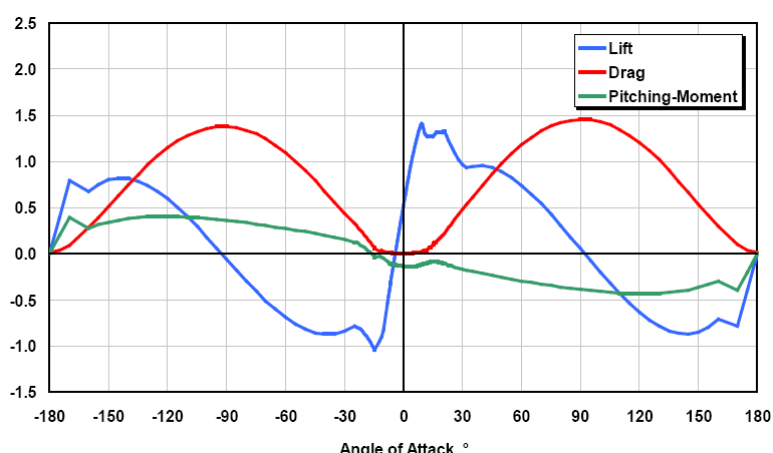


Figure 6.15 : Corrected coefficients of the DU21 airfoil

5.2. NREL - BLADE - DATA

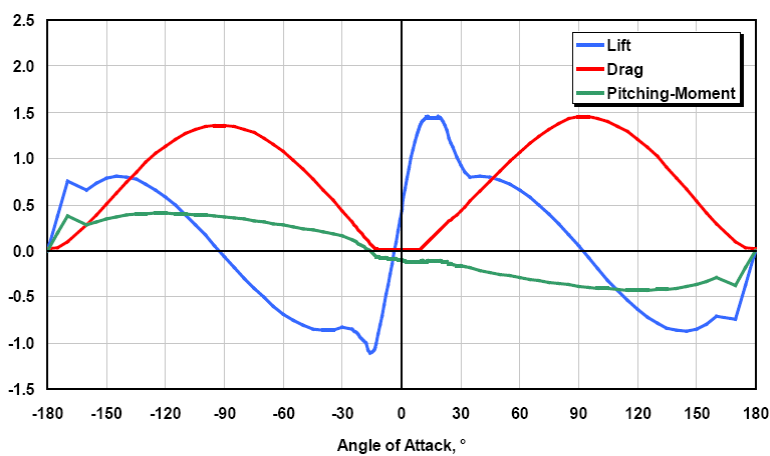


Figure 6.16 : Corrected coefficients of the NACA64 airfoil

5.3 L-profile

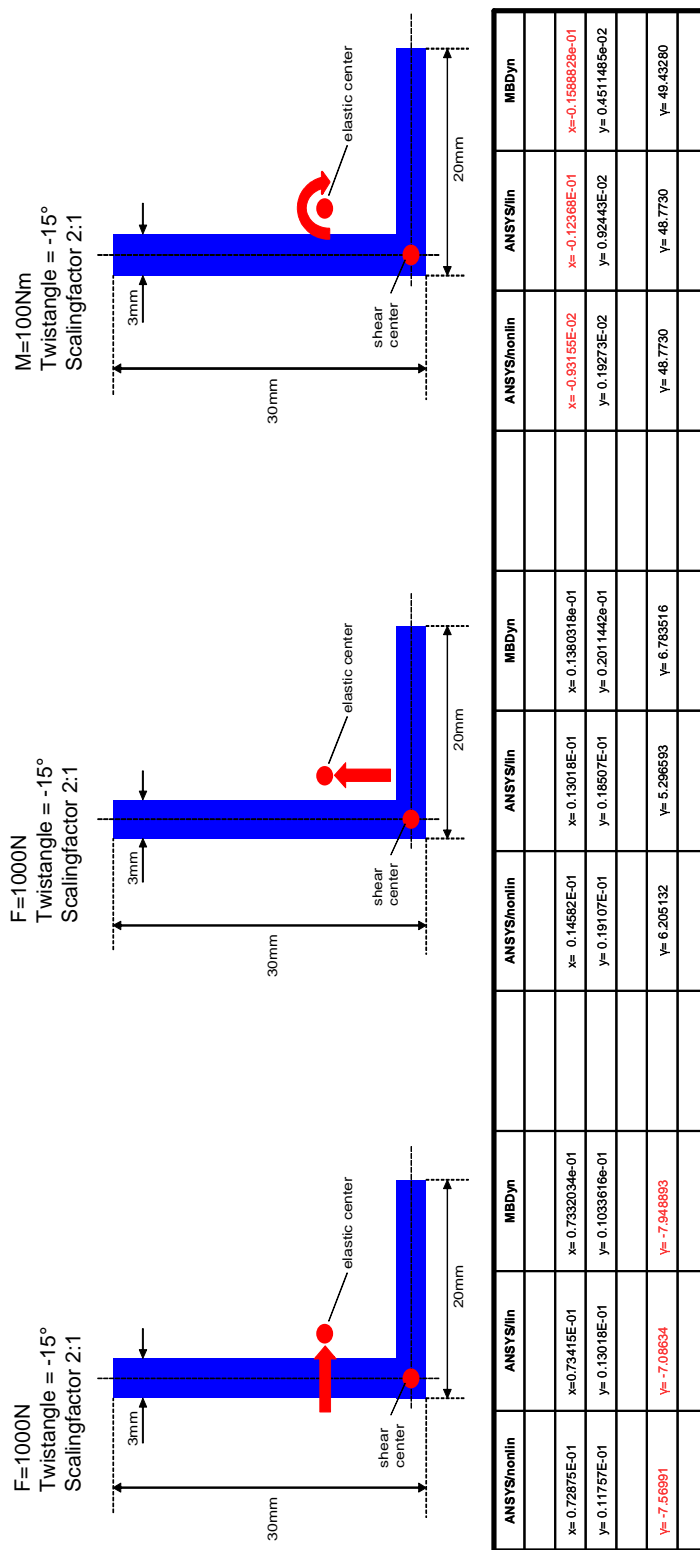


Figure 6.17 : L-profile, twist and scale

5.4 CD

Attached to this thesis is a CD where MBDyn NREL-blade models are included for testing purposes and illustration.

Descriptions of the included models:

- NREL_05abm_prebended_c81
 - Blades consist of five structural and aerodynamic beams
 - Adjusted aerodynamic is C81
- NREL_05abm_prebended_theodorsen
 - Blades consist of five structural and aerodynamic beams
 - Adjusted aerodynamic is Theodorsen
- NREL_10abm_prebended_c81
 - Blades consist of ten structural and aerodynamic beams
 - Adjusted aerodynamic is C81
- NREL_10abm_prebended_theodorsen
 - Blades consist of ten structural and aerodynamic beams
 - Adjusted aerodynamic is Theodorsen